63-4-2

NAVWEPS REPORT 8150 1 JUNE 1963

NAVWEPS REPORT 8150

Quarterly report:

FONDATIONAL RESEARCH PROJECTS

JANUARY–MARCH 1963

NAVAL ORDNANCE LABORATORY CORONA
CORONA, CALIFORNIA

NAVAL ORDNANCE LABORATORY CORONA

W. R. KURTZ, CAPT., USN
Commanding Officer

F. S. ATCHISON, Ph.D.
Technical Director

FOREWORD

This report includes papers on various aspects of work performed during the third quarter of fiscal year 1963 under the Foundational Research Program, whose aim is "to stimulate original work by scientific and technical personnel at the Naval Ordnance Laboratory Corona, in all fields of science and technology." The projects are supported by WepTask R360 FR-104/211-1/R011-01-001. Additional support is provided the High Temperature Polymer Program by WepTask RMGA-41-031/211-1/F009-07-002.

C. J. HUMPHREYS
Head, Research Department

CONTENTS

CODER COMPONENTS PROGRAM

THIN MAGNETIC FILM PARAMETRONS

by

R. L. King and J. H. Johnson

INTRODUCTION

The parametron, a solid-state digital component with high reliability, is generally constructed from a ferrite core, rolled ribbon magnetic core, or thin magnetic film. The theory of the thin film parametron was presented in a previous quarterly report (NAVWEPS Report 7214). This type differs from the ferrite core parametron (discussed in NAVWEPS Report 7229) in that the pumping field is applied at right angles to the signal field. It has the advantage over both ferrite and rolled ribbon (tape-wound) parametrons of being able to operate at higher pump and clock frequencies.

SUMMARY

Experiments were conducted at the Laboratory to test the basic theory and to determine the optimum parametron design under operating conditions. Figure 1 shows a circuit diagram of a commercially available thin film parametron used in these tests.[1] The primary winding is a single, straight, No. 20 AWG copper wire, on the surface of which is deposited a 25% iron 74% nickel alloy film, 14,900 A thick, to form the magnetic core. The primary winding carries the excitation current at the pumping frequency of 2f, and also the dc bias current. The secondary winding, which is around the axis of the single wire of the primary, is connected in parallel with a capacitor to form a circuit resonant at one-half the pumping frequency.

When two of these thin film parametrons were connected in series with the signal (secondary) windings opposing each other so as to cancel transformer action (see Figure 2), they functioned at frequencies up to 10 Mc. They were driven by a power supply constructed in the Laboratory. (A commercial power supply with an upper frequency limit of a

[1] Kanematsu New York, Inc.

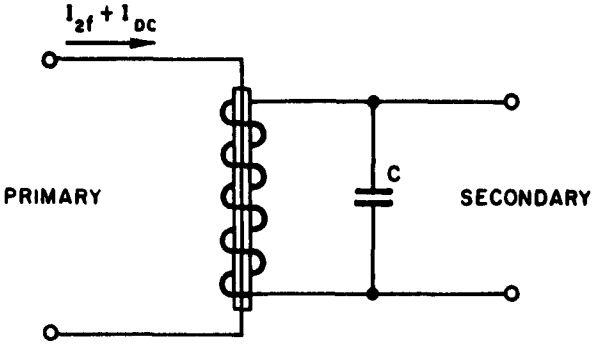

FIGURE 1. Thin Film Parametron

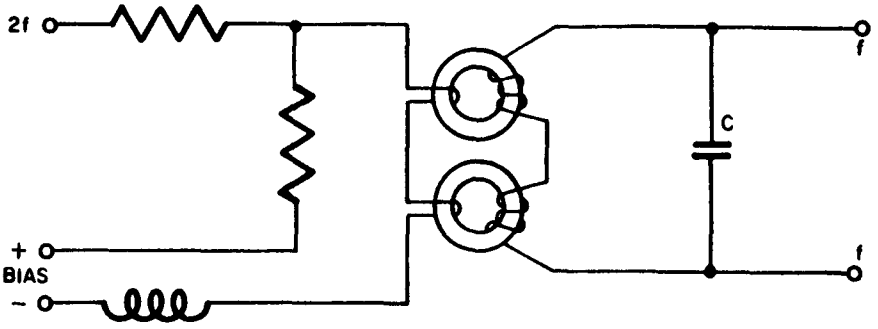

FIGURE 2. Parametron Circuit

little over 2 Mc was used for preliminary investigations with rolled ribbon cores.) Since the parametrons are designed for operation at a pump frequency of 10 to 20 Mc, additional capacitance was added to the resonant circuits for operation at the 2-Mc frequency.

EXPERIMENTAL DETAILS

Parametron design requires a critical choice of physical and electrical parameters, such as pump current, frequency, and bias. It is desirable, therefore, to establish criteria for predicting the optimum design and operating points for the various type of parametrons.

In order to develop a figure of merit for experimental parametrons, the basic parametron theory, as presented in NAVWEPS Report 7205, was reviewed. In this report, the required pumping power, P, is given by

$$P = \frac{2R}{\omega L} \tag{1}$$

where P is related to the change of inductance of the magnetic core. The relationship between the change in inductance, ΔL, and the Q of the parametron circuit is found to be

$$\frac{\Delta L}{L} \geq \frac{4}{Q} \tag{2}$$

This theory was based on high Q and low pumping power. For low Q and high pumping power, digital differential analyzer computations showed that $\Delta L/L$ could be smaller than this equation indicates. In any case, the ratio of $\Delta L/L$ to $1/Q$ should give a figure of merit for parametron operation.

To evaluate this figure of merit, several rolled ribbon and ferrite core parametrons were constructed and the ratio of $\Delta L/L$ to Q was determined. These parametrons functioned successfully in the parametron circuit at 2 Mc. However, the figure of merit did not prove as accurate in predicting optimum design parameters as had been anticipated. Measurements of ΔL were strongly dependent on the method of measurement and, similarly, the values of Q measured in different ways did not agree with each other.

To obtain the figure of merit measurements for the parametron, a pumping frequency of 2.0 Mc was used for the input, and the output or secondary winding was tuned to resonate at 1.0 Mc with the capacitor, C. Tape-wound cores having 10 wraps of 0.000125-inch Mo-Permalloy material were used. With the drive current set at approximately 0.2 amp, the cores have a switching time of 0.2 μsec. Figure 3 shows a resonant frequency curve of the output circuit with low-level input excitation.

Figure 4 is an oscilloscope picture of the output of the tape-wound parametron and the input current 2f, with settings of 1.0 volt/cm for the output and 1.0 amp/cm for the pump. Figure 5, a curve of inductance versus bias for these cores, shows that the area of optimum bias would be between 0.2 and 0.6 amp for successful operation.

Since the resonant peak of the parallel resonant circuit changed with the amplitude of the input signal, it follows that the inductance is

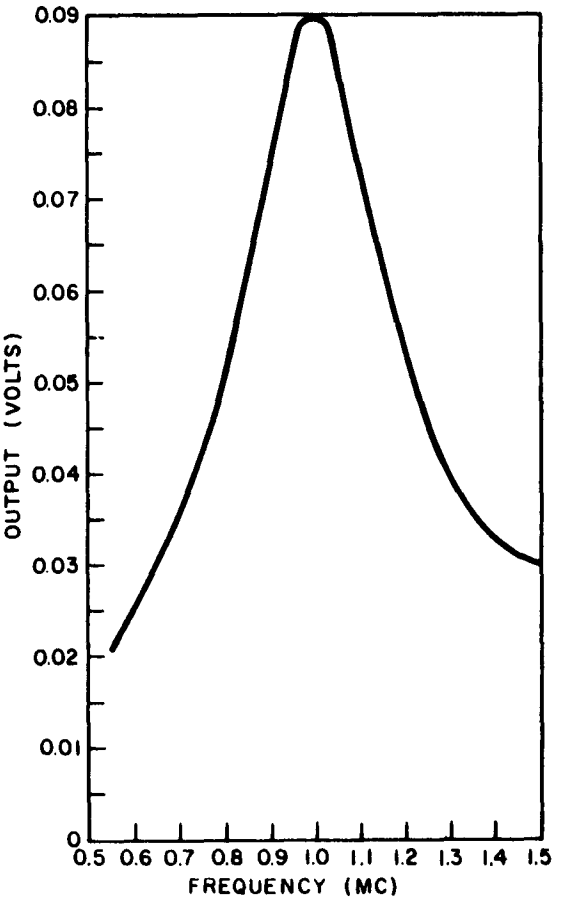

FIGURE 3. Resonant Frequency Curve

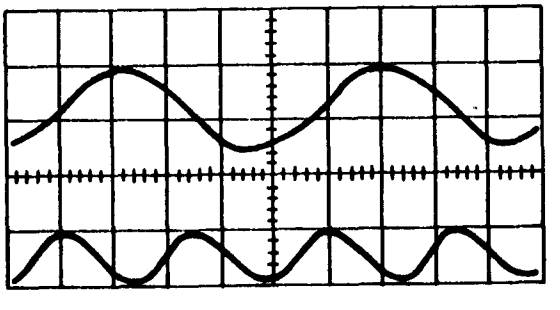

FIGURE 4. Output (top) and Input (bottom) of Tape-Wound Parametron

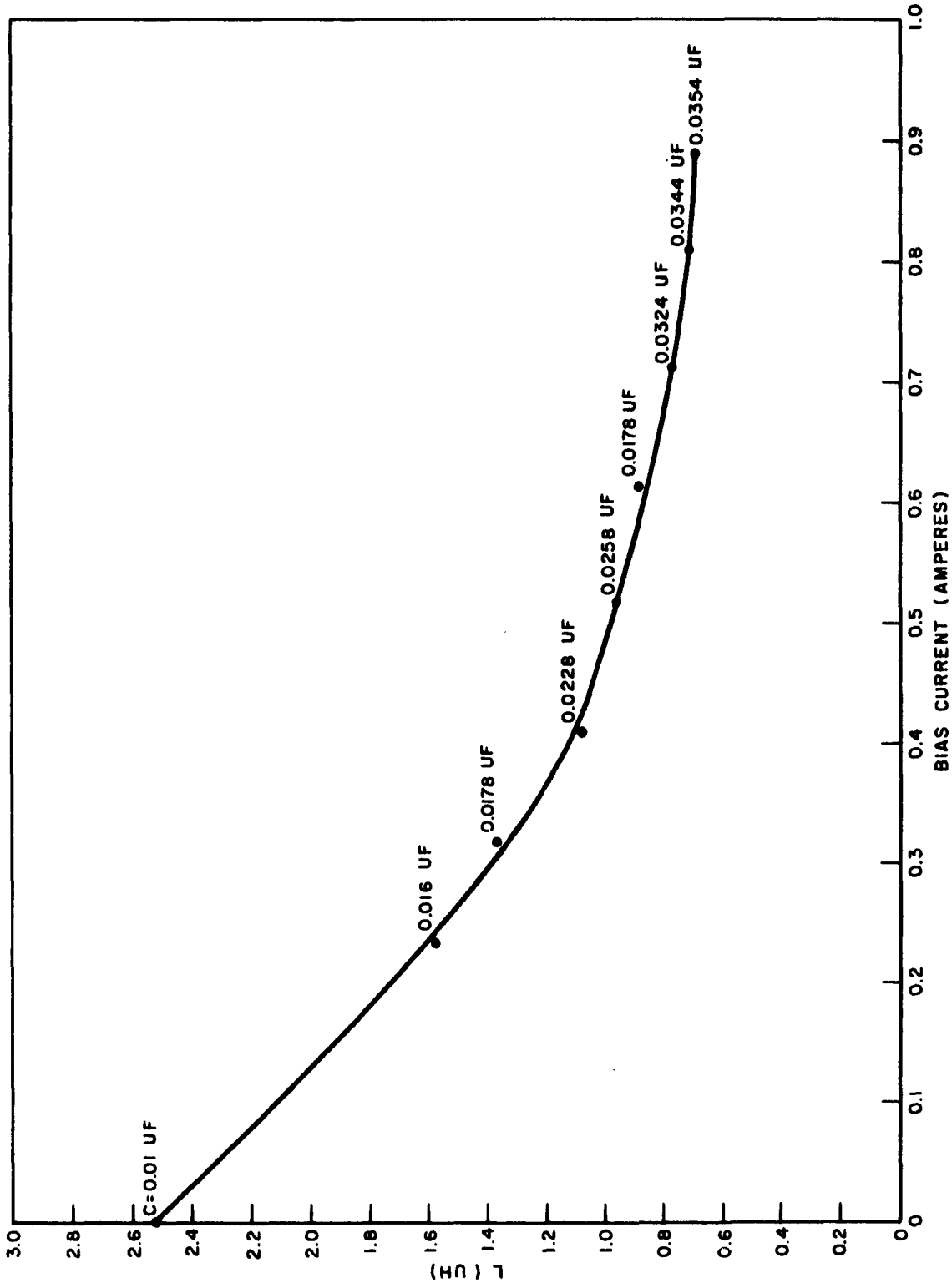

FIGURE 5. Inductance vs. Bias for Tape-Wound Parametron

changing due to saturation of the magnetic material in the core. If the circuit is tuned to resonance with a capacitance C_1, using very small input current, and then the magnetic material in the core is saturated by a strong permanent magnet and the value of capacitance (C_2) needed to restore resonance is noted, the difference inductance value can be calculated.

$$\Delta L = L_1 - L_2 = \frac{1}{(2\pi f)^2}\left(\frac{1}{C_1} - \frac{1}{C_2}\right) \tag{3}$$

Since $Q = \omega L/R$ and the inductance varies with the level of the input, R must be determined accurately. It was determined that a good method of obtaining R would be to use the impedance equation

$$Z^2 = R^2 + X_L^2 \tag{4}$$

where the impedance, Z, could be obtained from Thevenin's equivalent for the secondary circuit:

$$Z = \frac{E}{I} \tag{5}$$

Here E is the open circuit voltage of the secondary, and I is the current through the secondary windings with the circuit shorted. Since X_2 is known from the ωL measured previously,

$$R = \sqrt{Z^2 - X_2^2} \tag{6}$$

Data were obtained for parametrons in which a progressively smaller number of wraps of material, down to one wrap, were used. All of the data obtained for these parametrons under operating conditions resulted in a Q of approximately one ($Q \approx 1$). Information was obtained from some commercial thin-film parametron elements having capacitors encapsulated so that tuning should not be necessary up to a frequency of 20 Mc; however, capacitance was added and the elements were tuned at 2.0 Mc so that all the data would be at the same frequency. This also resulted in a $Q \approx 1$. With this low value, equation (2) would not be expected to apply.

HIGH TEMPERATURE POLYMER PROGRAM

SYNTHETIC STUDIES

by

D. L. Herring and C. M. Douglas

The study of the intermediates formed from the reaction of $(C_6H_5)_2PCl_3$ with NH_3 has been continued during the present reporting period. The reaction of $(C_6H_5)_2PCl_3$ with NH_3 in $CHCl_3$ solution, which is described by the equation

$$(C_6H_5)_2PCl_3 + NH_3 \longrightarrow \left[(C_6H_5)_2\overset{\overset{NH_2}{\|}}{P}-N=\overset{\overset{NH_2}{|}}{P}(C_6H_5)_2\right]Cl + \text{oil}$$

(I)

gave a 40-65% yield of the dimer (I) plus a 15-30% yield of an unidentified viscous oil. The infrared spectrum and molecular weight of the oil suggested that the material was

$$(C_6H_5)_2\overset{\overset{NH_2}{\|}}{P}-N=\overset{\overset{NH_2}{|}}{P}(C_6H_5)_2$$

(II)

Hydrolysis of samples of the oil gave

$$(C_6H_5)_2P(O)NHP(O)(C_6H_5)_2$$

(III)

Pyrolysis of the oil at 220-225°C under vacuum gave $[(C_6H_5)_2PN]_3$, compound (IV), in 16% yield (by weight), plus NH_3 and an unidentified residue. This result can be interpreted as further evidence that structure (II) is valid for the oil. However, since the elemental analysis did not confirm the proposed structure, the identity of the material was not established.

In a related experiment, (I) was heated with $(C_6H_5)_2PCl$ in an evacuated ampoule at 165-175°C for 72 hours. During the course of the

reaction, a rearrangement of (I) took place, giving NH_4Cl and a high yield of $[(C_6H_5)_2PN]_3$, together with a quantitative yield of $(C_6H_5)_2P(O)OH$ (based on $(C_6H_5)_2PCl$). Since it has been shown[1] that pyrolysis of (I) at 275-280°C yielded a product mixture composed of 85% $[(C_6H_5)_2PN]_4$, compound (V), and 10% $[(C_6H_5)_2PN]_3$, the $(C_6H_5)_2PCl$ in the above reaction apparently diverted the normal course of the reaction by catalyzing the cleavage of [P—N] bonds in compound (I).

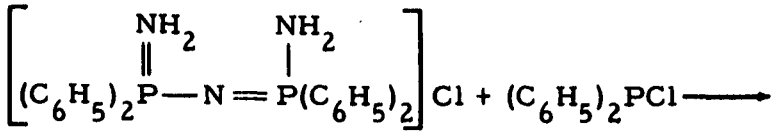

(1)

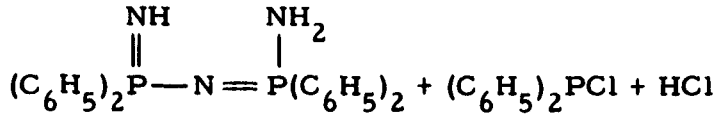

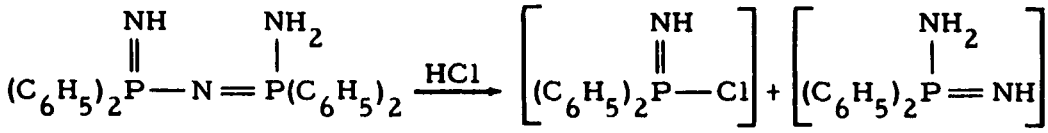

(2)

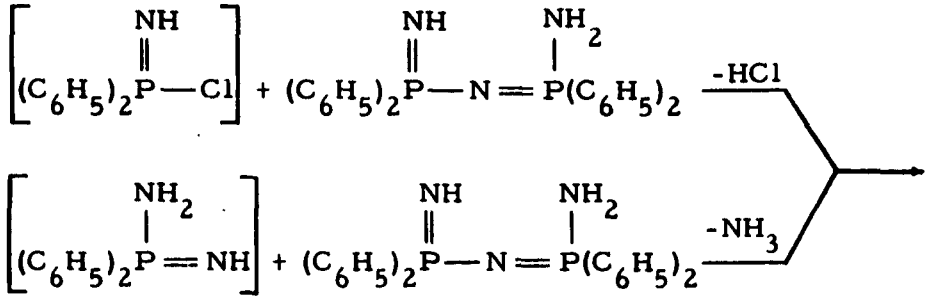

(3)

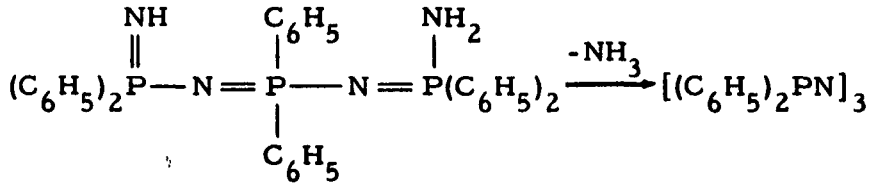

This series of reactions describes a possible route to the formation of $[(C_6H_5)_2PN]_3$ instead of the usual pyrolysis product, $[(C_6H_5)_2PN]_4$.

---

[1] C. P. Haber, D. L. Herring, and E. A. Lawton, J. Am. Chem. Soc., Vol. 80, p. 2116 (1958).

In the part of the investigation concerned with the formation of heterosubstituted cyclic compounds, it was initially postulated that (I) would react with the three classes of pentavalent phosphorus halides according to the following equations:

$$\text{Compound (I)} + R_2PCl_3 \longrightarrow HCl + (R_2PN)_3 \qquad (4)$$

$$\text{Compound (I)} + PCl_5 \longrightarrow HCl + R_4Cl_2P_3N_3 \qquad (5)$$

$$\text{Compound (I)} + RPCl_4 \longrightarrow HCl + R_5ClP_3N_3 \qquad (6)$$

to yield the corresponding cyclic trimer together with higher polymers. The preparation of $[(C_6H_5)_2PN]_3$ and $(C_6H_5)_4Cl_2P_3N_3$ by the above method has been described.[2,3] When (I) reacted with $C_6H_5PCl_4$ under vacuum over the range 140-145°C, about 75% of the amount of HCl was evolved that would be expected from the reaction

$$\left[(C_6H_5)_2P(NH_2)=N-P(NH_2)(C_6H_5)_2\right]Cl + C_6H_5PCl_4 \longrightarrow$$

$$4HCl + [(C_6H_5)_5ClP_3N_3]_x$$

The reaction product appeared to contain a polymeric material, which analyzed approximately for $[(C_6H_5)_5ClP_3N_3]_x$, together with some $[(C_6H_5)_2PN]_4$.

In a more informative experiment, $C_6H_5PCl_4$ and (I) were allowed to react at 75-80°C. The temperature was held at 75-80°C until one equivalent of HCl had been evolved, then increased to 135-140°C. Over the range of 135-140°C, a second equivalent of HCl was evolved during a 3-hour period. From the product mixture, by the process of fractional recrystallization from ligroine, the new compound (VI), $(C_6H_5)_6Cl_2P_4N_4$ (m.p. 192-193°C), was isolated. Since the synthesis of (VI) was not entirely unambiguous, it is not presently known whether the structure is that of (VIa) or (VIb).

---

[2] NAVWEPS Report 7237, Quarterly Report: Foundational Research Projects, July-September 1962, p. 39 (December 1962).

[3] NAVWEPS Report 8141, Quarterly Report: Foundational Research Projects, October-December 1962, p. 21 (March 1963).

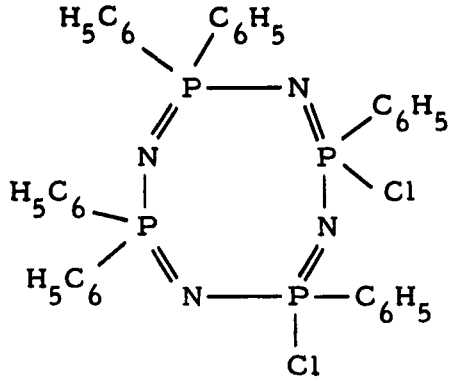

(VIa)

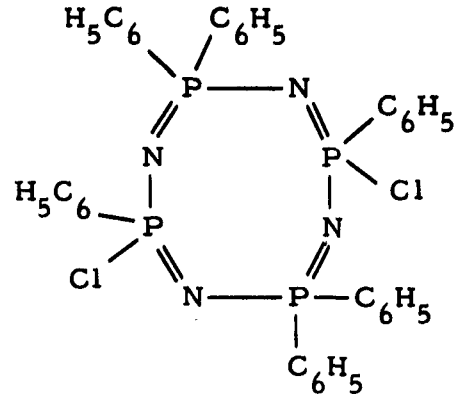

(VIb)

One may speculate that the course of the reaction leading to the formation of (VIa) was

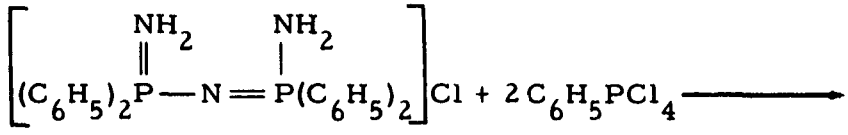

(I)

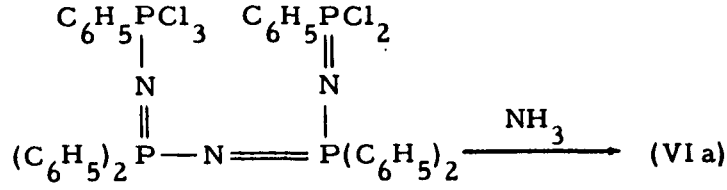

To explain the formation of (VIb) would require a mechanism involving the low-temperature cleavage of (I). Under the conditions of the experiment, such a reaction is considered unlikely.

Compound (VII), $(C_6H_5)_6Cl_2P_4N_4$, with a melting point at 153-155°C, was also isolated from the above reaction by fractional recrystallization from ligroine. On the basis of the infrared spectra, (VII) was an isomer of (VI).

EXPERIMENTAL

Hydrolysis and Pyrolysis of the Intermediate Oil

The infrared spectra of $(C_6H_5)_2PCl_3$, which was used in the preparation of (I) and the oil, are shown in Figure 1. A 25-g sample of the

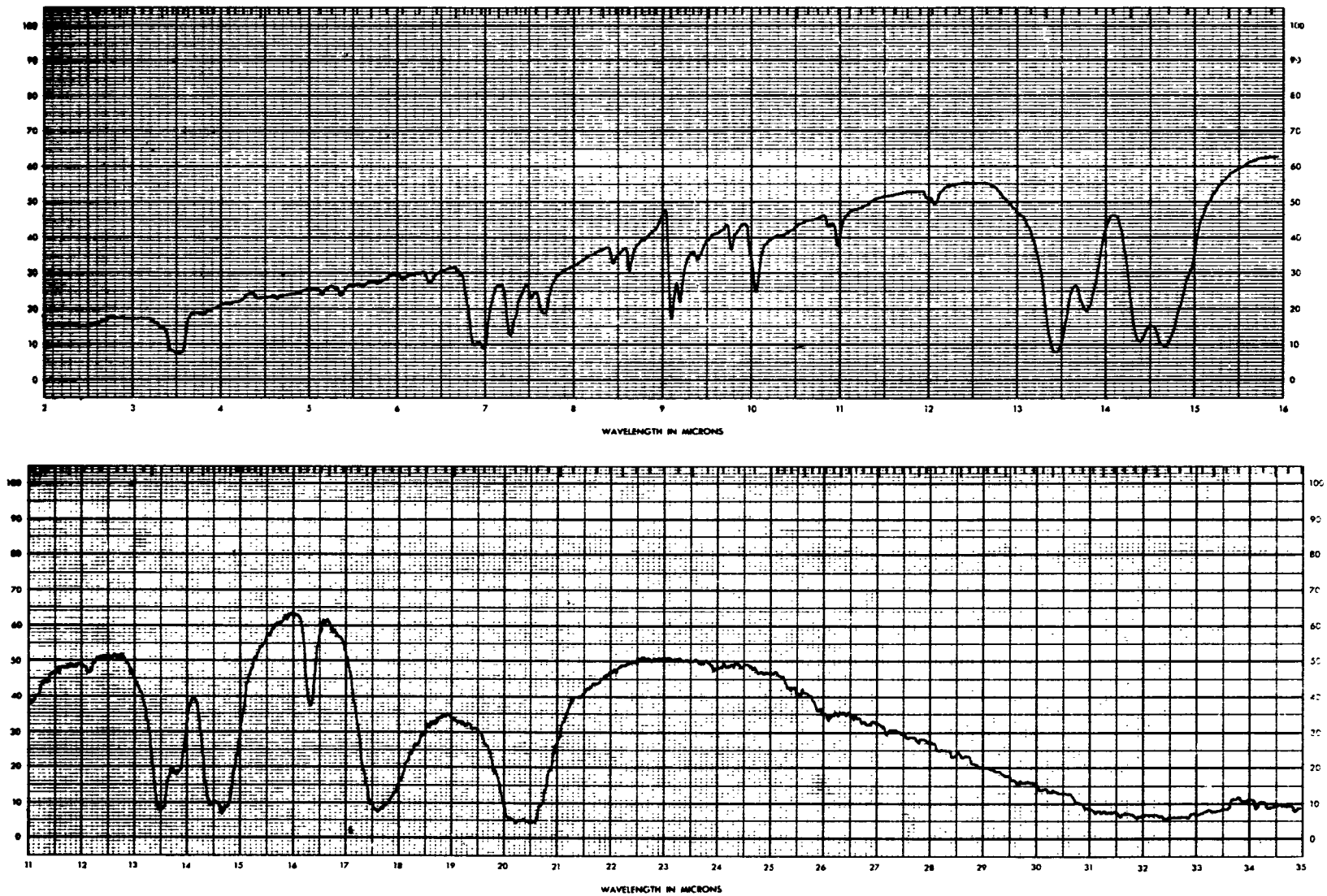

FIGURE 1. Infrared Spectra of $(C_6H_5)_2PCl_3$

crude oil obtained as a by-product from the reaction of $(C_6H_5)_2PCl_3$ with ammonia was heated for 8 hours under vacuum at 120-125°C to remove $CHCl_3$ and benzene. Then a 5-g sample of the material was refluxed with concentrated HCl for 8 hours, yielding a white crystalline precipitate which was removed by filtration. By the process of recrystallization from $C_6H_5NO_2$, 1.5 g of $(C_6H_5)_2P(O)NHP(O)(C_6H_5)_2$, compound (III) (m.p. 271-272°C), was isolated. The appearance and properties of the oily residue indicated that only partial hydrolysis had taken place.

A second 5-g sample was heated under vacuum at 225-230°C for 8 hours. An unmeasured amount of NH_3 was evolved during the heating cycle. The resulting oily material was allowed to set undisturbed at room temperature for 72 hours, during which time a crystalline material formed in the oily mixture. Next, the mixture was extracted with 50 ml of ether and the insoluble crystalline material removed by filtration. Then, by the process of recrystallization from benzene, 1.3 g of $[(C_6H_5)_2PN]_3$(m.p. 228-230°C) was isolated. The oily residue appeared to be starting material.

Reaction of Diphenylchlorophosphine with the Dimer (I)

A mixture of 1.4 g (0.0063 mole) of $(C_6H_5)_2PCl$ and 2.9 g (0.0063 mole) of dimer was heated in an evacuated ampoule for 72 hours at 165-175°C. The crude product was extracted with boiling benzene in the drybox to remove any unreacted $(C_6H_5)_2PCl$. The benzene-insoluble material (1.6 g, m.p. 224-227°C) was dried and recrystallized from a pyridine mixture (m.p. 232-233°C). The infrared spectra of this material was identical with that of $[(C_6H_5)_2PN]_3$.

Preparation of Trimeric Diphenyltetrachlorophosphonitrile

A mixture of 236 g (0.68 mole) of $(PNCl_2)_3$, 268 g (2.0 mole) of anhydrous $AlCl_3$, and 3000 ml of dry benzene was introduced into a 5-liter flask fitted with a mechanical stirrer, reflux condenser, and thermometer. The mixture was heated at reflux temperature for 70 hours in the drybox. It was then cooled, removed from the drybox, poured into 2 liters of ice water, and stirred vigorously. The organic layer was separated and dried over anhydrous sodium sulfate. After filtration, the dried solution was treated with activated charcoal and refiltered. The benzene was distilled from the mixture. About 30 g of $(PNCl_2)_3$ was removed at 135-150°C/15 mm Hg. The 195-g residue was recrystallized from ligroine (60-90°C boiling range) to yield 160 g of white crystals melting over the range 71-86°C. Recrystallization from absolute ethanol yielded white crystals melting at 92-93°C (lit.[4] 92.5°C).

[4] H. Bode and H. Bach, Ber, Vol. 75B, p. 215 (1942).

The use of absolute ethanol for the recrystallization of this compound appears to be mandatory, inasmuch as attempts to dissolve the material in ethanol that contained a very small amount of water resulted in the formation of an oil. Over 60% of the product was unrecovered.

The infrared spectrum of $(C_6H_5)_2Cl_4P_3N_3$ is presented in Figure 2.

Reaction of the Dimer with PCl_5 in Acetonitrile in the Presence of Triethylamine

In the drybox, 2.1 g (0.01 mole) of freshly sublimed PCl_5 was dissolved in 75 cc acetonitrile which had previously been refluxed over and distilled from P_2O_5. This solution was introduced into a 3-necked, 250-ml, round-bottomed flask equipped with mechanical stirrer, dropping funnel, and reflux condenser. Triethylamine (4.0 g, 0.04 mole) was added to the acetonitrile solution, and a solution containing 4.5 g (0.01 mole) of the dimer (I) in 100 cc of acetonitrile was added dropwise to the vigorously stirred reaction mixture. Addition of the dimer was complete in about 2 hours. Stirring was continued overnight, and the reaction mixture was then refluxed for one hour. No insoluble products were formed during the course of the reaction. The acetonitrile was distilled under vacuum and the residue was extracted with boiling benzene. From the benzene solution, 1.08 g (24%) of unreacted dimer was recrystallized. The solvent was then removed under reduced pressure and the residue extracted with ligroine (90-120°C boiling range). Eventually, 0.1350 g (2.6%) of the geminally substituted tetraphenyldichlorophosphonitrilic trimer was recovered (m.p. 142-143°C).

Calcd. for $C_{24}H_{20}Cl_2N_3P_3$: C, 56.1; H, 3.9; Cl, 13.8; N, 8.2; P, 18.1; mol. wt. 513

Found: C, 56.2; H, 4.0; Cl, 13.7; N, 8.3; P, 18.2; mol. wt. (cryosocopically in benzene) 509

Reaction of the Dimer with $C_6H_5PCl_4$

A mixture of 10.2 g (0.023 mole) of the dimer (I) and 5.6 g (0.023 mole) of $C_6H_5PCl_4$ was loaded into a heavy wall glass ampoule in the drybox, then heated on the vacuum line for 8 hours at 150-155°C. The reaction was carried out as previously described. The product was extracted with boiling benzene and the insoluble material removed by filtration. The benzene solution, which was strongly acidic, was washed with water until neutral, then dried over sodium sulfate and filtered. Upon standing overnight, 2.1 g of material was precipitated. While the infrared spectrum of this product was nearly identical with $[(C_6H_5)_2PN]_4$, the material melted over a wide range, 220-300°C. However, recrystallization from pyridine yielded 2 g of $[(C_6H_5)_2PN]_4$ (m.p. 320°C).

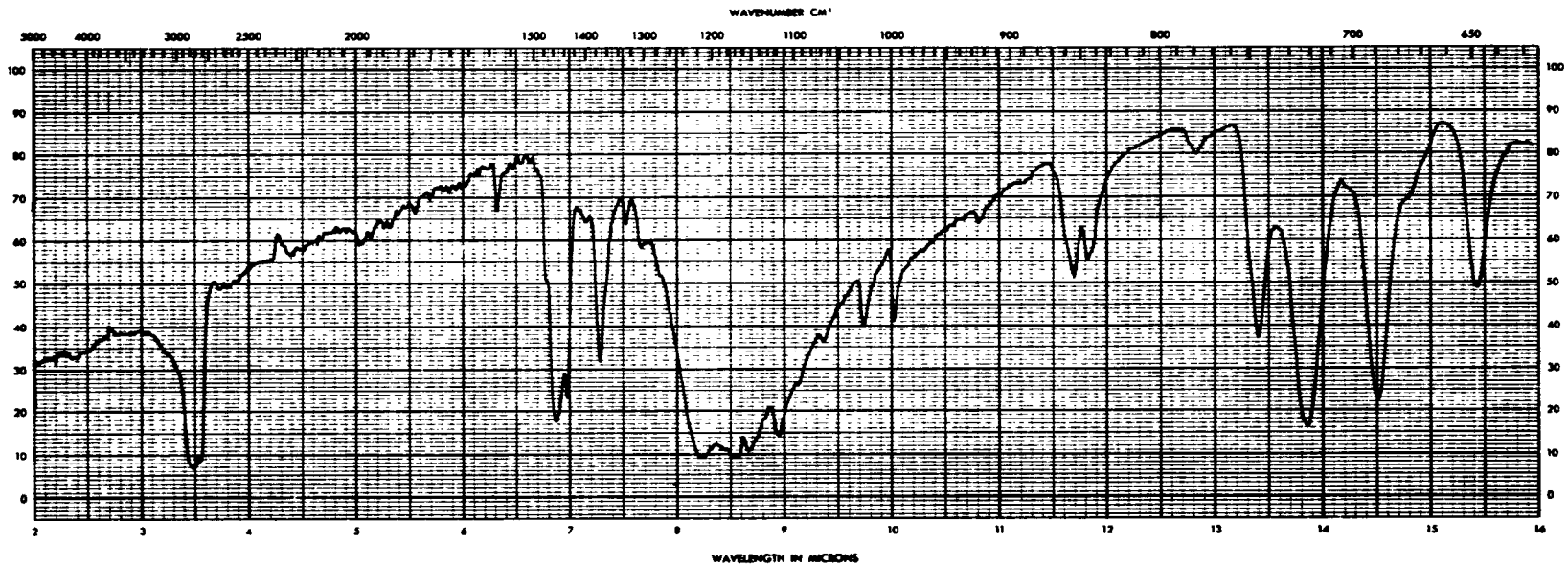

FIGURE 2. Infrared Spectrum of $(C_6H_5)_2Cl_4P_3N_3$

The remainder of the benzene-soluble portion was a low-melting oily material from which no other identifiable products were isolated.

The benzene-insoluble fraction was repeatedly extracted with boiling ligroine, and yielded a compound whose melting point (171-172°C) and infrared spectra are identical with those reported for the compound

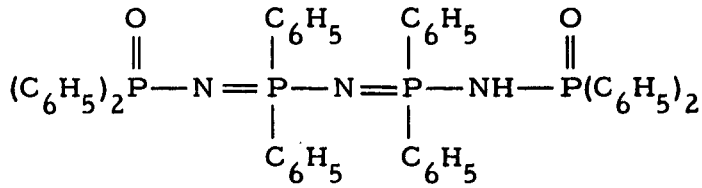

The reaction between the dimer and $C_6H_5PCl_4$ was repeated under exactly the same conditions as those outlined above. The benzene-soluble portion of the reaction product was treated with diethylamine. The diethylamine hydrochloride was removed by filtration and the benzene evaporated under reduced pressure. The residue melted over the range 50-70°C.

Calcd. for $C_{30}H_{25}ClP_3N_3$: C, 64.8; H, 4.5; P, 16.7; N, 7.5; Cl, 6.3

Found: C, 60.5; H, 4.9; P, 16.4; N, 7.3; Cl, 7.9

With the exception of 0.21 g of $[(C_6H_5)_2PN]_4$, which was recovered from the benzene-insoluble portion, no other identifiable products were isolated from this reaction.

The dimer (10.2 g, 0.023 mole) and 5.2 g (0.021 mole) of $C_6H_5PCl_4$ were heated in a heavy wall glass ampoule on the vacuum line. Evolution of hydrogen chloride commenced at about 80°C (bath temperature). This temperature was maintained for 5 hours, during which time one equivalent of HCl was collected. When the temperature of the oil bath was gradually raised to 140°C, one additional equivalent of HCl was evolved over a period of 16 hours. The heating was discontinued and the ampoule removed to the drybox, where the reaction mixture was dissolved in 500 ml of dry acetonitrile and 4.1 g (0.04 mole) of triethylamine was added. The mixture was refluxed for 1.5 hours. A portion of the material remained insoluble in refluxing acetonitrile. This compound was recovered and identified as 1.4 g of $[(C_6H_5)_2PN]_4$ (m.p. 319-321°C).

The CH_3CN was evaporated under reduced pressure and the residue extracted with boiling benzene to remove $Et_3N{\cdot}HCl$. The solvent was evaporated to dryness and the residue extracted with two 250-ml portions of ligroine. A white solid (m.p. 150-160°C) crystallized upon

concentration of the solvent. Recrystallization from ligroine yielded 0.5 g of a compound melting at 192-193°C. The infrared spectra are shown in Figure 3.

Calcd. for $C_{36}H_{30}P_4N_4Cl_2$: C, 60.7; H, 4.2; P, 17.4; N, 7.8; Cl, 9.9; mol. wt. 713

Found: C, 60.7; H, 4.2; P, 17.4; N, 8.0; Cl, 9.7; mol. wt. (cryosocopically in benzene) 695

Also recrystallized from the ligroine solution was a product that melted at 153-155°C. Its infrared spectrum (Figure 4) is similar to the compound mentioned above. On the basis of the infrared spectrum and an elemental analysis, the product was identified as compound (VII), an isomer of (VI).

Calcd. for $C_{36}H_{30}P_4N_4Cl_2$: C, 60.7; H, 4.2; P, 17.4; N, 7.8; Cl, 9.9; mol. wt. 713

Found: C, 60.9; H, 4.4; P, 17.4; N, 7.9; Cl, 9.7; mol. wt. 685

Preparation of Phenyltetrachlorophosphorane

In the drybox, 84.0 g (0.47 mole) of phenyldichlorophosphine was dissolved in 500 cc of dry carbon tetrachloride and introduced into a 1-liter stainless steel bomb. The bomb, with the valve attached, was removed to the vacuum line and cooled with liquid nitrogen. Chlorine (33.4 g, 0.47 mole) was gassed into the bomb, and the resulting mixture was allowed to warm to room temperature.

The contents of the bomb was then emptied into a 1-liter flask in the drybox. The solvent was evaporated under reduced pressure to about one-half the original volume. The small amount (about 2 g) of white, crystalline material which precipitated was filtered and dried in vacuum (m.p. 75-76°C).

Calcd. for $C_6H_5PCl_4$: C, 28.8; H, 2.0; P, 12.4; Cl, 56.8

Found: C, 28.6; H, 2.1; P, 12.3; Cl, 56.9

The remaining solution was evaporated to near dryness and the precipitate recovered. The infrared spectra of $C_6H_5PCl_4$ are presented in Figure 5.

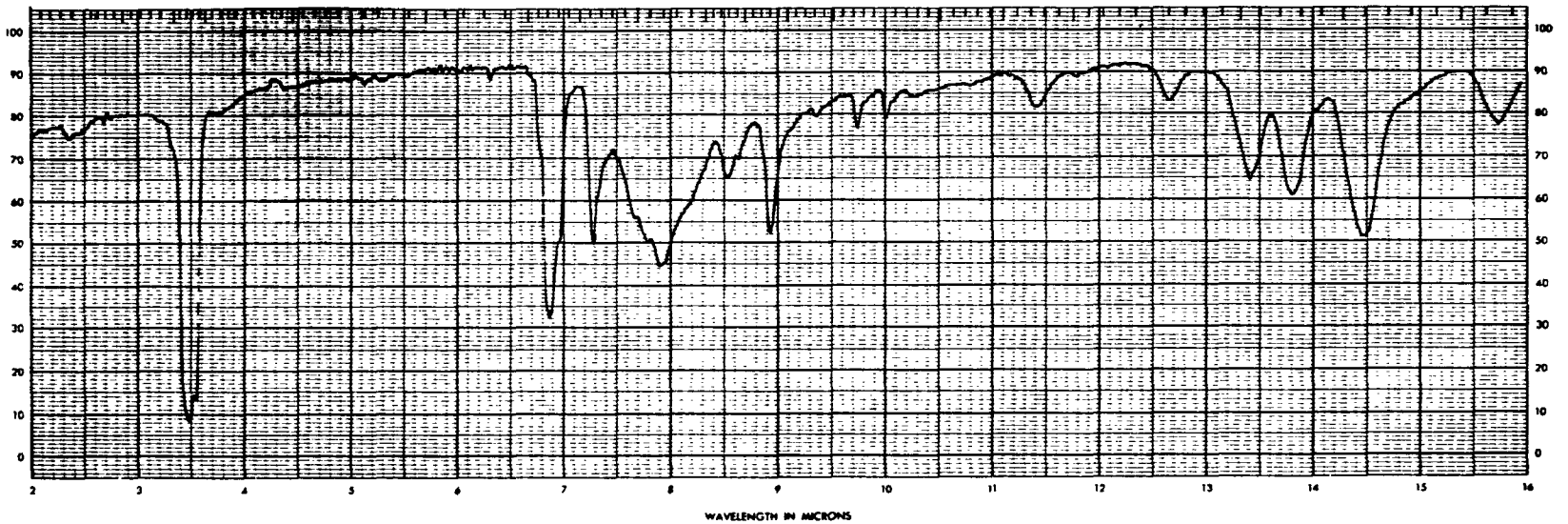

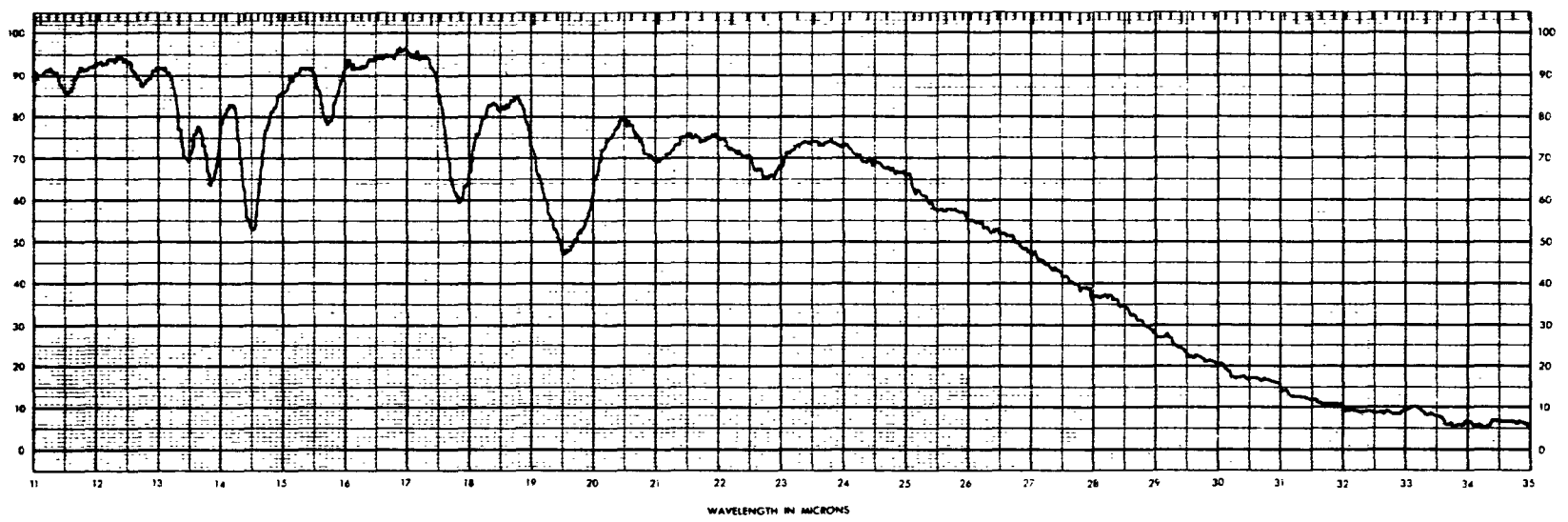

FIGURE 3. Infrared Spectra of $(C_6H_5)_6Cl_2P_4N_4$ (m.p. 192-193°C)

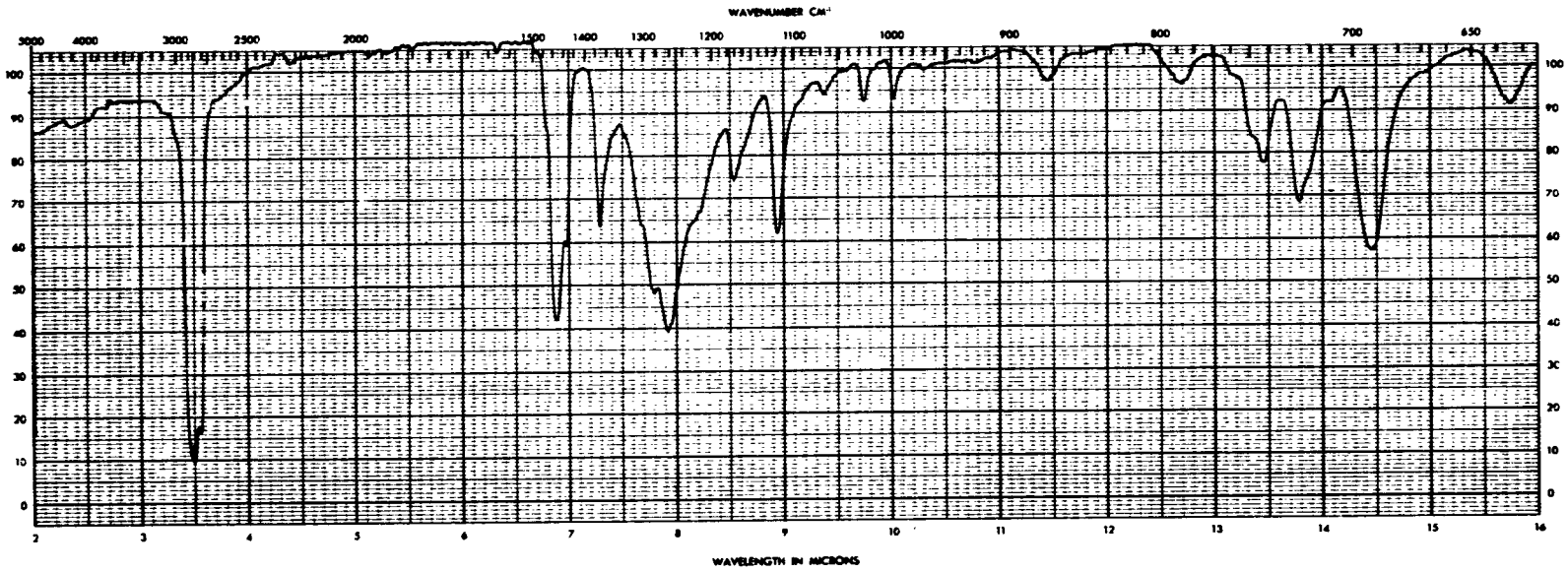

FIGURE 4. Infrared Spectrum of $(C_6H_5)_6Cl_2P_4N_4$ (m.p. 153-155°C)

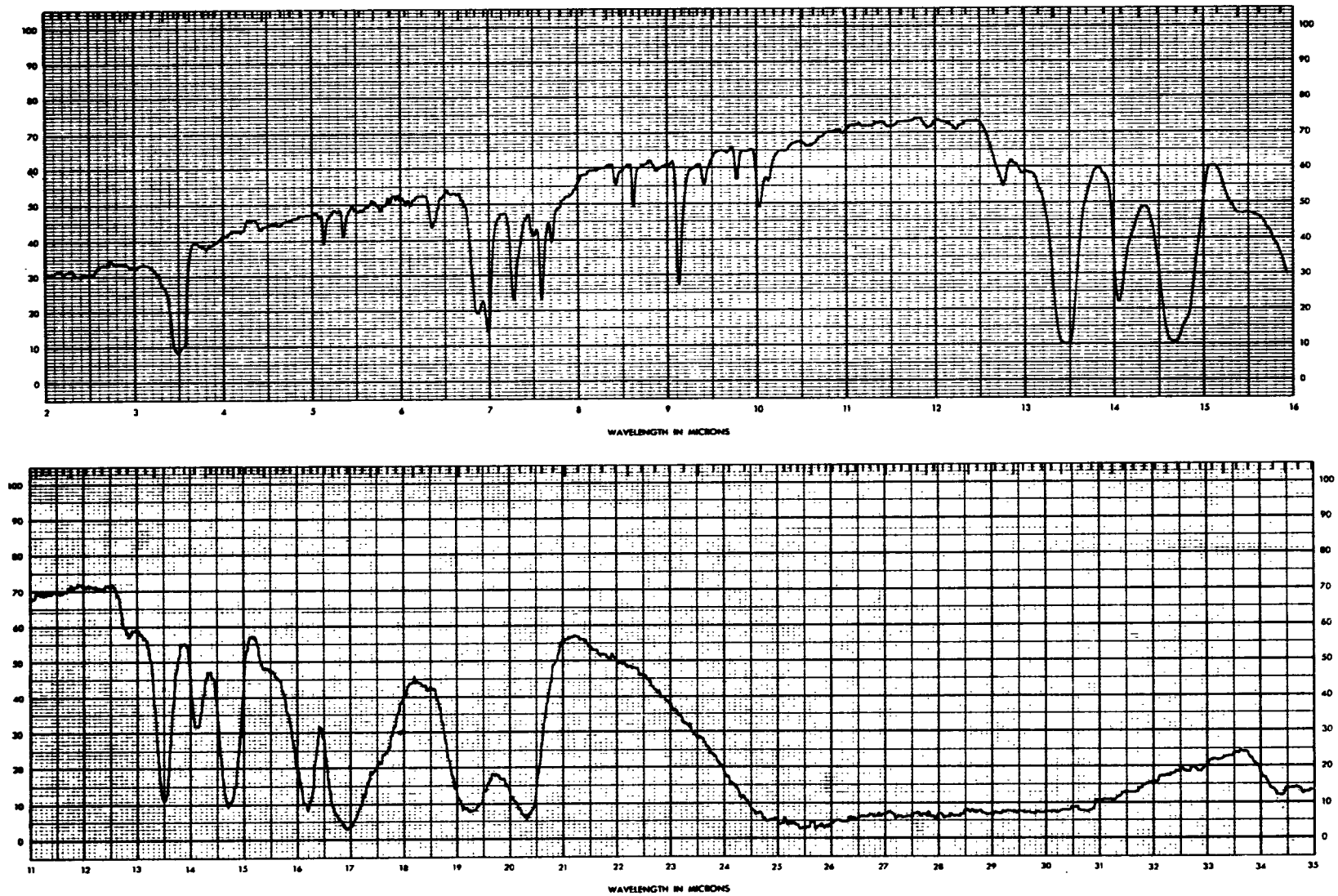

FIGURE 5. Infrared Spectra of $C_6H_5PCl_4$

POLYMERIZATION MECHANISM STUDIES

by

K. L. Paciorek and R. H. Kratzer

The study of the mechanism of phosphonitrile polymer formation via the reaction of organophosphinous halide with a metal azide was continued. To determine the existence of diphenylphosphinous azide, the reaction of diphenylphosphinous chloride with lithium azide in acetonitrile (at ca. -15°C) was reinvestigated. The decomposition of the reaction solution (filtered at ca. -20°C from the lithium salts) afforded 1.09 mole of nitrogen for each mole of phosphorus present in the filtrate. This value indicates that all the phosphorus present prior to the decomposition is in the form of diphenylphosphinous azide or its association product. Interestingly, 92% of the nitrogen was given off at room temperature, and the remainder only after heating at 90°C with triphenylphosphine. Later work has shown that this additional nitrogen is given off on heating above 100°C, even in the absence of triphenylphosphine. The analysis of the decomposition products showed the presence of chloride and azide ions. Since the combined molal quantity of these ions is equal to the moles of lithium, it is apparent that they were derived from lithium salts dissolved in the acetonitrile. This evidence confirms the absence of diphenylphosphinous chloride and shows that the reaction of diphenylphosphinous chloride and lithium azide proceeds to completion under the conditions selected.

To establish whether diphenylphosphinous azide existed in the form of a monomer ϕ_2PN_3 or as an associated moiety of a form such as shown by (I), the molecular weight was determined in butane by the technique of vapor pressure lowering.

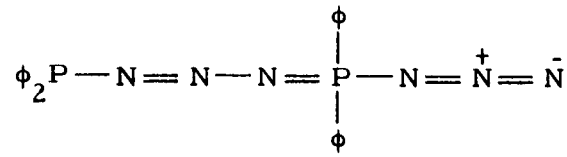

(I)

For the molecular weight determination and the elemental analysis, diphenylphosphinous azide was purified by recrystallization from pentane at -78°C; accordingly, this sample was completely free from lithium salts. The molecular weight found by this procedure was 278 (theoretical 227), which points to some association. The pure diphenylphosphinous azide, in the absence of solvent, decomposed sharply at 13.6-13.8°C and became bright yellow. At ca. 100°C additional nitrogen was evolved and the material turned white. The infrared spectrum of the decomposition product was typical of a phosphonitrilic system; the presence of

trimer was evident; and no absorption due to an azido moiety was observed.

To elucidate the type of products obtained from the room-temperature decomposition of diphenylphosphinous azide in acetonitrile, a larger-scale experiment was devised. The products were separated into acetonitrile-soluble and insoluble materials. Diphenylphosphonitrilic trimer (total yield, 25%) constituted the bulk of the insoluble fraction; the acetonitrile solubles (mol. wt., 1560) formed 57% of the total product. A small part of this substance (handled only in nitrogen atmosphere) was heated at 158°C for 2 hours and yielded 0.000286 mole of nitrogen. Based on the molecular weight of 1560, 0.000279 mole of the polymer was used. These values tend to indicate that the chains were azide terminated. After the heat treatment the molecular weight increased to 1950.

Attempts to purify another part of this substance by recrystallization from several solvents (outside the drybox) were unsuccessful. The material was soluble in benzene, except for 3.0% of the residue, which was shown to be a mixture of lithium chloride and lithium azide. The benzene-soluble fraction was subsequently treated with acetonitrile and ligroine. The product thus obtained had a molecular weight of 1450. The amount of nitrogen evolved at 185°C corresponded to only one-third of azido-terminated chains. The analytical figures agree relatively well with an assumption that the other two-thirds of the chains were oxygen terminated.

In addition to diphenylphosphonitrilic trimer, the acetonitrile-insoluble portion consisted of higher molecular weight material (above 2156), the elemental analysis of which was almost identical with that of the acetonitrile-soluble fraction.

It is noteworthy that the infrared spectra of the acetonitrile-soluble and insoluble portions (after removal of diphenylphosphonitrilic trimer) are almost identical, both exhibiting a weak band at 4.7 μ, most likely due to an azido moiety. Consequently, based mainly on the investigation of the acetonitrile-soluble portion, it can be safely deduced that the decomposition of diphenylphosphinous azide in a solvent such as acetonitrile in the absence of a chain-terminating agent yields at least 50% of azido-terminated polymers.

In a previous report[5] the decomposition of diphenylphosphinous azide in the presence of triphenylphosphine was described; however, the product was not examined adequately at that time. Subsequently, unreacted triphenylphosphine was removed from the phosphonitrilates.

[5]NAVWEPS Report 7237, Quarterly Report: Foundational Research Projects, July-September 1962, p. 49 (December 1962).

If the chains are assumed to be triphenylphosphine terminated, the quantity of combined triphenylphosphine corresponded to a molecular weight of 972; the molecular weight determined directly on the polymer was 785. The discrepancy in the molecular weights could be due to the presence of some ϕ_2PN material admixed with the recovered triphenylphosphine. The elemental analysis agrees fairly well with the compound of a structure $\phi_2P-N=P\phi_2-N=P\phi_2-N=P\phi_3$ (mol. wt. 860).

The model system program that had been initiated previously was continued. Reaction of the azide (II) with triphenylphosphine afforded the compound (III) in good yield.

$$\phi_2\overset{O}{\overset{\|}{P}}-(N=P\phi_2)_3N_3 + \phi_3P \longrightarrow \phi_2\overset{O}{\overset{\|}{P}}-(N=P\phi_2)_4\phi$$

(II) (III)

Also, from the chloride (IV) the phenoxy derivative (V) was obtained on treatment with sodium phenoxide.

$$\phi_2\overset{O}{\overset{\|}{P}}-(N=P\phi_2)_3Cl \xrightarrow{\phi OH + Na} \phi_2\overset{O}{\overset{\|}{P}}-(N=P\phi_2)_3O\phi$$

(IV) (V)

SPECTRAL INVESTIGATIONS

In several articles concerning phosphonitriles,[6,7,8] absorptions in the 7.4- to 8.3-μ region have been ascribed to vibrations associated with $-P=N-$ systems. The published data pertain mainly to cyclic compounds. The results of infrared spectral examinations of the compounds prepared for the model system program are compiled in Table 1, and the ultraviolet data are shown in Table 2.

It is clear from the tabulated values that the infrared absorptions of the $-P=N-$ moiety in the linear phosphonitrilic derivatives are well within the limits found for the cyclic compounds. The weak absorption exhibited by compound (VII) at 7.50 and 7.62 μ suggests that the

---

[6] L. W. Daasch and D. C. Smith, Anal. Chem., Vol. 23, p. 853 (1951).

[7] L. W. Daasch, J. Am. Chem. Soc., Vol. 76, p. 3403 (1954).

[8] L. G. Lund, N. L. Paddock, J. E. Proctor, and H. T. Searle, J. Chem. Soc., p. 2542 (1960).

TABLE 1. Infrared Absorption Spectra of Phosphonitrilic Derivatives and Related Compounds in the 7.4- to 9.0-μ and 10- to 11-μ Regions

Compound		Infrared Bands[a]	
Formula	Number		
ϕ_2POOH	VI	7.65 w	8.86 s
		8.40 s	8.94 s
		8.50 s	10.42 vs
		8.68 w	
$\phi_2P(O)-NH-P(O)\phi_2$	VII	7.50 w	8.90 s
		7.62 w	9.00 s
		8.42 m	10.80 m
$\phi_2P(O)-N=P\phi_3$	VIII	7.70 vs	
		8.58 vs	
		9.00 s	
$\phi_2P(O)-N=P\phi_2-NH-P(O)\phi_2$	IX	7.60 vw	8.90 s
		8.15 s	10.80 vw
		8.50 m	
$\phi_2P(O)-(N=P\phi_2)_2NH-P(O)\phi_2$	X	7.78 s	8.50 m
		7.90 s	8.95 s
		8.25 s	10.80 vw
$\phi_2P(O)-(N=P\phi_2)_3Cl$	IV	7.50 vw	8.40 s
		8.00 s	8.52 s
		8.25 s	8.92 s
$\phi_2P(O)-(N=P\phi_2)_4\phi$	III	7.78 s	8.50 m
		7.95 s	8.72 m
		8.15 s	8.97 s

[a]Code: w = weak; m = medium; s = strong; vs = very strong; vw = very weak.

TABLE 2. Ultraviolet Absorption Spectra of Phosphonitrilic Derivatives and Related Compounds for Wavelengths at Which Maxima Occurred

Compound		Maxima for wavelengths indicated (in mμ)			
Formula	Number	247	260	266	273
ϕ_2POOH [a]	VI	956	1142	1392	1179
$\phi_2P(O)-NH-P(O)\phi_2$	VII		1982	2479	1982
$\phi_2P(O)-N=P\phi_3$	VIII		2370	2140	1850
$\phi_2P(O)-N=P\phi_2-NH-P(O)\phi_2$	IX		2820	2996	2239
$\phi_2P(O)-(N=P\phi_2)_2NH-P(O)\phi_2$	X		4362	4117	2597
$\phi_2P(O)-(N=P\phi_2)_4\phi$ [b]	III			6337	3885
$(\phi_2PN)_3$ [c]	XI			1239	769

[a] This and other spectra in ethanol.

[b] In acetonitrile.

[c] In hexane.

TABLE 2. Ultraviolet Absorption Spectra of Phosphonitrilic Derivatives and Related Compounds for Wavelengths at Which Maxima Occurred

Compound		Maxima for wavelengths indicated (in mμ)			
Formula	Number	247	260	266	273
ϕ_2POOH [a]	VI	956	1142	1392	1179
$\phi_2P(O)-NH-P(O)\phi_2$	VII		1982	2479	1982
$\phi_2P(O)-N=P\phi_3$	VIII		2370	2140	1850
$\phi_2P(O)-N=P\phi_2-NH-P(O)\phi_2$	IX		2820	2996	2239
$\phi_2P(O)-(N=P\phi_2)_2NH-P(O)\phi_2$	X		4362	4117	2597
$\phi_2P(O)-(N=P\phi_2)_4\phi$ [b]	III			6337	3885
$(\phi_2PN)_3$ [c]	XI			1239	769

[a] This and other spectra in ethanol.

[b] In acetonitrile.

[c] In hexane.

material exists predominantly as $\phi_2P(=O)-NH-P(=O)\phi_2$ and not as a $\phi_2P(=O)-N=P(OH)\phi_2$ arrangement. This is further confirmed by the presence of a medium band at 10.80 μ, which is indicative of —P—NH—P— linkage.[9] Similar reasoning can be applied to compounds (IX) and (X).

Ultraviolet electronic spectra of cyclic phosphonitriles have been discussed by several authors.[8,10,11,12,13] The maxima for $(PNX_2)_n$ rings are found at very short wave lengths, their positions varying with the halogen substituent. On this basis Lund et al.[8] assigned them tentatively to an excitation of the unshared electrons on the exocyclic halogens. This theory was supported by Lakatos et al.[14]

According to Dewar et al.[12] the π-electrons of the phosphonitrilic system are localized in definite three-center π-bonds. This is an entirely different situation from that holding in organic aromatic systems where no transformation into localized equivalent orbitals is possible. Craig and Paddock,[15] in their consideration of the aromaticity of phosphonitriles, emphasize the participation of d-orbitals in π-bonds, though neither the three-center "islands" of conjugation around the ring nor the cyclic configuration have been positively established.

The maxima observed for the phenyl-substituted phosphonitrilic derivatives (see Table 2) cannot be attributed to a conjugated —P=N— system, since with chain lengthening the absorption should shift toward the visible region, and the increase in Σmax. should be much more pronounced. Thus these absorptions are most likely due to vibrational components of the electronic spectrum of phosphorus-substituted benzenes. It is noteworthy that the spectral pattern of diphenylphosphinic acid tends to confirm this hypothesis.

---

[9] E. Steger, Chem. Ber., Vol. 94, p. 266 (1961).

[10] H. J. Krause, Z. Elektrochem., Vol. 59, p. 1004 (1955).

[11] R. A. Shaw and F. B. G. Wells, Chem. & Ind., p. 1189 (1960).

[12] M. J. S. Dewar, E. A. C. Lucken, and M. A. Whitehead, J. Chem. Soc., p. 2423 (1960).

[13] R. Foster, L. Mayor, P. Warsop, and A. D. Walsh, Chem. & Ind., p. 1445 (1960).

[14] B. Lakatos, A. Hess, S. Holly, and S. Horvath, Naturwiss., Vol. 49, p. 493 (1962).

[15] D. P. Craig and N. L. Paddock, J. Chem. Soc., p. 4118 (1962).

EXPERIMENTAL

All experiments were carried out in an inert atmosphere, unless otherwise specified. Reagent-grade solvents and chemicals were used. Acetonitrile was refluxed over and distilled from phosphorus pentoxide. The molecular weights were determined in benzene by employing a Mechrolab vapor pressure osmometer.

Reaction of ϕ_2PCl with LiN_3 in Acetonitrile

Three sets of experiments were conducted to study the reaction of diphenylphosphinous chloride with lithium azide in acetonitrile. In each instance an excess of lithium azide was employed.

(1) The apparatus employed for the first experiment consisted of a 150-ml, 3-necked, round-bottomed flask. One of the necks served as connection to the vacuum line via an adapter; the second one was closed by a device for slow addition of solid dry lithium azide; and the third neck (bent horizontally) was equipped with a sintered glass disc and attached to a second 150-ml flask via a silicone-greased ground joint.

Into the flask, which contained a Teflon-coated stirring bar, was introduced freshly distilled diphenylphosphinous chloride (0.6699 g, 0.003036 mole); the system was then assembled and evacuated on the vacuum line. Subsequently, acetonitrile (50 ml, v.p. at 0°C, 25.4 mm) was distilled onto the diphenylphosphinous chloride at -78°C. Solution of diphenylphosphinous chloride was effected by warming the contents to room temperature, cooling the flask to -28°C, and slowly adding lithium azide (0.3 g, 0.00612 mole) over a period of 30 minutes. Stirring was continued for 11 hours, the solution being kept between -28 and -22°C. After the entire system was removed from the vacuum line and cooled to -25°C, filtration was accomplished by turning the system through 90 degrees and cooling the second flask to liquid nitrogen temperature. Dry nitrogen was admitted, and the flask containing the filtrate was removed from the rest of the apparatus and attached directly to the vacuum system, where the solution was allowed to warm to room temperature. The amount of nitrogen evolved was 2.3865 mmole. Subsequently, triphenylphosphine (0.3543 g, 0.0013507 mole) was added and the mixture heated at 82-92°C for 3 hours. An additional 0.1991 mmole of nitrogen was formed, bringing to 2.5856 mmole the total amount of nitrogen given off. The solid residue was analyzed for phosphorus and 3.7185 mmole was found. Since the amount obtained from triphenylphosphorus was 1.3507 mmole, the total phosphorus derived from the compound was 2.368 mmole. This gives the ratio of nitrogen to phosphorus formed in the thermal decomposition as 2.586:2.368 or 1.09:1.

(2) The apparatus employed for the second experiment consisted of a 150-ml flask equipped with a horizontal sidearm with a sealed-in sintered glass disc, and a ground joint which permitted the attachment of another similar flask.

In the first flask, 1.24 g of finely powdered lithium azide was suspended in 25 ml of acetonitrile. To this vigorously stirred mixture was added diphenylphosphinous chloride (1.229 g) in 10 ml of acetonitrile over a period of 45 minutes. A mercury valve protected the system from the atmosphere. The stirring was continued for 7 hours at -18 to -14°C, during which period no pressure change could be observed. After the connection to the mercury valve was sealed, the system was attached to the vacuum line and evacuated, and the acetonitrile was removed completely at -18°C. Then 55 ml of n-pentane (v. p. at 0°C, 185.0 mm) was distilled onto the residue, the system warmed to -20°C for 1 hour, and the solution filtered into the second 150-ml flask. There the product, diphenylphosphinous azide, was crystallized from the solution by cooling to -78°C and the mother liquor was filtered off. The solid, colorless residue left in the flask formed a clear, colorless solution at -20°C when 60 ml of fresh pentane (same purity as above) was distilled onto it.

A 22.5-ml portion of this solution was filtered into a long-necked, 100-ml flask, the solvent removed completely, and the flask warmed slowly from -15°C in a clear-sight Dewar vessel. The colorless solid became slightly wet at 13.5°C, and between 13.6 and 13.8°C it changed to deep yellow with a simultaneous gas evolution. (The temperatures were measured with a calibrated mercury thermometer.) After the contents of the flask was heated for 2 hours to 170°C (during which treatment the material remained solid), the pressure in the system had increased 25% over the pressure measured before heating. The total amount of nitrogen evolved was 0.62513 mmole, the identity of which was checked by a mass spectra of the collected gas which showed only the presence of masses 14, 28, and 29. Analysis of the residue, which consisted of more than 100 mg of substance, gave the following composition:

Anal. Calcd. for $(\phi_2PN)_x$: P, 15.55; N, 7.03

Found: P, 14.63; N, 6.89; Cl^-, 0.07; N_3^-, <0.1

The analysis showed that no materials containing Cl^- or N_3^- were present, and that the ratio of P:N in the material after heating was 1:1.042.

About a 3.2-ml portion of the same solution as that used for the above analysis was transferred, by filtration at -20°C, into an apparatus for determining molecular weights by vapor pressure lowering of a

solvent. The n-pentane was removed completely from the solution at -15°C, a measured amount of butane (v. p. at 0°C, 781.0 mm) was distilled onto it, and the pressure difference between solution and solvent was measured at 0°C with a cathetometer on a mercury differential manometer. From this value the presence of 0.05274 mmole of substance was calculated.

After removal of the solvent, the material was decomposed thermally as described above; it yielded 0.06404 mmole of nitrogen, the purity of which was checked by mass spectral analysis. The ratio of nitrogen evolved to mmole substance present is therefore 6.404:5.274 or 1.214:1, implying a molecular weight of 275.9 (calcd. for ϕ_2PN_3, 227.21).

(3) The apparatus used for this experiment was the same as that described for the previous experiment, the only difference being that the sidearm was connected directly to a mercury valve, not to another flask. To the stirred acetonitrile solution (50 ml) containing lithium azide (4.0 g, 0.0817 mole) was added diphenylphosphinous chloride (7.374 g 0.05342 mole) in acetonitrile (20 ml) at -20°C over a period of 45 minutes. Subsequently the mixture was stirred for 9 hours at -20 to -15°C. During this time the solution turned slightly yellow, indicating slight decomposition. At the conclusion of the reaction the outlet, which was previously connected to the mercury valve, was attached to a 200-ml, round-bottomed flask containing a magnetic stirring bar. The system was then cooled in dry ice and evacuated. The contents of the reaction flask was warmed to -20°C and filtration via the sintered glass disc was accomplished by applying a slight nitrogen pressure. The flask containing the filtrate was then attached to the mercury valve and stirred initially at 0°C (for ca. 2 hours), then overnight at room temperature. During that time the stirring stopped because of the formed precipitate. The acetonitrile-insoluble material, 1.752 g, was filtered off in the drybox. A 1.164-g portion of this material was continuously extracted with ligroine (b. p. 65-75°C), by means of a Soxhlet extractor, for 6 days, and 0.560 g of trimer was obtained. Thus the total amount of trimer in the insoluble portion was 0.843 g. Only a small part (0.083 g) of the residue left in the Soxhlet container was benzene soluble; the molecular weight of this portion was 2156.

Anal. Found: C, 70.64; H, 5.83; Cl, 0; N, 7.35; P, 14.27

The acetonitrile filtrate, on removal of acetonitrile (on the vacuum line), yielded 2.313 g of yellow residue (mol. wt., 1560). This material exhibited an absorption at 4.7 μ indicative of azido moiety. A 0.4358-g portion of the material was heated in vacuo for 2 hours at 158°C, and 0.000286 mmole of nitrogen was obtained. The molecular weight of the heat-treated substance was 1950. When the bulk of the material (1.520 g) was removed from the drybox and dissolved in benzene (25 ml), only 0.047 g failed to dissolve. This portion was shown to consist of lithium

azide and lithium chloride. Benzene was then removed from the filtrate and the precipitate was treated with ca. 10 ml of acetonitrile; 0.3256 g of precipitate resulted. This material was then continuously extracted with ligroine (b.p. 65-75°C) over a period of 14 days, yielding 0.127 g of phosphonitrilic trimer. Thus the total amount of trimer obtained was 1.033 g, or 25% of reaction products.

A 0.422-g portion of the acetonitrile-soluble fraction was boiled repeatedly with ligroine, but the material appeared to be completely ligroine-insoluble.

Anal. Found: C, 71.0; H, 5.09; P, 14.55; N, 7.51; O, 1.0; mol. wt. 1450

The ligroine-treated sample (0.1457 g, 0.0001 mole), after being heated under vacuum at 185°C for 3 hours, gave 0.00003053 mole of nitrogen. Addition of triphenylphosphine followed by 48 hours of heating at 90°C failed to afford more nitrogen. Since only one-third of the chains appeared to be azide terminated (after removal of the sample from the drybox), it seemed likely that this was due to hydrolysis of the other two-thirds of the sample.

Anal. Calcd. for a mixture of 1/3 $\phi_2P-(N=P\phi_2)_5-N=\overset{N_3}{\underset{|}{P}}\phi_2$

and 2/3 $\phi_2P-(N=P\phi_2)_5-NH\overset{O}{\underset{\|}{P}}\phi_2$: C, 71.82; H, 5.07; N, 6.87; P, 15.43; O, 0.8

Treatment of ϕ_2PN_3 with ϕ_3P

Into a 3-necked flask equipped with a magnetic stirrer, reflux condenser, gas inlet, and a solid addition device were introduced acetonitrile (25 ml) and diphenylphosphinous chloride (1.843 g, 0.00836 mole). To the stirred solution of diphenylphosphinous chloride in acetonitrile, which had been cooled to -25°C, was added finely ground lithium azide (0.6 g, 0.0123 mole) over a period of 30 minutes. The mixture was stirred for an additional $5\frac{1}{2}$ hours at -20 to -25°C, and then filtered under nitrogen atmosphere through a thimble into an evacuated flask into which were previously introduced a magnetic stirring bar and a solution of triphenylphosphine (3.2 g, 0.0122 mole) in acetonitrile (40 ml). The temperature of the triphenylphosphine solution was about -25°C, whereas the diphenylphosphinous azide solution prior to filtration was -35 to -40°C. Combination of the two solutions resulted in yellow discoloration and precipitation of a white solid. Subsequently, nitrogen was allowed into the system (to bring it to atmospheric pressure), the outlet was connected to a mercury bubbler, and the solution was stirred

at 0°C. The white precipitate, which was probably crystalline triphenylphosphine, started to dissolve slowly. Stirring was continued overnight. During this period all the solid dissolved and the solution was only slightly discolored. The failure of the infrared spectrum to exhibit any absorption in the vicinity of 4.6-4.8 μ pointed to the absence of an azide linkage. The presence of unreacted triphenylphosphine was also evident.

A 0.600-g sample of this material, heated in a sublimation apparatus at 75-80°C for 24 hours, yielded 0.256 g of triphenylphosphine. The sublimation residue was then refluxed several times with ligroine, and the ligroine filtrates afforded an additional 0.050 g of triphenylphosphine. Thus the ratio of diphenylphosphinic nitride to triphenylphosphine combined chemically (0.001029/0.0003393) is 3.2:1, giving a molecular weight of 972. The ligroine-insoluble residue (m.p. 57-61°C) is believed to be mainly $(\phi_2PN)_3P\phi_3$.

Anal. Calcd. for $(\phi_2PN)_3P\phi_3$: C, 75.43; H, 5.29; P, 14.40; N, 4.89; mol. wt. 860

Found: C, 73.06; H, 5.42; P, 14.08; N, 4.90; mol. wt. 785

Preparation of Compound (III)

To 1.05 g (0.00125 mole) of the azide in benzene (20 ml) was added triphenylphosphine (0.85 g, 0.00324 mole), and the resulting solution was refluxed overnight. The solvent and excess triphenylphosphine were removed by distillation and vacuum sublimation at 80°C. Crystallization from acetonitrile-ethanol of the residue that remained after sublimation of the reaction mixture gave compound (III) (m.p. 157-160°C).

Anal. Calcd. for $C_{66}H_{55}P_5N_4O$: C, 73.72; H, 5.16; P, 14.41; N, 5.21; O, 1.49; mol. wt. 1052

Found: C, 73.85; H, 5.36; P, 14.43; N, 5.39; O, 1.42; mol. wt. 1075 (in chloroform using Mechrolab osmometer)

Preparation of (V)

To xylene (30 ml) was added finely divided sodium (0.060 g, 0.00261 mole) followed by phenol (0.6 g, 0.00638 mole) and compound (IV) (2.10 g, 0.00252 mole). After the mixture was refluxed overnight the precipitate (sodium chloride) was filtered. The filtrate, after removal of solvent and excess phenol by distillation and vacuum sublimation at 120°C, yielded (V), which, after recrystallization from ether-heptane mixture, melted at 65-70°C.

Anal. Calcd. for $C_{54}H_{45}P_4N_3O_2$: C, 72.72; H, 5.09; P, 13.89; N, 4.71
Found: C, 71.67; H, 5.32; P, 13.23; N, 4.50

The infrared spectrum of (V) exhibited a band at 10.85 μ which indicated the presence of a phenoxy group attached to phosphorus.

INFRARED ATOMIC SPECTRA

THE FIRST SPECTRUM OF XENON IN THE 4-MICRON REGION AND ITS INTERPRETATION

by

C. J. Humphreys and E. Paul, Jr.

The material included here may be regarded as an extension of the corresponding section of the preceding quarterly issue of this report.[1] It is intended to supplement the previous discussion by considering the spectrum of xenon in the 4-micron region, which, although observed as of the earlier date, required further study for interpretation. For the essential features of the interpretation, the authors are greatly indebted to Robert D. Cowan of the University of California, Los Alamos Scientific Laboratory. Both this and the preceding report are to be regarded as preliminary to more detailed and rigorous treatment of the material. A tentative plan has been worked out between Dr. Cowan, Dr. Kenneth L. Andrew of Purdue University, and the senior author of this report for the preparation of two papers for journal publication. As described by Dr. Andrew, the first paper, to be written by Cowan and Andrew, would discuss the general background material that seems not to have been given in sufficient detail in the literature—for example, clarification of the pair-degeneracy approximation and the fact that it is distinct from $j\ell$ coupling (or, as Cowan prefers to call it, jK coupling) and could occur also in jj or LS coupling. In addition, it would include a derivation of selection rules for the $j\ell$-coupling case and some descriptive information concerning the code employed for the least-squares determination of the Slater parameters. The second paper, a joint one by the three authors, would apply the relations discussed in the first paper to the cases of neon, argon, krypton, and xenon, and would show how they were used to carry out the term analysis and how the parameters which are zero in the pair-degeneracy approximation account qualitatively for the features actually observed, particularly in the cases of Kr and Xe. The pair-coupling approximation, which was reported[1] to be satisfied in the instances of the energy levels originating in the p^5g configurations of Ne I, Ar I, and Kr I to within the limits of observational error, is formulated by a set of equations derived by Shortley

[1] C. J. Humphreys and E. Paul, Jr., NAVWEPS Report 8141, Quarterly Report: Foundational Research Projects, October-December 1962, pp. 29-46 (March 1963).

and Fried,[2] which express the energies in terms of only three of the Slater parameters, F_0, F_2, and p, whose significance was explained in the previous report. Examination of the experimental material from Xe I showed not only that the approximation was not satisfied for the $5p^5\,5g$ levels, but that even in the instance of $5p^5\,4f$ the distribution of the level pairs departed significantly from that required by the equations. It therefore became evident that more rigorous formulations would be required, retaining additional parameters.

Dr. Cowan[3] has kindly supplied the sets of equations that describe the distribution of the pairs and the pair splittings for the respective configurations noted above. These equations, which are quite general with an appropriate choice of element and total quantum numbers, are displayed as Tables 1 and 2. The equations listed in Table 1, giving the pair separations for the p^5f configuration in pure jK coupling, are obtained by differencing the equations in Table 1 of the previous report that describe levels converging to the $^2P_{3/2}$ limit, except for the terms in ζ_f, the spin-orbit interaction of the f-electron. In parentheses are shown the j-value of the limiting term, and the intermediate quantum number K. The number following the parentheses is the J-value of the lowest member of the degenerate pair, or in the usual notation we have $(j_1\,K)J$. Neglecting the small terms in ζ_f, the separations should be in the ratio 7:8:7. Whereas this is very nearly true for the 4f levels of Ne I, Ar I, and Kr I, it is rather poorly satisfied for Xe I. It is apparent therefore that ζ_f is not negligible in the instance of the latter spectrum. Cowan has contributed the following qualitative explanation: A 4f wave function lies pretty well outside the $3s^23p^5$ core of Ar I or even the $4s^24p^5$ core of Kr I, but can be expected to be appreciably perturbed by the $5s^25p^5$ core of Xe; that is, correlation effects can be expected to be so strong for Xe that the one-electron wave function approximation in the Slater theory can be expected to be rather poor. This explanation is consistent with the fact that the 7:8:7 ratio holds successively better for the 5f, 6f, 7f, and 8f levels of Xe I.

The pair splittings for the p^5f levels involving the two exchange integrals G_2 and G_4 as well as ζ_f are shown in Table 1b. G_2 is expected to be larger than G_4. Of the observed splittings, that for K = 3/2 is the largest; the others, in descending order corresponding to K, 5/2, 9/2, and 7/2. This is of course obvious qualitatively on the basis of the magnitudes of the coefficients and algebraic signs in the appropriate equations. It turns out, however, that the value of ζ_f required to explain the large splitting of the K = 3/2 pair and the somewhat smaller splitting

---

[2] G. H. Shortley and B. Fried, Phys. Rev., Vol. 54, p. 749 (1938).

[3] R. D. Cowan, private communication.

TABLE 1. Pair Separations (a) and Pair Splittings (b) of p^5f Levels in Pure jK Coupling

$\left(\frac{3}{2}\ \frac{9}{2}\right)5 - \left(\frac{3}{2}\ \frac{3}{2}\right)1 = 7F_2 + 3.5\zeta_f$	
$\left(\frac{3}{2}\ \frac{5}{2}\right)3 - \left(\frac{3}{2}\ \frac{9}{2}\right)5 = 8F_2 - 0.29\zeta_f$	(a)
$\left(\frac{3}{2}\ \frac{7}{2}\right)3 - \left(\frac{3}{2}\ \frac{5}{2}\right)3 = 7F_2 - 2.9\zeta_f$	
$\left(\frac{3}{2}\ \frac{3}{2}\right)2\text{-}1 = 50.4G_2 + 3.2\zeta_f$	
$\left(\frac{3}{2}\ \frac{9}{2}\right)4\text{-}5 = 31.1G_4 - 3.3\zeta_f$	
$\left(\frac{3}{2}\ \frac{5}{2}\right)2\text{-}3 = 33.6G_2 - 2.9\zeta_f$	(b)
$\left(\frac{3}{2}\ \frac{7}{2}\right)4\text{-}3 = 6.2G_4 + 3.0\zeta_f$	

TABLE 2. Pair Separations (a) and Pair Splittings (b) of p^5g Levels in Pure jK Coupling

$\left(\frac{3}{2}\ \frac{11}{2}\right)6 - \left(\frac{3}{2}\ \frac{5}{2}\right)2 = 27F_2 + 4.5\zeta_g$	
$\left(\frac{3}{2}\ \frac{7}{2}\right)4 - \left(\frac{3}{2}\ \frac{11}{2}\right)6 = 50F_2 - 0.22\zeta_g$	(a)
$\left(\frac{3}{2}\ \frac{9}{2}\right)4 - \left(\frac{3}{2}\ \frac{7}{2}\right)4 = 27F_2 - 4.06\zeta_g$	
$\left(\frac{3}{2}\ \frac{5}{2}\right)3\text{-}2 = 30.9G_3 + 4.3\zeta_g$	
$\left(\frac{3}{2}\ \frac{11}{2}\right)5\text{-}6 = 49.1G_5 - 4.4\zeta_g$	
$\left(\frac{3}{2}\ \frac{7}{2}\right)3\text{-}4 = 17.1G_3 - 4.1\zeta_g$	(b)
$\left(\frac{3}{2}\ \frac{9}{2}\right)5\text{-}4 = 10.9G_5 - 4.1\zeta_g$	

of the K = 5/2 pair is inconsistent with the observed extremely small splitting of the K = 7/2 pair.

The similar sets of equations for p^5g in pure jK coupling that describe the pair separations and the splitting of the pairs are listed in Table 2a and 2b. These have the same general form as those of Table 1a and 1b but with different coefficients for the parameters. The large splitting of the 3,2 pair (K = 5/2) is explainable as before through the additive effects of G_3 and ζ_g. In accordance with the equations of Table 2a, the pair separations should be in the ratio 27:50:27. The actually observed separations are 6, 13, and 23 cm^{-1} when one reckons with the lowest members of the respective pairs.

Figure 1 is a reproduction of a record chart showing the observed transitions belonging to the 4f-5g array. This should be compared with Figure 3 of the previous report which correlates the features of the spectra of the various noble gases associated with the transitions of the class 4f-5g. Some of these features have already been noted: (1) the same relative positions of transitions described by the same K and j-values, and (2) the shift of position of the arrays to shorter wavelengths with increasing atomic number, resulting from augmented influence of the atom core and, consequently, the large quantum defect.

The array of observed wave numbers of the 4f-5g combinations in Xe I is shown as Table 2a and includes the derived values of the 5g energy levels. The identifications are based solely on the appearance of the splittings of the 4f pairs as double transitions. Although the array superficially resembles the corresponding ones for the other rare gases, it could not be established on the basis of the pair-coupling approximation. Only in the instance of the 3,2 pair was the splitting of the 5g levels observable, amounting to 8.8 cm. This has already been mentioned. Regarding the other pairs, it cannot be decided on presently available experimental evidence whether the splittings are extremely small, masked by those of the 4f levels, or unobservable under conditions of the experiments.

The interpretation of the actual features will require further study. That is one of the reasons for planning additional publications. The computer code developed by Cowan and Andrew[4] for determining the Slater parameters which give the best fit between the calculated values, eigenvalues of the Hamiltonian matrix, and the experimental levels, has been utilized in a study of the 4f levels, with substantial verification of the qualitative theoretical discussion. In spite of somewhat poor energy-level fit, a comparison of eigenvectors computed on the basis of jK, SL,

[4] R. D. Cowan and K. L. Andrew. Program of Atomic Spectroscopy Symposium, Argonne National Laboratory, 7-9 June (1961).

① λ 38725.5 A, σ 2581.58 cm^{-1} — $4f[1\frac{1}{2}]_1 - 5g[2\frac{1}{2}]^\circ_2$

② λ 38737.7 A, σ 2580.76 cm^{-1} — $4f[1\frac{1}{2}]_2 - 5g[2\frac{1}{2}]^\circ_3$

③ λ 38869.1 A, σ 2572.04 cm^{-1} — $4f[1\frac{1}{2}]_2 - 5g[2\frac{1}{2}]^\circ_2$

④ λ 38939.74 A

⑤ λ 38950.4 A, σ 2566.67 cm^{-1} — $4f[4\frac{1}{2}]_5 - 5g[5\frac{1}{2}]^\circ_{5,6}$

⑥ λ 38963.0 A, σ 2565.84 cm^{-1} — $4f[4\frac{1}{2}]_4 - 5g[5\frac{1}{2}]^\circ_{5,6}$

⑦ λ 39199.0 A, σ 2550.39 cm^{-1} — $4f'[3\frac{1}{2}]_{3,4} - 5g'[4\frac{1}{2}]^\circ_{4,5}$; $4f'[2\frac{1}{2}]_{2,3} - 5g'[3\frac{1}{2}]^\circ_{3,4}$

⑧ λ 39472.9 A, σ 2532.69 cm^{-1} — $4f[2\frac{1}{2}]_3 - 5g[3\frac{1}{2}]^\circ_{3,4}$

⑨ λ 39518.5 A, σ 2529.77 cm^{-1} — $4f[2\frac{1}{2}]_2 - 5g[3\frac{1}{2}]^\circ_{3,4}$

⑩ λ 39691.8 A, σ 2518.76 cm^{-1} — $4f[3\frac{1}{2}]_{3,4} - 5g[4\frac{1}{2}]^\circ_{4,5}$

⑪ λ 39954.75 A

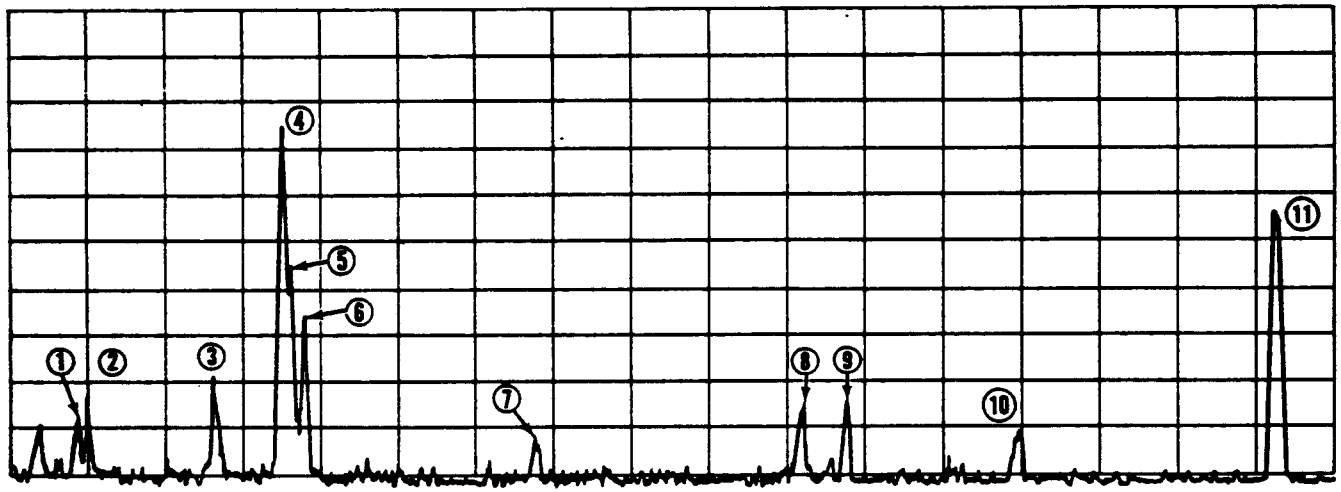

FIGURE 1. Section of a Recording of the First Spectrum of Xenon in the 4-Micron Region, with Identifications of the 4f-5g Transitions

and jj coupling, respectively, indicate that the first is realized to a closer approximation than the others. Cowan points out also that the calculated g-values are much closer to the pure coupling values, g_{kk} for jK, than for SL or jj coupling, and that the calculated values agree well with the experimental ones.

The 5g runs using the computer code led to similar conclusions, but no experimental g-values are known for these levels.

LASER PROGRAM

LASERS

by

R. L. Conger, J. H. Johnson,
L. T. Long, and J. A. Parks

DELAY IN LASER OUTPUT

The output of a ruby laser as a function of time has been observed by means of a phototube. Five hundred volts was applied to the phototube in series with a 93-ohm load resistor. (The tube can be coupled to 93-ohm transmission lines without having the response time deteriorate.) Figure 1 shows a picture of the oscilloscope trace of the output of the phototube with a laser input, taken at a time scale of 10 μsec/cm. At a voltage so low that the laser produces only a broad beam of red light, a series of spikes of about 1 μsec duration and spaced 2 or 3 μsec apart began to appear in the output of the phototube. The number of these spikes increased as the laser beam width decreased. The spikes were not of the same height nor were the spacings uniform. When the ruby was excited by two U-shaped xenon tubes placed beside it, the output of the xenon tubes appeared on the oscilloscope trace along with the output of the ruby, as shown in Figure 2. Here the time scale is 20 μsec/cm. The broad peak in Figure 2 is from the xenon tube, and the spikes are laser pulses. It was observed that the xenon light output had dropped to a very low level about 100 μsec before laser action started. In experiments with a large helical xenon tube, the output of the tube could not be seen on the same trace as the laser pulse, but separate observations of xenon tube output showed a similar delay in laser output.

BEAM-WIDTH MEASUREMENTS

To obtain laser beam-width measurements, a $2\frac{1}{2}$ inch by $\frac{1}{4}$-inch ruby rod was placed inside a large xenon tube helix powered by a 250-μf capacitor charged to 5000 volts. At a distance of 60 feet, the laser beam had spread to about 6 inches, indicating a beam width of about 0.5 degree. A small telescope was then placed in front of the ruby so that laser light entered the eyepiece of the telescope. The telescope was focused first at infinity and then adjusted to decrease the width of the laser beam.

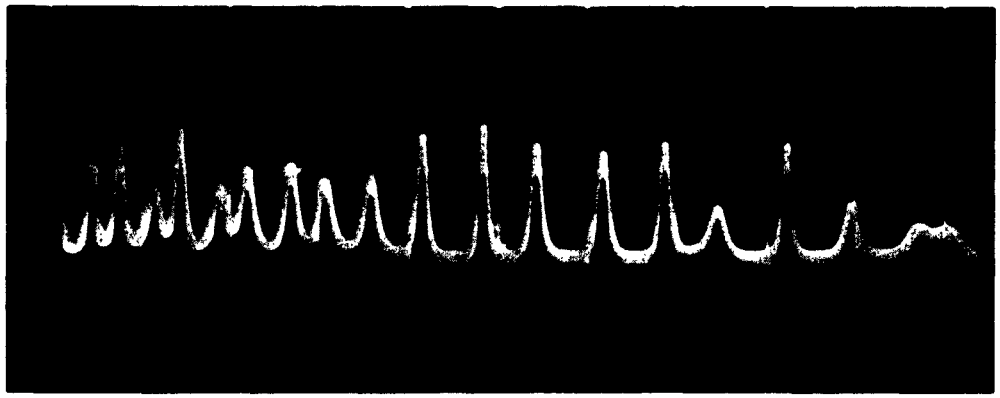

FIGURE 1. Laser Pulses

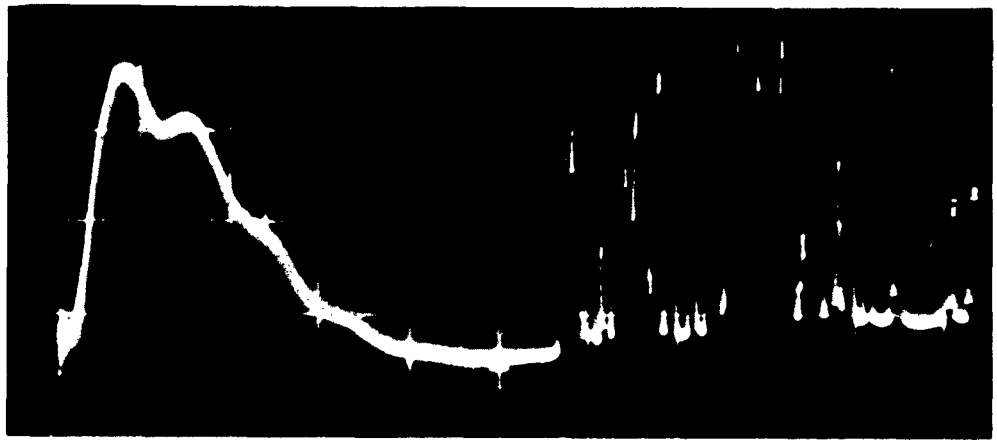

FIGURE 2. Delay in Laser Output

At a distance of 120 feet, the spot size was about 2 inches. This indicates an angular spread of about 0.07 degree. It is felt that the beam width probably could be reduced from 0.07 to about 0.02 degree if greater care were used in adjusting the apparatus.

LASER EFFICIENCY

A calorimeter was constructed by rolling 0.1 gram of blackened brass shim stock into a cone and welding a thermocouple to the point of the cone. The area of the open base of the cone was 0.71 cm^2. Because the heat capacity of brass is 0.09 calorie per gram, this calorimeter should experience a 27°C temperature rise per joule of energy absorbed. To check the calorimeter, it was placed 3 inches from the center of a No. 3 flash bulb, and heat-absorbing glass was put between the two items. Since the flash bulb is rated at 1.1×10^5 lumen seconds of light, the cone should receive 0.16 joule at this distance. According to the temperature rise indicated by the thermocouple, the energy received was 0.22 joule.

The calorimeter was then used for measuring the energy output of the ruby laser. When the ruby was cooled with cold nitrogen gas to -85°C, it produced about 0.04 joule of coherent light energy. Proof that the energy was actually coming from the laser beam was shown by the fact that in several cases the laser beam missed the calorimeter, and in these cases no reading was obtained.

A Dewar was constructed that could fit inside the xenon tube helix. The inside of the Dewar was filled with liquid nitrogen and the ruby was placed in the liquid nitrogen. It was found that the threshold of laser operation was reduced from 4000 volts to less than 3500 volts applied to the capacitor bank. Although the threshold had not changed much, efficiency was considerably increased. Each flash of the xenon tube caused boiling liquid nitrogen to spurt from the Dewar. A deflector with a glass window was placed in the beam to stop the liquid nitrogen from hitting the calorimeter, and energy measurements were repeated. The energy output was now 0.25 joule. Since the energy input was 2500 joules, the efficiency was only 0.01 of 1%.

Most of the energy losses can be accounted for in the following way. The xenon tube is about 2.5% efficient in converting electrical energy to light. About 10% of this light strikes the ruby and perhaps 20% of this amount is in the part of the spectrum where it is absorbed. Half the energy is dissipated non-radiatively in going from energy level 3 to energy level 2. From these factors, the maximum efficiency with this geometry would be about 0.02 of 1%. This still leaves a factor of 2

unaccounted for. This factor is probably caused by only certain portions of the ruby producing laser radiation, while all parts of it absorb energy.

When the ruby was placed inside a Dewar filled with liquid nitrogen and the Dewar was placed inside a helical xenon tube, optical coupling from the xenon tube to the ruby was only one-fifth as efficient as when the ruby was placed at one axis of an elliptic cylinder and a straight xenon tube placed along the other axis. This elliptic cylinder arrangement was found to work about as satisfactorily as a previous arrangement in which the xenon tubes were placed beside the ruby and the entire assembly was wrapped in aluminum foil. It has the advantage, however, of being more efficient for cooling the ruby. With the tighter optical coupling of the elliptic cylinder design, the over-all laser efficiency would be increased to 0.05 of 1%.

PYROTECHNIC LIGHT SOURCES

A test was made of pyrotechnic bombs as possible sources of pumping light for lasers. Since the pyrotechnic devices produce light only one-hundredth as intense as that of the xenon tube, these bombs cannot be used for pumping ruby rods, but they may be useful for other laser materials with lower thresholds.

A bomb was made with approximately one gram of a pyrotechnic mixture composed of 40% aluminum, 30% potassium perchlorate, and 30% barium nitrate. This is one of the brightest pyrotechnic compositions. The flash was observed by using the photomultiplier with Fresnel lenses to concentrate the light on it. Figure 3 is an oscilloscope trace of the output of the photomultiplier; the time scale is 10 msec/cm. The light intensity was only about one-fourth that of a No. 3 flash bulb, but the duration of the light pulse was about the same as that of the flash bulb—about 0.01 sec. Although there was considerable blast, the Fresnel lenses were not damaged. It was observed that the light output had an initial spike; the light intensity then dipped down and was followed by a second pulse of longer duration, as shown in Figure 3. The first

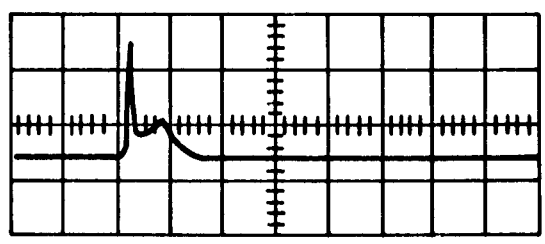

FIGURE 3. Light From Pyrotechnic Bomb

spike may be due to the explosion of the bomb and the second to the combustion of aluminum in oxygen in a large fire ball about 6 inches in diameter about the bomb. It appeared from this test that pyrotechnic bombs are of no merit in laser experiments, since they produce less light than flash bulbs and have the disadvantages of noise and smoke.

THE ELECTROREDUCTION OF SUBSTITUTED AROMATIC NITRO COMPOUNDS IN LIQUID AMMONIA SOLUTIONS

by

W. S. Harris

The preceding quarterly report presented data that showed the great difference in behavior when m-dinitrobenzene was electrochemically reduced in neutral liquid ammonia solutions and when it was reduced in acid liquid ammonia solutions. By using the method and apparatus described in previous reports, it was found that the low rate reduction of this compound uses 8 electrons in acid solution but only about 2 electrons in neutral solution. Because of the heavy weight of acids (ammonium salts in the ammonia system) that take part in and are necessary for the efficient utilization of materials such as m-dinitrobenzene, a severe weight penalty is placed upon their use in high power density batteries. It is therefore desirable to find materials that can operate in neutral solutions where NH_3 or H_2O can be the source of the hydrogen ions used in the reductions. The molecular weight of NH_3 or H_2O is two-ninths that of NH_4SCN, a commonly used source of H ions in acid ammonia solution.

Marked changes in the course of electroreduction of aromatic nitro compounds have been observed when various substituents have been placed on the aromatic ring. In acid solutions, the addition of the proper substituents to the aromatic ring has given more electrons and a more constant discharge voltage. Figure 1 illustrates this behavior for 1,3, 5-trinitrobenzenes and Figure 2 illustrates it for m-dinitrobenzenes. In neutral solutions, a similar effect may be noted. Figure 3 shows the reduction of nitrobenzene and a substituted nitrobenzene in neutral (NaSCN) solution. The effect of the substituent in this case is a great improvement in the voltage regulation, with resultant doubling of the "useful" capacity.

Research is continuing on the effect of the spatial relationships of different kinds of substituents upon the electroreduction of aromatic nitro compounds. It is hoped that one of the results of this research will be the discovery of nitrocompounds that will satisfactorily operate at high efficiencies in neutral ammonia solutions.

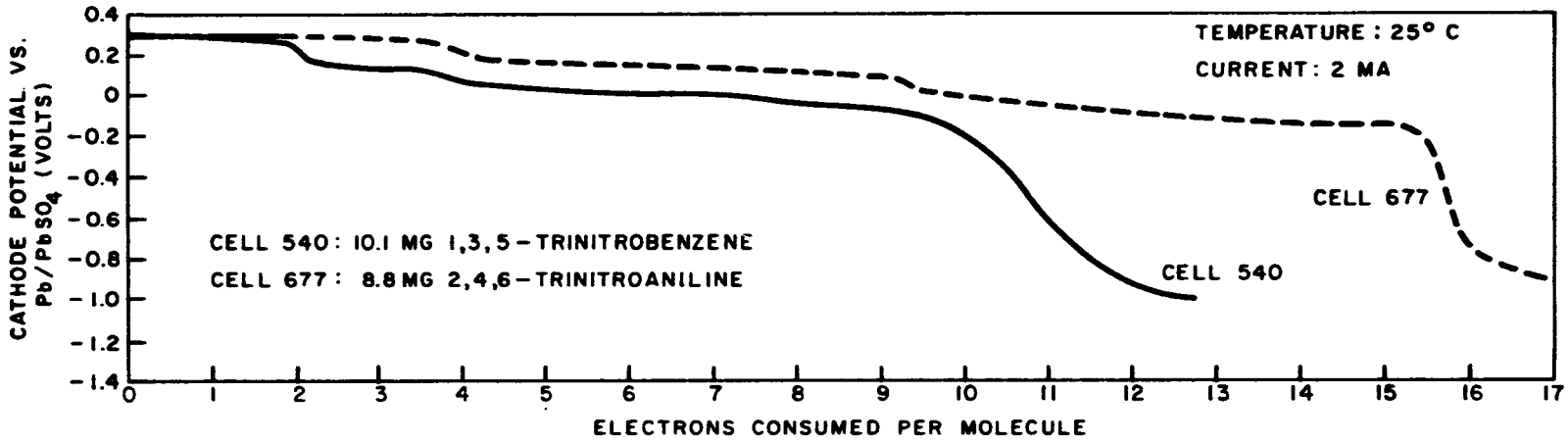

FIGURE 1. Low-Rate Reduction of 1, 3, 5-Trinitrobenzenes on Hg Cathode in NH_4SCN-NH_3

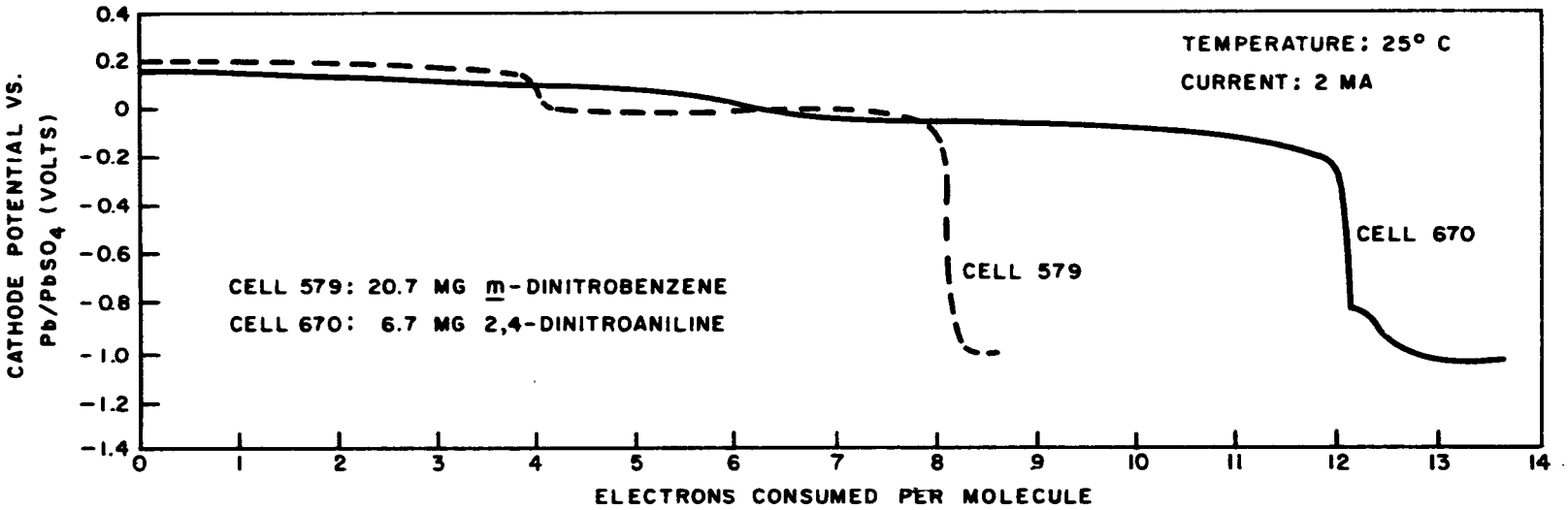

FIGURE 2. Low-Rate Reduction of m-Dinitrobenzenes on Hg Cathode in NH_4SCN-NH_3

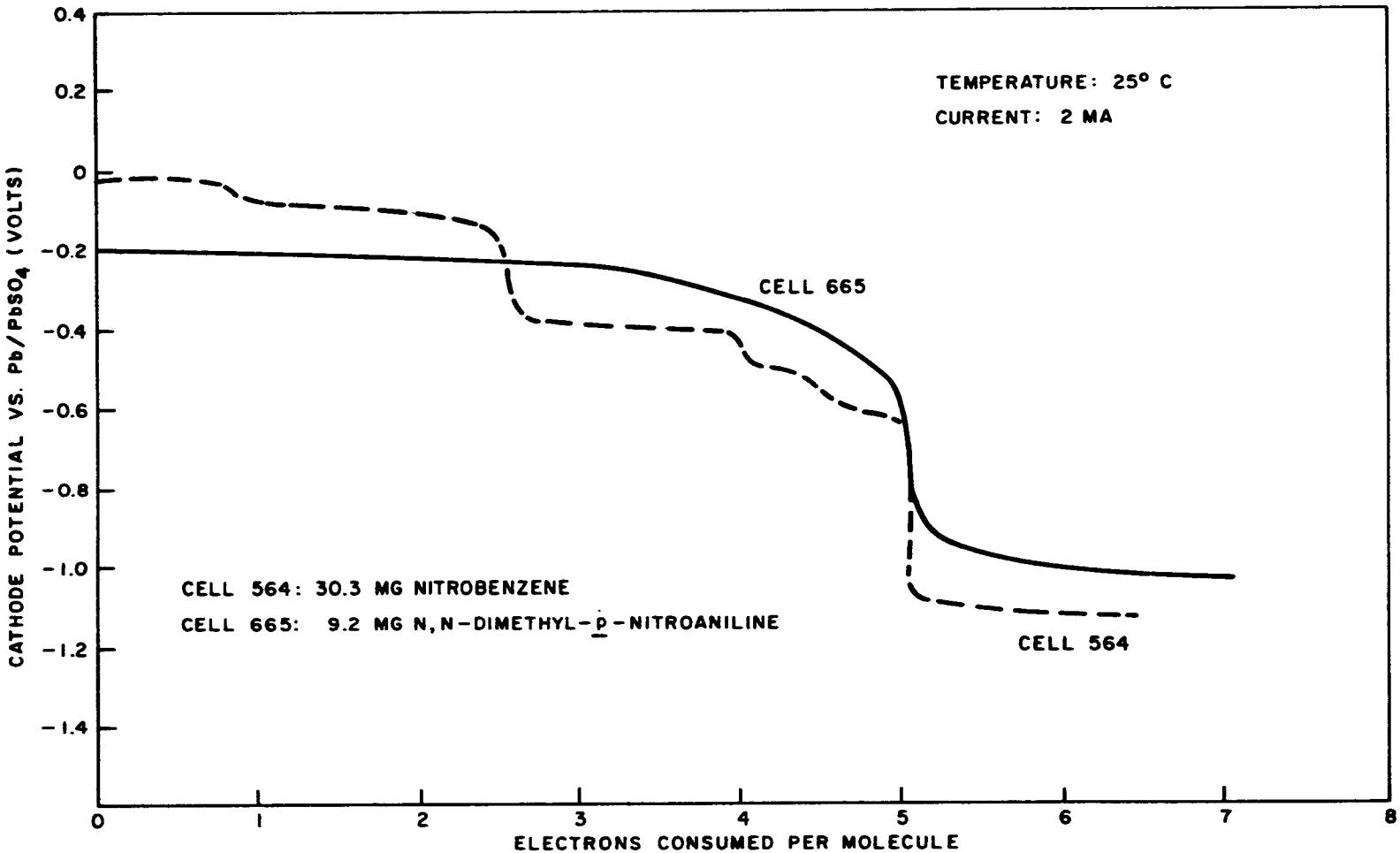

FIGURE 3. Low-Rate Reduction of Nitrobenzenes on Hg Cathode in $NaSCN-NH_3$

IONIC MELT ELECTROCHEMISTRY

by

R. E. Panzer

INTRODUCTION

Investigations in ionic melts during the past quarter have been based on salts or systems melting in the range of 120 to 180°C. Analysis of the first set (SED-1) of factorial-designed cells was completed, and three other sets (SED-2, 3, and 4) were set up, run, and analyzed. Very promising results have been obtained in this type of experimentation. Determination of the specific conductivity of various alkali thiocyanate systems has given new (unpublished) data.

EXPERIMENTAL METHODS AND RESULTS

The following tabulation shows the factors and levels used in set SED-1. Although previously given in an earlier report,[1] it is repeated here for convenient referral and because minor changes were made.

Alloy Anode	Cathode	Electrolyte	Temperature, °C	Resistive Load, ohms
Li-Ca	$CaCrO_4$	KSCN	200	40 (low)
Li-Mg	AgBr	KSCN-LiBr	250	10 (high)
Li-Zn	UO_3		300	

Changes from the original plan were the use of AgBr instead of AgCl, which interacted with LiBr in the electrolyte, and the raising of temperature levels to 200, 250, and 300°C. It will be noted that this design involves both qualitative and quantitative factors.

After the cell tests were conducted in the hardware cell apparatus previously described, an initial analysis of the results was made. In this analysis, ΔE_{FCCV}^{PCCV}, the change of emf from the peak closed circuit voltage to the final closed circuit voltage during a 5-minute period, was used as the dependent variable. The main effects and interactions due to the various treatment combinations were estimated by the method of

[1] NAVWEPS Report 7237, Quarterly Report: Foundational Research Projects, July-September 1962, pp. 70-79 (December 1962).

least squares. The significance of the results was determined by the analysis-of-variance technique. Because of an overshadowing of interactions caused by the load factor, some of these evaluations were not so conclusive as desired. (Since the same conditions existed in SED-2, later designs were modified to give better interaction evaluation.) An examination of the original evaluation showed that a cell starting at a low peak voltage could have a nearly flat discharge and hence a low ΔE. Although this would be a desirable criterion, the cell would not be particularly good in an over-all evaluation because of its generally low voltage. In view of this possibility, the data from SED-1 were subsequently reanalyzed, using the sum of PCCV and FCCV as the dependent variable. The main results of SED-1 are summarized briefly below.

(1) The KSCN-LiBr electrolyte gave better cell performance at low load, but KSCN was a far better electrolyte at high load.

(2) Of the alloy anodes, Li-Mg gave slightly better over-all performance, probably because it had a higher melting point (205°C) than Li-Ca (130°C) or Li-Zn (165°C).

(3) The best cell performance resulted from the combination of UO_3 in KSCN-LiBr with Li-Mg anodes at high load. It was consistently outstanding at the lower temperatures, but at 350°C the differences were leveled somewhat.

SED-2 had a different design than SED-1. It was a 2^5 design having 5 factors at 2 levels each; 16 cell tests were run of a possible 32 combinations.[2] The dependent variable was PCCV plus FCCV. The 2^5 design is particularly convenient for voltaic cell tests because the factors can be standardized for anode, electrolyte, and cathode, plus two other variables such as load, temperature, cathector, or a cell constituent. The following factors were tabulated for SED-2.

Electrolyte	Anode	Cathode	Load, ohms	Temperature, °C
KSCN-NaSCN eutectic	Li	H_4UO_6	40	150
KSCN-NaSCN + 10% NaCl	Li-Mg	Na-DNBA	10	200

The symbol Na-DNBA is an abbreviation of the formula for the sodium salt of 3, 5-dinitrobenzoic acid. The hydroxyperuranic acid (H_4UO_6)

[2] Fractional Factorial Experiment Designs for Factors at Two Levels, NBS Report AMS-48 (April 1957).

was prepared according to methods given by Katz and Rabinowitz.[3] The following statements summarize the results from SED-2.

(1) The electrolyte factor was significant at the 1% level of the F-test; the KSCN-NaSCN + 10% NaCl gave an average of 20% higher PCCV than the eutectic.

(2) Li-Mg gave slightly better cell performance than Li metal, but the difference was not significant.

(3) H_4UO_6 was slightly better than Na-DNBA, but neither gave a top-level cell performance, based on previous experience. The expected interaction cathode-temperature was significant at the 5% level, indicating that an operating temperature of 200°C results in better cells.

SED-3 was a half-fraction of a 2^5 design with the following factors and levels.

Electrolyte	Anode	Cathode	Absorbent	Temp., °C
KSCN-NaSCN eutectic	Li	H_4UO_6	Al_2O_3	150
KSCN-NaSCN + NaCl	Li-Mg	Na-DNBA	Kaolin	200

This design was nearly a duplicate of SED-2, but a constant resistive load of 25 ohms was used and anolyte absorbent was substituted for the load factor. It was not expected that the absorbent would prove a very significant factor. The following conclusions were derived from SED-3.

(1) Significant at the 1% level, the absorbent factor was closely analyzed. Kaolin was present in all but one of the cells producing the highest response (PCCV plus FCCV).

(2) The cathode factor, significant at the 5% level, disclosed on examination that Na-DNBA was superior to H_4UO_6 at all levels of electrolyte, anode, and temperature.

(3) Li metal performed best at 150°C but was equaled by Li-Mg at 200°C.

---

[3] J. L. Katz and E. Rabinowitz, The Chemistry of Uranium, National Nuclear Energy Series, Div. XII, Vol. 5, New York: McGraw-Hill, 1951.

SED-4 was a half-fraction of a 2^5 design with the following factors and levels.

Alloy Anode	Electrolyte	Cathode	Absorbent	Load, ohms
Li-Mg	KSCN-LiBr	UO_3	Al_2O_3	34
Li-Pb	KSCN-NaSCN	Na-DNBA	Kaolin	43

The Li-Pb alloy is the intermetallic compound Li_4Pb_7, and KSCN-LiBr has a 90-10 wt-% composition. From this series, the following conclusions were obtained.

(1) The electrolyte was nearly significant at the 1% level and very significant at the 5% level of the F-test. KSCN-NaSCN gave much better cell performance.

(2) Li-Mg alloy anodes gave much better performance than Li-Pb; the difference was significant at the 1% level.

(3) The UO_3 cathode operated far better than the Na-DNBA cathode; the difference was very significant, exceeding the 0.1% level.

(4) The load factor was nearly significant at the 5% level. This was the result of bringing the load levels close together; had there been a greater difference, the load would have had greater significance in the analysis.

(5) Significant at the 5% level, kaolin was superior to alumina.

The statistical design of cell experimentation has materially reduced the labor involved in screening a number of anode, cathode, and electrolyte materials. Furthermore, it has shown that kaolin is an excellent anolyte absorbent for thermal cells—a fact known from contractors' data at 450°C, but unknown at 200°C. From set SED-4, cell Li-Mg/KSCN-NaSCN-kaolin/UO_3-C-KSCN-NaSCN/Ni gave the following performance:

PCCV	2.59 volts
FCCV	2.01 volts
Peak current density	84 ma/cm^2
Final current density	65 ma/cm^2
Life to 80% PCCV	474 seconds
Temperature	200°C
Resistive load	34 ohms

This excellent level of performance has not been previously observed at 200°C, and it is hoped that even higher performance may be achieved through optimizing cell construction and operating conditions.

Prior to their use in the SED series of cells, the various electrolytes or mixtures had been screened for acceptable conductivity. The conductivity cell was described in NAVWEPS Report 7237.[1] In the temperature range observed (120-360°C), it was possible to use platinum black electrodes in the fused systems without deterioration to the gray form. These electrodes effectively reduced polarization phenomena on the electrodes and also reduced the error from frequency change to less than the experimental error from all other sources. The General Radio 1650A bridge, which was subsequently used for all conductivity measurements, has a built-in 1-kc oscillator. Original plans were to use a special diode circuit and to record resistivity versus temperature on an X-Y recorder. However, troubles with the recorder, plus the non-linearity of the resistance-diode circuit over the conductivity range studied, caused a return to hand recording.

The conductivities of the following electrolytes were determined or checked against known literature values: KSCN, KSCN-NH_4SCN (50-50 wt-%), and KSCN-NaSCN eutectic. The data for KSCN-NaSCN eutectic temperatures from 123.5°C (m.p.) to 360°C have not been previously reported. These data are plotted in Figure 4, where the logarithm of the specific conductivity $\times 10^3$ versus $1/T \times 10^4$ gives a curve that is essentially straight until the melting point of NaSCN is reached. With a further temperature drop, more curvature is observed. This behavior corresponds with that predicted by Delimarski and Markov[4] for ideal eutectic salt mixtures.

In addition to the data obtained from pure salts or eutectic melts, conductivity parameters were determined when various materials were combined with the melts. It was expected that the additives would enhance the conductivity of KSCN-NaSCN eutectic or of KSCN only. Measured quantities of water were introduced and the effects observed. Salts added to this eutectic were AgBr, NaI, NaCl, NaBr, KCl, LiCl, and LiSCN. The LiSCN was prepared at NOLC by dissolving stoichiometric amounts of LiOH and NH_4SCN in distilled water and then evaporating the mixture to dryness. Following long vacuum drying, the anhydrous LiSCN was obtained, as proven by an analysis for sulfur. The material is extremely hygroscopic, requiring drybox handling.

---

[4] I. U. K. Delimarski and B. F. Markov, Electrochemistry of Fused Salts, Sigma Press, 1961, translated by Adam Peiperly, National Bureau of Standards.

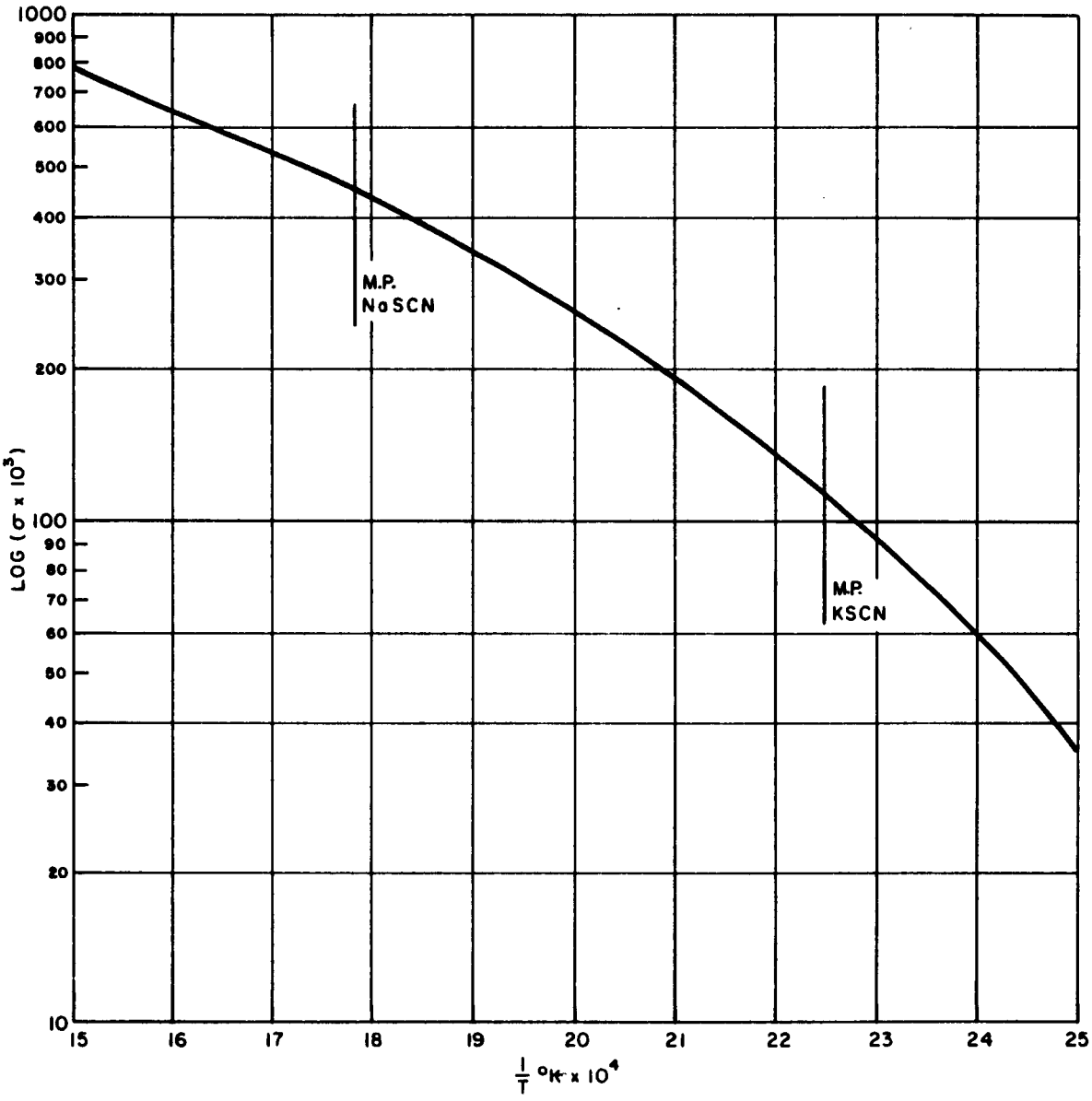

FIGURE 4. Specific Conductivity vs. Temperature (°K) for KSCN-NaSCN Eutectic

Results of all the conductivity tests with the above salts in KSCN-NaSCN eutectic indicated that no gross changes in conductivity could be obtained by such additions. In some cases the conductivity was even slightly lower at a given temperature with the added salt present. Sodium chloride seemed to cause a slightly increased conductivity, but there were other reasons for its subsequent use in KSCN-NaSCN for cell tests:

(1) The Cl^- ion tends to aid anodic depolarization.

(2) Na^+ has a much smaller charge-to-radius ratio than Li^+ ion. Because it does not so readily attract oppositely charged ions, its mobility is not reduced.

(3) Na^+ is a cation species common to one of the eutectic partners, NaSCN, and would be expected to be more mobile than a completely strange additive cation.

Addition of water to KSCN-NaSCN melts before and while melted would be expected to cause some hydrolysis and the formation of products such as HCN and H_2S. While evidence indicated such to be the case, hydrolysis was minimal, most of the water boiling out of the melt as it was heated. Typical specific conductivities at 232°C were: KSCN-NaSCN eutectic, 0.276 mho; KSCN-NaSCN eutectic + 10% water (mostly removed on heating), 0.369 mho.

When a slight amount of powdered sulfur was added to a fresh, clear KSCN-NaSCN eutectic melt at 175°C, the resulting melt was typically dark blue and retained a greenish-yellow tinge when solid. Although numerous investigators have reported this color phenomenon with heating above 300°C, this is the first time it has been reported as resulting from the addition of sulfur at a lower temperature.

The conductivity of KSCN-NaSCN-alumina pills was determined. Later, when cell tests showed that kaolin absorbent contributed to better cell performance, those anolyte pills, too, were checked for conductivity. In all cases the composition was 65% salt mixture, 35% absorbent, and the temperature was 200 ± 3°C. The specific conductivities were: KSCN-NaSCN-Al_2O_3, 0.0606 mho; KSCN-NaSCN-kaolin, 0.127 mho.

It is believed that the improved cell performance with kaolin is due to lesser ohmic polarization. Possibly the laminar structure of kaolin allows easier passage of the conducting ions than does alumina, which has an irregular shape that results in grossly lengthened path distance across the cell.

FUTURE PLANS

In the forthcoming quarter, the results from the previous statistically designed cells are to be applied to optimizing composition, conditions, and performance of ionic melt voltaic cells. New SED series are to be set up, run, and evaluated. The search for other electrolytes and nonaqueous ionizing solvents is continuing. It is hoped that the techniques of chronopotentiometry may be applied to pill cells, though the problems of concentration control and cell geometry still exist.

NARROW PULSE GENERATION BY NONLINEAR TRANSMISSION LINE METHODS

by

J. R. Alday

INTRODUCTION

It has been shown[1] that the electromagnetic analogy of mechanical shock waves can be generated electrically if an electromagnetic wave is propagated either in a nondispersive active medium or down a nondispersive nonlinear transmission line. By differentiation, this electromagnetic shock function can be transformed into pulses of very narrow duration.

This paper treats in some detail the most obvious properties that degrade the rise or decay time of the shock function in a lumped-element varactor-diode-loaded nonlinear transmisssion line of infinite length.

MECHANISM OF ELECTROMAGNETIC SHOCK-WAVE FORMATION

A propagating electromagnetic wave is transformed into an electromagnetic shock wave because the velocity of the wave is a function of the instantaneous magnitude of the wave. This transformation may be illustrated by the following example.

Consider the hypothetical case in which a pure sine function is applied to the input of a lossless varactor-loaded nonlinear transmission line of unbounded length. The phase velocity of a wave traveling down such a line is inversely proportional to the square root of its distributed capacity, which in turn is a function of the instantaneous voltage appearing across the capacitive admittance elements. Therefore, it can be stipulated that the positive peaks of the sine function will have higher or lower phase velocity (depending upon the orientation of the diodes) than the negative peaks. Since the line length is boundless and the line is

[1] R. Landauer, "Shock Waves in Nonlinear Transmission Lines and Their Effect on Parametric Amplification," IBM Journal, Vol. 4, p. 391 (1960).

lossless, there is a point along the line where the faster traveling peak will nearly coincide with the slower traveling peak to form a near singularity. From this point on the shock function is said to propagate.

Although the varactor example is used as an illustration here, there are certain ferroelectrics, ferrites, plasmas, magnetoplasmas, thermistors, bolometers, and conducting diodes that have nonlinear voltage, current, or power properties and can possibly be adapted for the formation of electromagnetic shock waves.

The topic of electromagnetic shock-wave formation along distributed nonlinear transmission lines has been treated in detail by other authors.[1,2]

DEGRADATION OF SHOCK FUNCTION RISE TIME

Even when the best examples are considered, there exist conditions that degrade or even prevent the formation of the shock function. Such conditions are primarily the result of dispersion due to the frequency-sensitivity of the elements, joule heating, and radiation losses of high order harmonics. The latter appears negligible in comparison to the others.

Consider first the properties that a nonlinear transmission line must exhibit to be ideally suited to the generation of narrow pulses. In order to achieve perfect pulses upon differentiation, the line must form the forcing function into a perfect sawtooth wave.

From Fourier's theorem, a perfect sawtooth function, neglecting the dc component, may be represented by

$$f(t) = \sum_{n=1}^{\infty} C_n(t) \sin [n\omega t + \delta_n(t)] \qquad (1)$$

where

$$n = 1, 2 \ldots$$

$$C_n(t) = \frac{1}{n\pi}$$

$$\delta_n(t) = 0$$

[2] R. B. Riley, Technical Report No. 1707-1, An Analysis of a Nonlinear Transmission Line, Stanford University, January 1961.

ω = forcing frequency

$$-\frac{2\pi}{\omega} \leq t \leq \frac{2\pi}{\omega}$$

It seems likely that the amplitudes and respective phases of the harmonics generated in the course of propagation down the line will be inconsistent with the conditions of equation (1). These inconsistencies will be shown to be the result of dispersion.

Dispersion can be treated by a small signal analysis using a distributed line approximation.

The differential equations describing the line are derived from the voltage and current drops in an infinitesimal section of infinite transmission line. These equations are then used to develop the one-dimensional wave equations for voltage and current from which the small signal propagation coefficient $\gamma = \alpha + i\beta$ is developed.

Given the TEM configuration shown in Figure 1, where Z is the series impedance and Y(V) is the voltage variable shunt admittance, the one-dimensional electric wave equation resulting from the application of a modified[3] transmission line theory is

$$\frac{\partial^2 V}{\partial z^2} = Z\frac{\partial}{\partial t}\left[Y(V)\frac{\partial V}{\partial t}\right] \qquad (2)$$

where Z is static (i.e., $\partial Z/\partial t = 0$) and Y(V) and V are arbitrary functions of z and t.

Equation (2) is essentially general except it does not include the possibility of the existence of higher order modes. No evidence of these modes has been experimentally encountered in a lumped TEM configuration; however, they may be present in a distributed line at microwave frequencies.[4,5]

---

[3] Previous unreported analysis.

[4] M. DiDomenico, Jr., Microwave Laboratory Report 960, The Microwave Characteristics and Applications of Ferroelectric Ceramics, Stanford University, October 1962.

[5] B. A. Auld, M. DiDomenico, Jr., and R. H. Panell, "Traveling-Wave Harmonic Generation Along Nonlinear Transmission Lines," J. Appl. Phys., Vol. 33, p. 3537 (1962).

An approximate solution of equation (2) for the case of a distributed line with voltage-variable capacitance and conductance admittance is obtained (from DiDomenico) by the use of perturbation theory.[4] Riley and Landauer use the method of characteristics to obtain solutions for distributed lines.

If the approximation

$$\frac{\partial Y(V)}{\partial t} \simeq 0$$

can be made, the linear wave equation may be used. In such a case the propagation coefficient is

$$\gamma = [ZY(V)]^{\frac{1}{2}} \tag{3}$$

Consider now the equivalent circuit of an incremental section of an infinite length lumped-element varactor-diode-loaded transmission line (Figure 2), where

R_r = radiation resistance

L = series inductance

R_L = series resistance

C_L = distributed capacity of L

G = leakage conductance

$C(V)$ = shunt voltage variable capacity

R_S = series diode resistance

L_S = series diode inductance

C_S = shunt leakage capacity

The discussion is somewhat simplified if it is assumed that the effects of some elements are negligible compared with the effects of others. These assumptions result in the approximations $R_r \simeq 0$, $G \simeq 0$, $L_S \simeq 0$, and $C_S \simeq 0$.

With reference to Figure 2 and the above approximations, the series impedance is

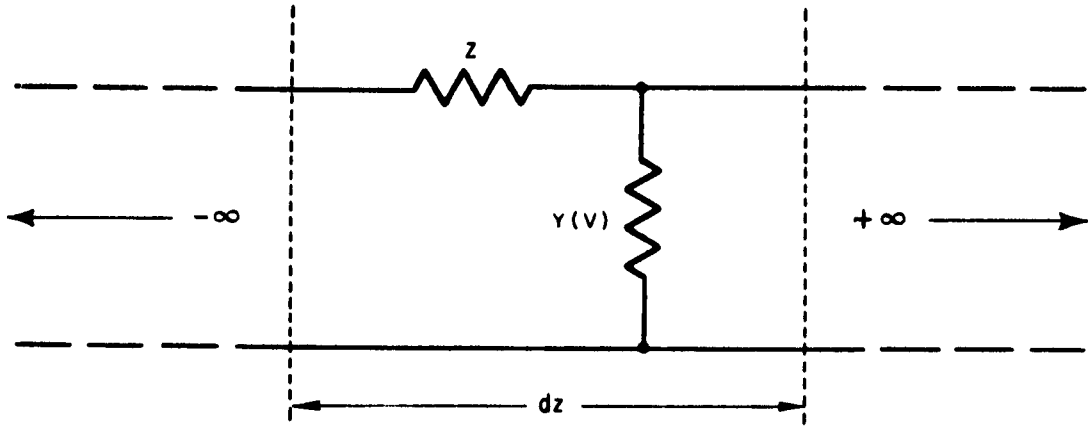

FIGURE 1. Infinitesimal Section of Line

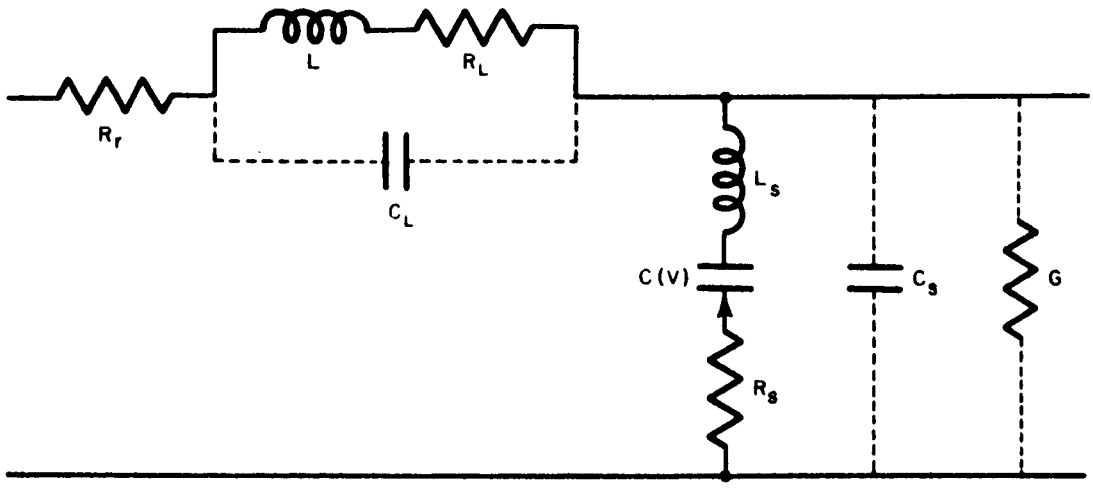

FIGURE 2. Equivalent Circuit

$$Z = \frac{R_L + i\omega\left[L\left(1 - \omega^2 L C_L\right) - C_L R_L\right]}{\left(1 - \omega^2 L C_L\right) + \omega^2 C_L^2 R_L^2} \tag{4}$$

The expression Q_L may be defined as the Q of the tank circuit L, R_L, C_L; and ω_L as its antiresonant frequency. Then, by proceeding algebraically,

$$Z = \omega L \Psi_z \exp(i\theta_z) \tag{5}$$

where

$$\Psi_z = \left[\frac{1 + Q_L}{\left(1 - \omega^2/\omega_L^2\right) + \omega^4/\omega_L^4}\right]^{\frac{1}{2}}$$

and

$$\theta_z = \tan^{-1}\left[\frac{\left(1 - \omega^2/\omega_L^2\right)Q_L^2 + \omega^2/\omega_L^2}{Q_L}\right]$$

Similarly, the shunt admittance is

$$Y(V) = \frac{R_S + i/\omega C(V)}{R_S^2 + 1/\omega^2 C(V)^2}$$

or

$$Y(V) = \omega C(V) \Psi_y \exp(i\theta_y)$$

where

$$\Psi_y = Q_c\left(1 + Q_c^2\right)^{-\frac{1}{2}}$$

Q_c = the Q of the varactor diode

$$\theta_y = \tan^{-1} Q_c$$

From the relationship $\gamma = \alpha + i\beta$, the following are obtained:

$$\alpha = \omega[L C(V)]^{\frac{1}{2}}\left(\Psi_z \Psi_y\right)^{\frac{1}{2}} \cos\theta \equiv \beta \cot\theta \tag{6}$$

and

$$\beta = \omega[LC(V)]^{\frac{1}{2}}\left(\psi_z \psi_y\right)^{\frac{1}{2}} \sin\theta = \alpha \tan\theta \tag{7}$$

where

$$\theta = \frac{\theta_z + \theta_y}{2}$$

The characteristic line impedance is given by

$$Z_o = \left[\frac{L}{C(V)}\right]^{\frac{1}{2}}\left(\frac{\psi_z}{\psi_y}\right)^{\frac{1}{2}} \exp(i\theta') \tag{8}$$

where

$$\theta' = \frac{\theta_z - \theta_y}{2}$$

The effect of joule heating upon the dispersion of the line can be shown graphically by considering a slight rearrangement of equation (5). This rearrangement consists of allowing Q_1 to represent the Q of the series inductance (L and R) evaluated at ω_L, and Q_2 to represent the Q of the shunt capacitance evaluated at ω_L. Also, let P be the ratio of the forcing frequency to the antiresonant frequency of L and C_L. With this arrangement the absorption factor can then be written as a function of these parameters. That is, from equation (7),

$$D(P) = \frac{\beta V_p}{\omega} = \left[\psi_z(Q_1, P)\, \psi_y(Q_2, P)\right]^{\frac{1}{2}} \sin\theta(Q_1, Q_2, P) \tag{9}$$

where V_p is the zero dispersion phase velocity.

A numerical value of unity for D(P) in equation (9) depicts a dispersionless transmission line. Figures 3, 4, and 5, which show D(P) as a function of P for various Q_1 and Q_2, illustrate the evolution of D(P) from a highly dispersive line to a relatively low dispersion line. As would be expected, D(P) is shown to approach the ideal case whenever the Q's are large.

Dispersion not due to joule heating, i.e., reflective dispersion, can be shown to exist by allowing Q_1 and Q_2 to approach infinity.

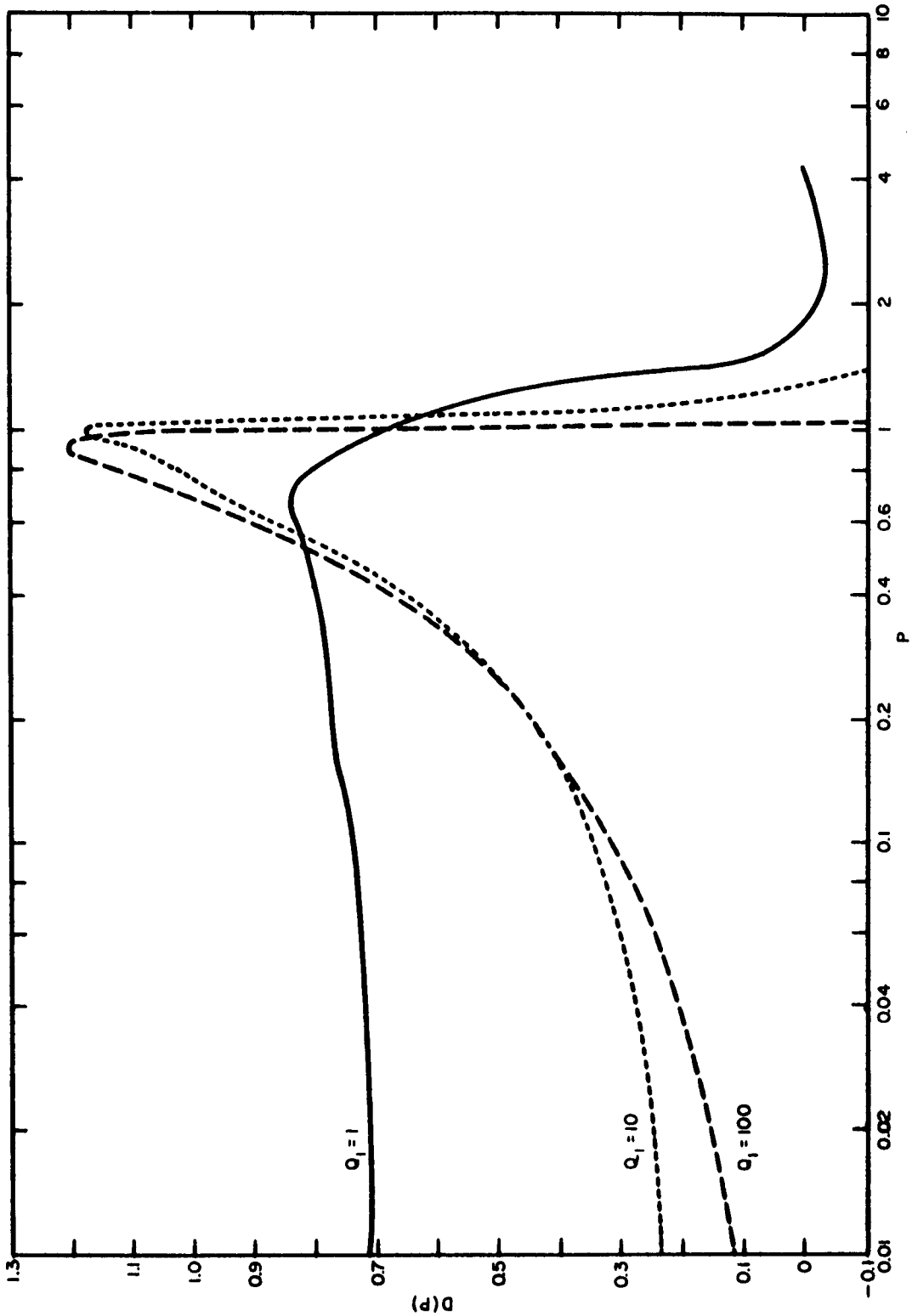

FIGURE 3. D(P) as a Function of P for $Q_2 = 1$

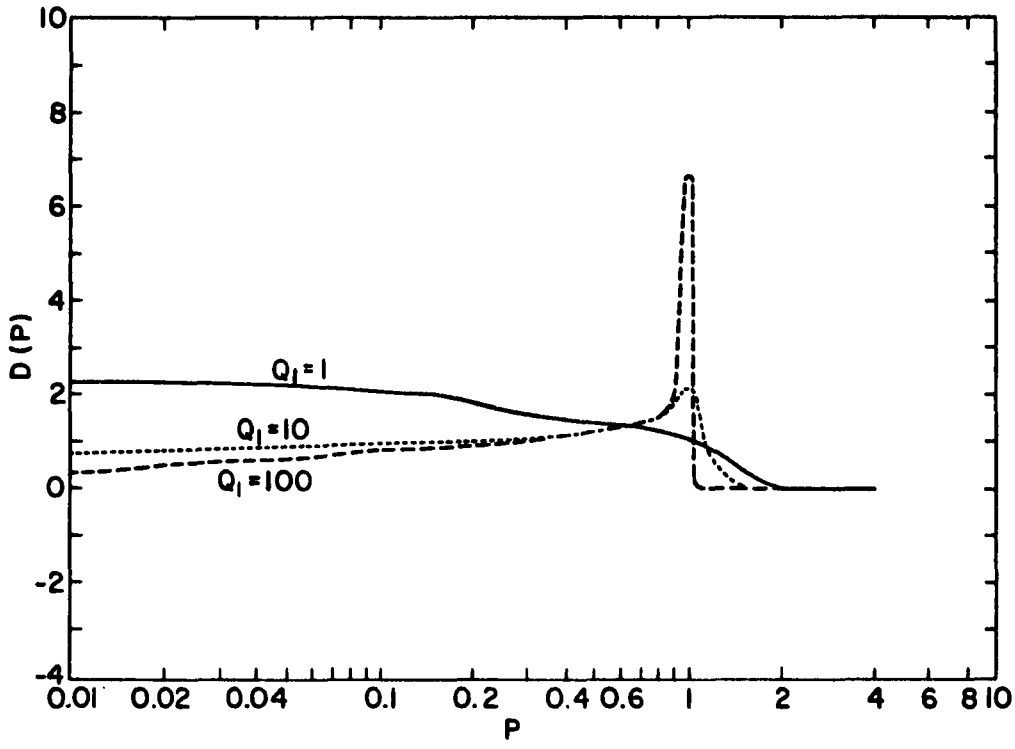

FIGURE 4. D(P) as a Function of P for Q_2 = 10

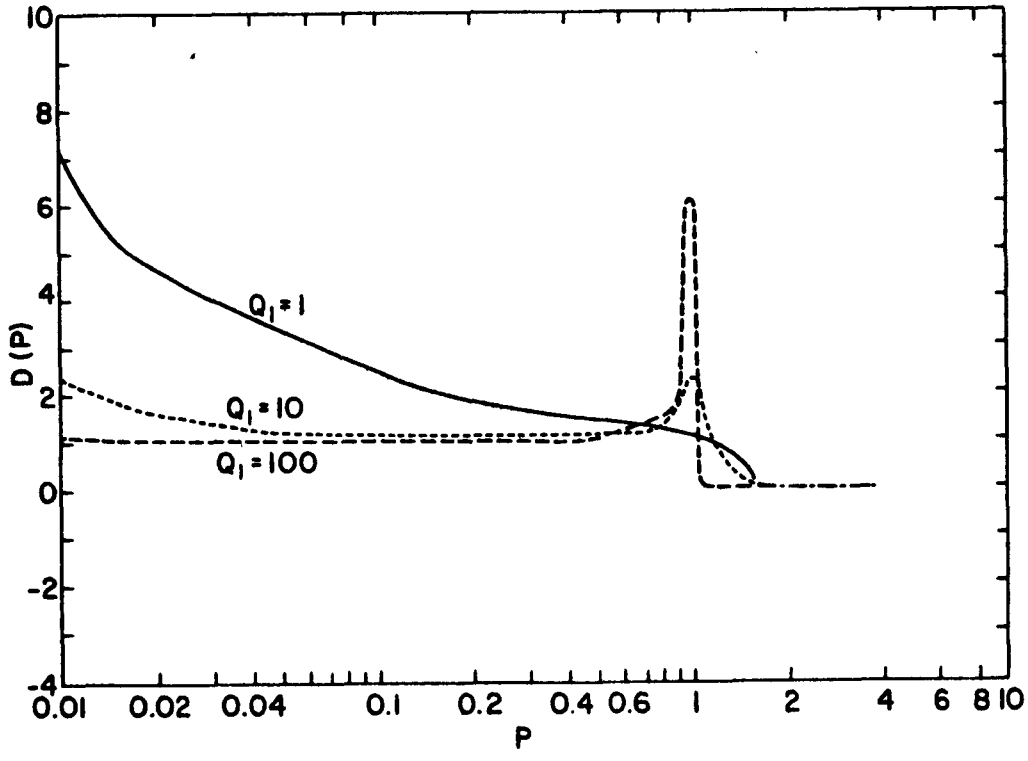

FIGURE 5. D(P) as a Function of P for Q_2 = 100

$$\lim_{Q_1, Q_2 \to \infty} D(P) = \begin{cases} (1 - P^2)^{-\frac{1}{2}} & P < 1 \\ 0 & P > 1 \\ \text{undetermined} & P = 1 \end{cases}$$

The example states, in effect, that there will always be an upper cutoff frequency in a lumped-element nonlinear line when it is operated in the dominant TEM mode. The elementary theory used here does not include the case of a possible mode-coupling to a higher order mode when $P \geq 1$.

The problem of impedance matching also depends upon the dispersive properties of a lumped-element nonlinear transmission line. A measure of the relative requirements of a proper matching can be speculated upon by considering the normalized characteristic impedance of the line as a function of P for various Q_1 and Q_2. From equation (8), the normalized characteristic line impedance is

$$\tilde{Z}_o = \left[\Psi_z(Q_1, P)/\Psi_y(Q_2, P)\right]^{\frac{1}{2}} \exp(i\theta')$$

Figures 6-11 show $\mathrm{Re}\,\tilde{Z}_o$ and $\mathrm{Im}\,\tilde{Z}_o$ as functions of P for various Q_1 and Q_2's. Again, the ideal case is approached as the element Q's are raised.

When the Q's are unlimited, the normalized characteristic impedance of the line is

$$\tilde{Z}_o = \begin{cases} (1 - P^2)^{-\frac{1}{2}} & P < 1 \\ \infty & P \geq 1 \end{cases}$$

This type of result would be expected since the line in the given configuration closely resembles that of a low pass filter.

EXPERIMENTS

An experimental diode-loaded transmission line was constructed as shown in the block diagram of Figure 12. This 155-section line uses Pacific Semiconductor V-15E Varicap diodes for shunt elements and 0.19-μh inductors (Q is 160 at 25 Mc) for series elements. After completion, the line was tested for narrow pulse generation capabilities. The results of these experiments are shown in the oscillographs in Figures 13, 14, 15, and 16, which depict the input, output, differentiated

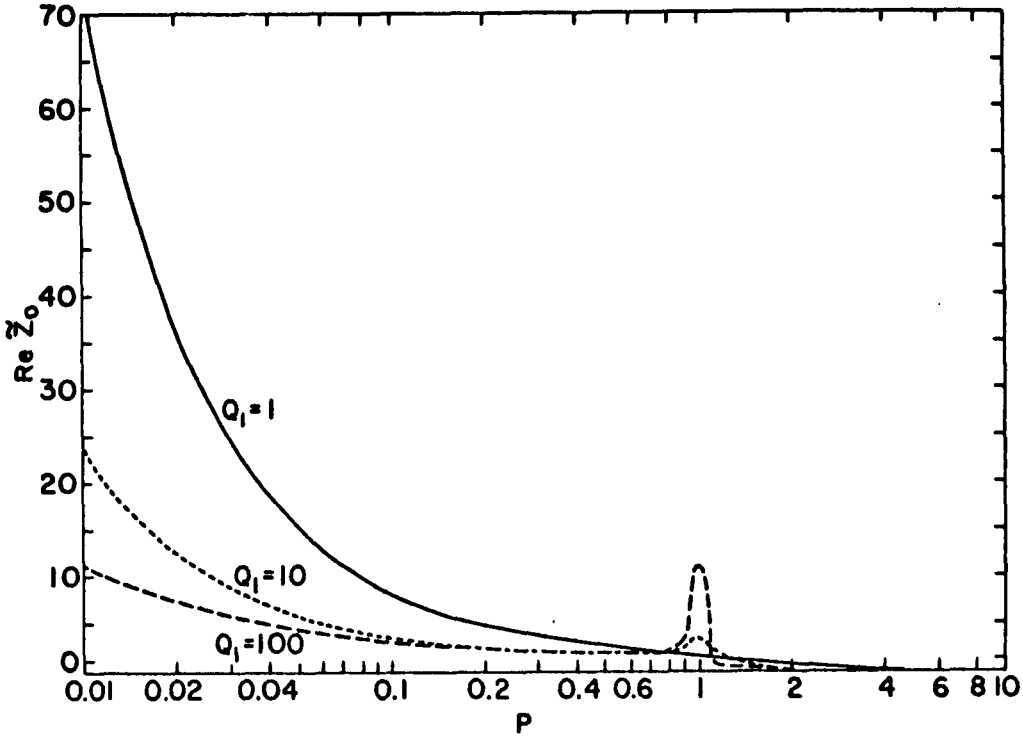

FIGURE 6. Re $\tilde{Z}_o$ as a Function of P for Q_2 = 1

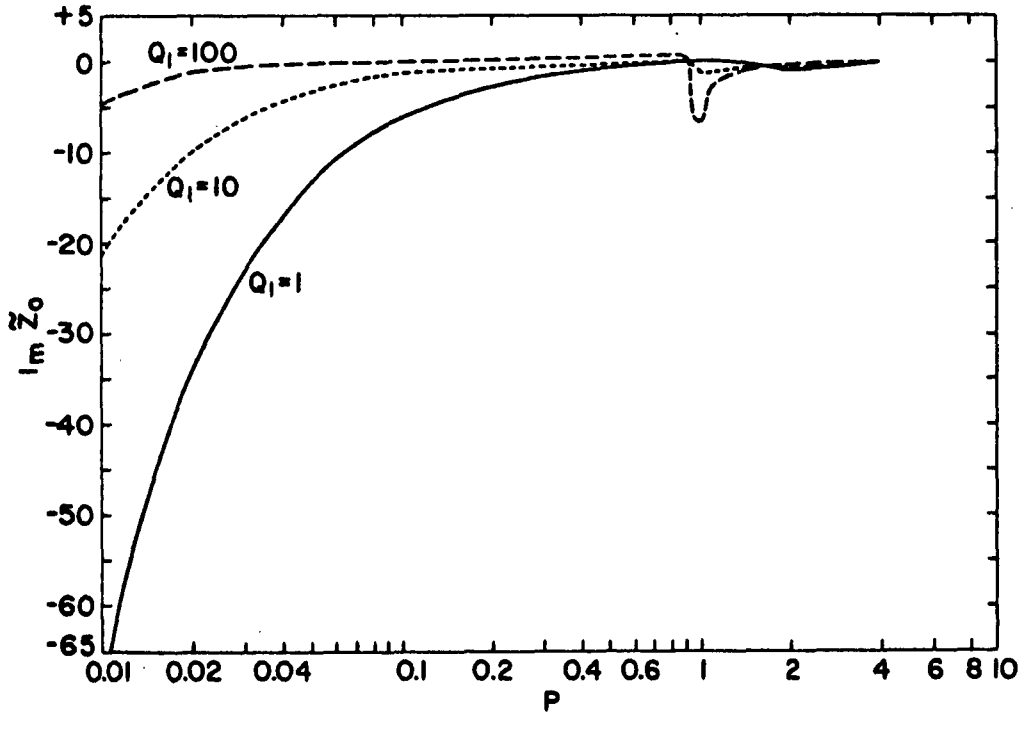

FIGURE 7. Im $\tilde{Z}_o$ as a Function of P for Q_2 = 1

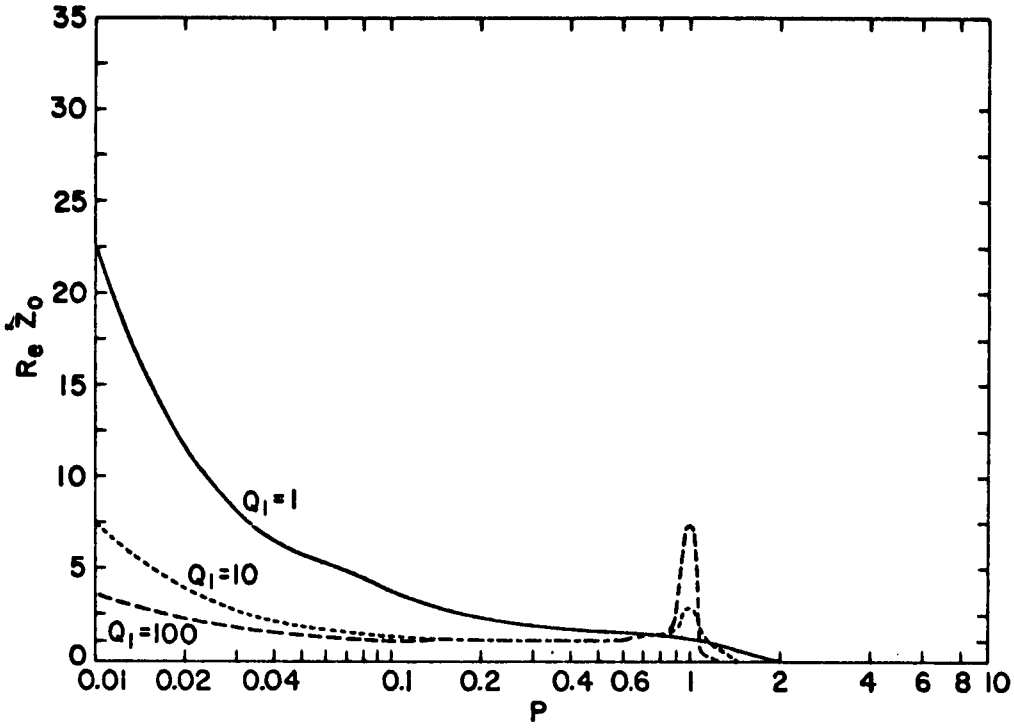

FIGURE 8. Re $\tilde{Z}_o$ as a Function of P for Q_2 = 10

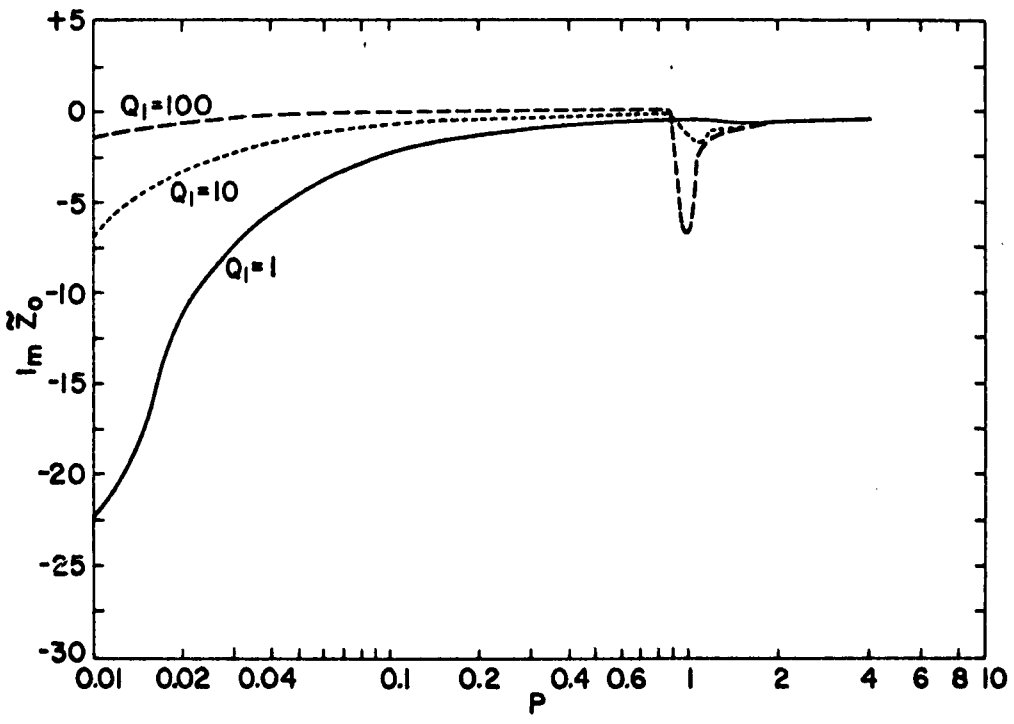

FIGURE 9. Im $\tilde{Z}_o$ as a Function of P for Q_2 = 10

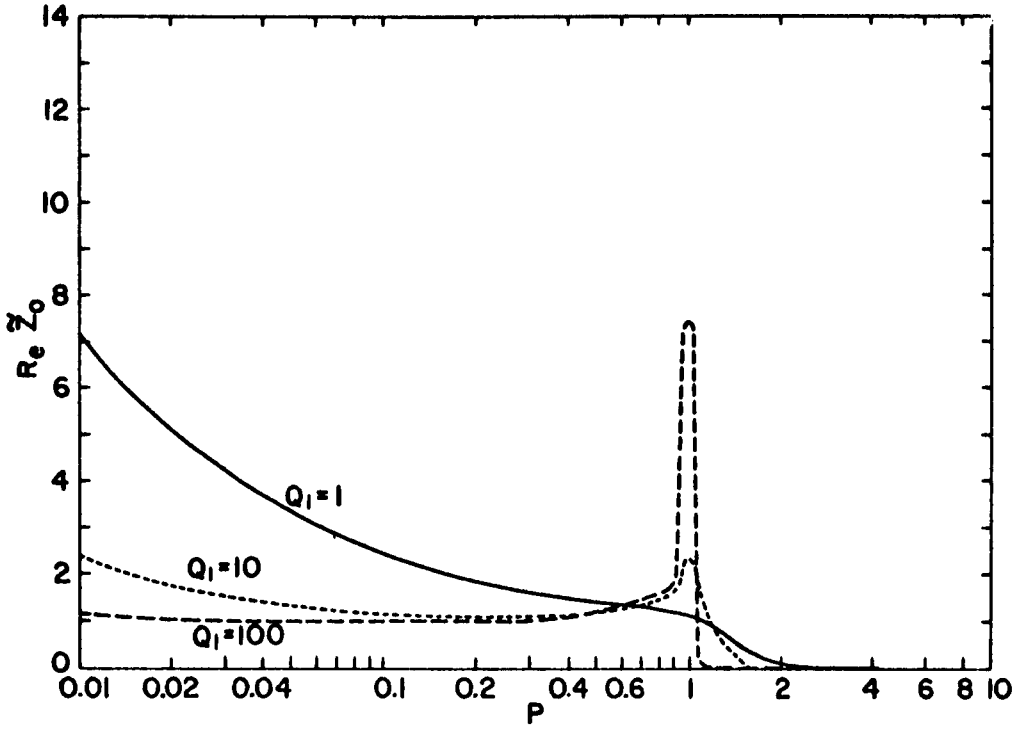

FIGURE 10. Re $\tilde{Z}_o$ as a Function of P for Q_2 = 100

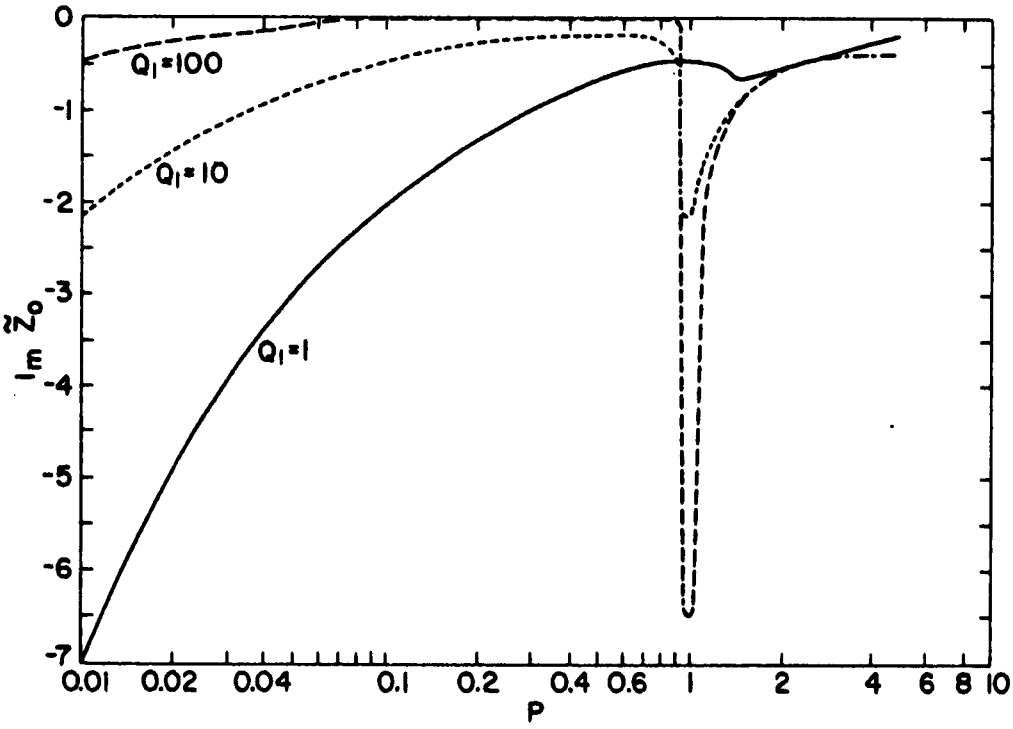

FIGURE 11. Im $\tilde{Z}_o$ as a Function of P for Q_2 = 100

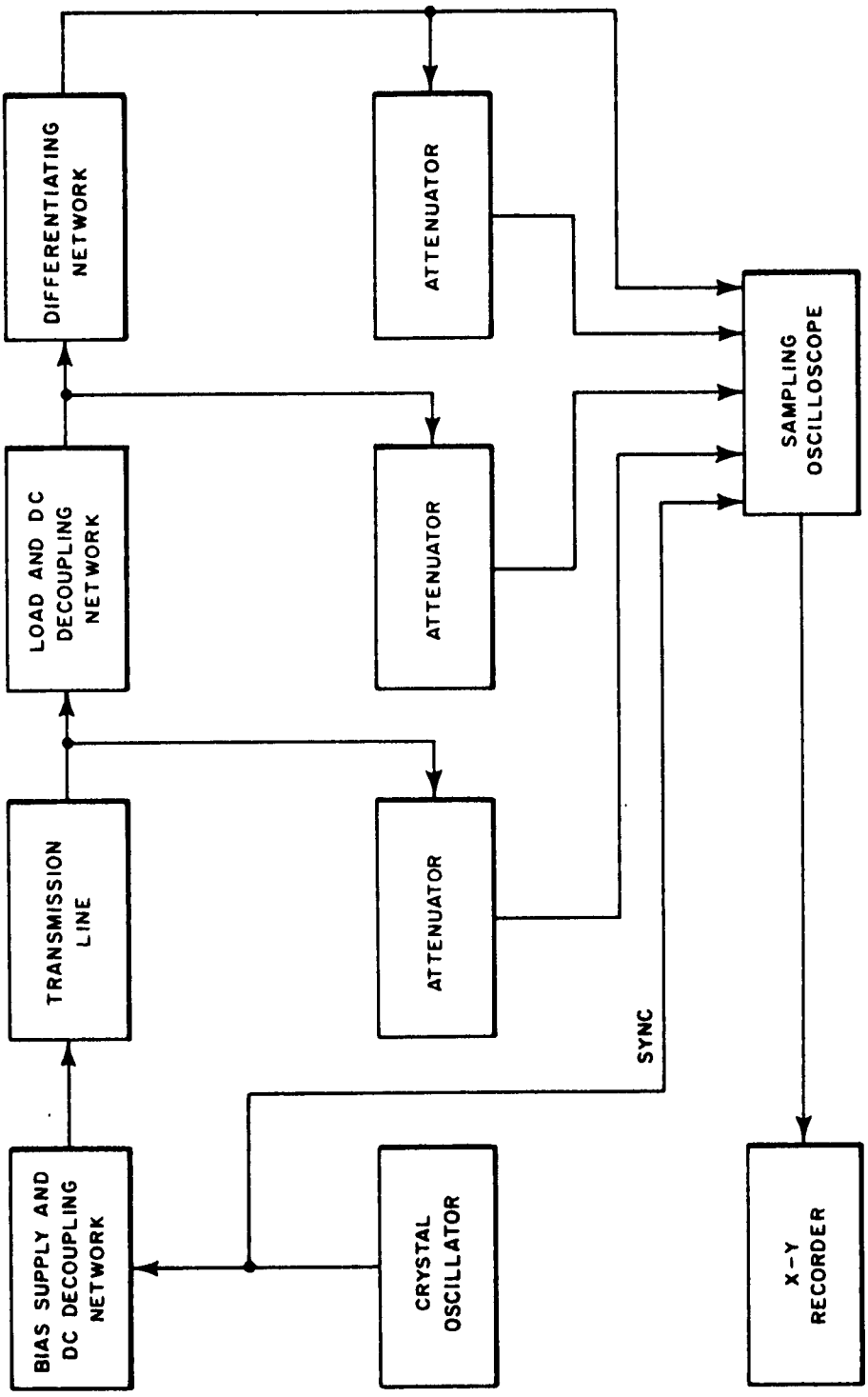

FIGURE 12. Block Diagram of Experimental Setup

output, and expanded differentiated output functions, respectively, for a forcing frequency of 7.810 Mc. Similar results are observed at 4.735 and 10.4 Mc.

Under the same conditions, some experiments were conducted with a low-level forcing signal. The purpose of these experiments was two-fold: (1) to experimentally show the dispersion effects, and (2) to gather a relative idea of the forcing frequency vs. narrow-pulse-producing capabilities of the line. Figure 17 shows the pulse width and peak pulse voltage output with a constant 4-volt peak-to-peak input voltage. The extreme ends of the curve illustrate the effects of dispersion upon the degradation of pulse width (or rise time of the shock function). The figure also shows that the most favorable pulse generation capabilities of this particular line are for repetition frequencies on the order of 1 to 10 Mc.

CONCLUSION

It has been demonstrated theoretically and experimentally that the dispersional effects due to joule heating and frequency-sensitive transmission line elements degrade the intuitive narrow-pulse-producing capabilities of a lumped-element nonlinear transmission line. However, as shown experimentally, it is possible to generate very narrow pulses of high repetition rates with far less than state-of-the-art components if the dispersional effects are small over the range of the forcing frequency and its highest order harmonic.

By the utilization of varactor diodes with relatively low series resistance and high reverse bias properties, pulse widths much less than the 1 nsec shown here would be expected.

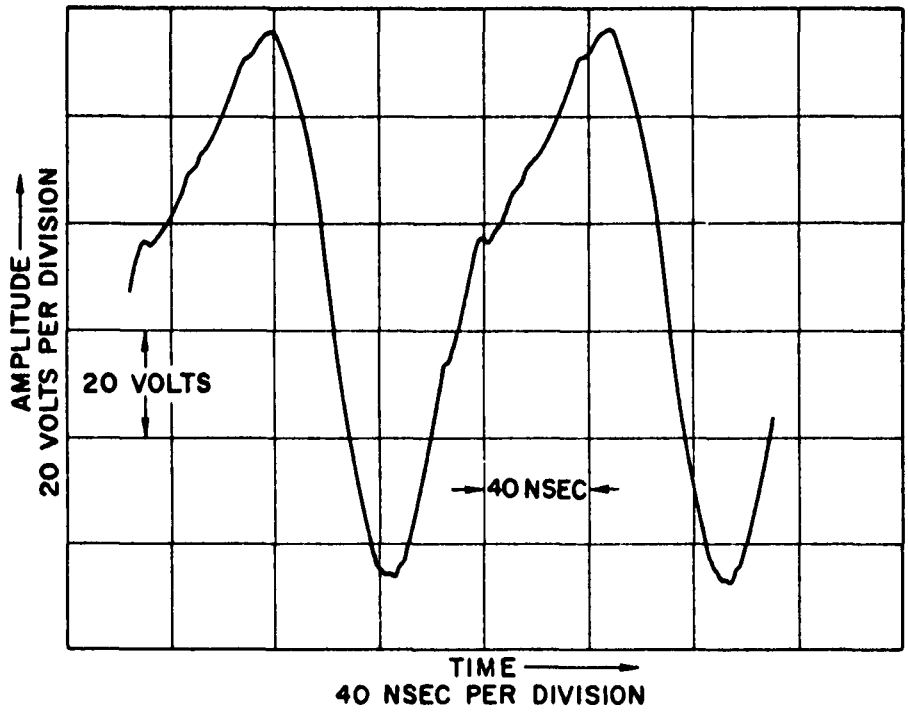

FIGURE 13. Input Wave Form

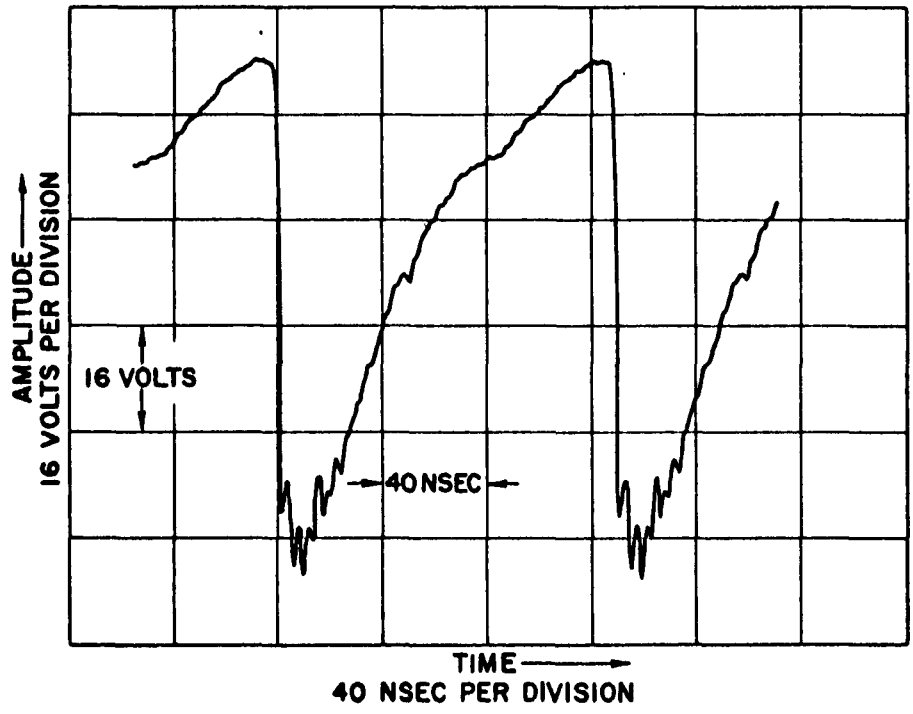

FIGURE 14. Output Wave Form

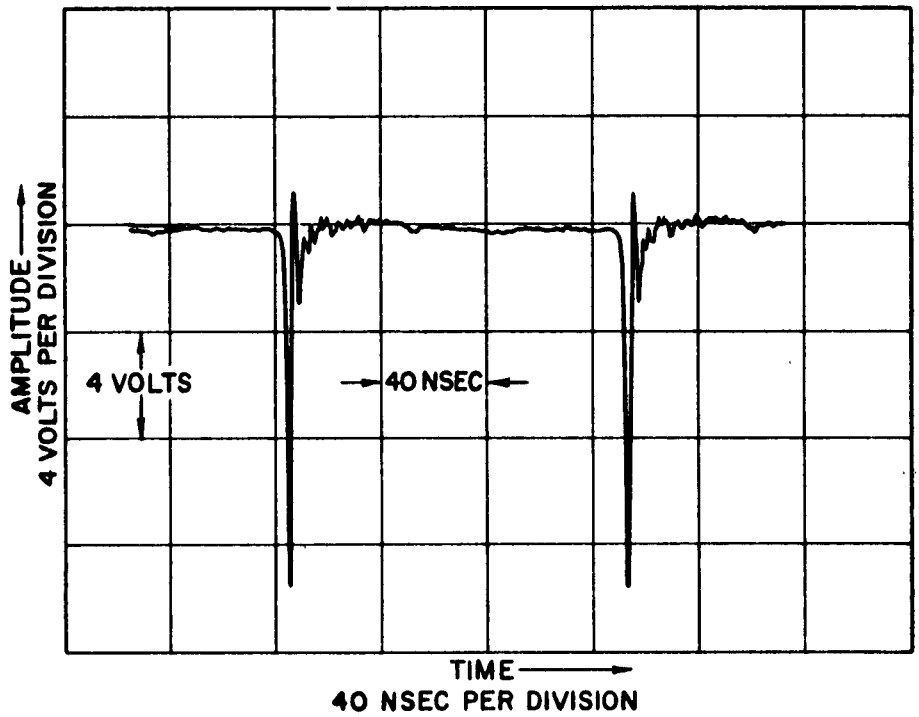

FIGURE 15. Differentiated Output Wave Form

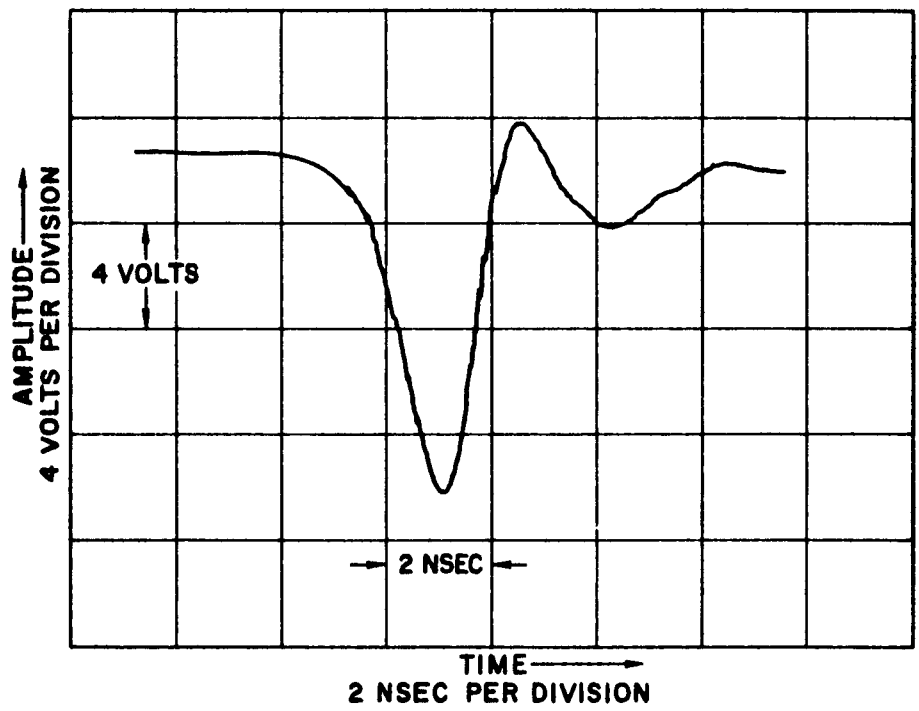

FIGURE 16. Expanded Differentiated Output Wave Form

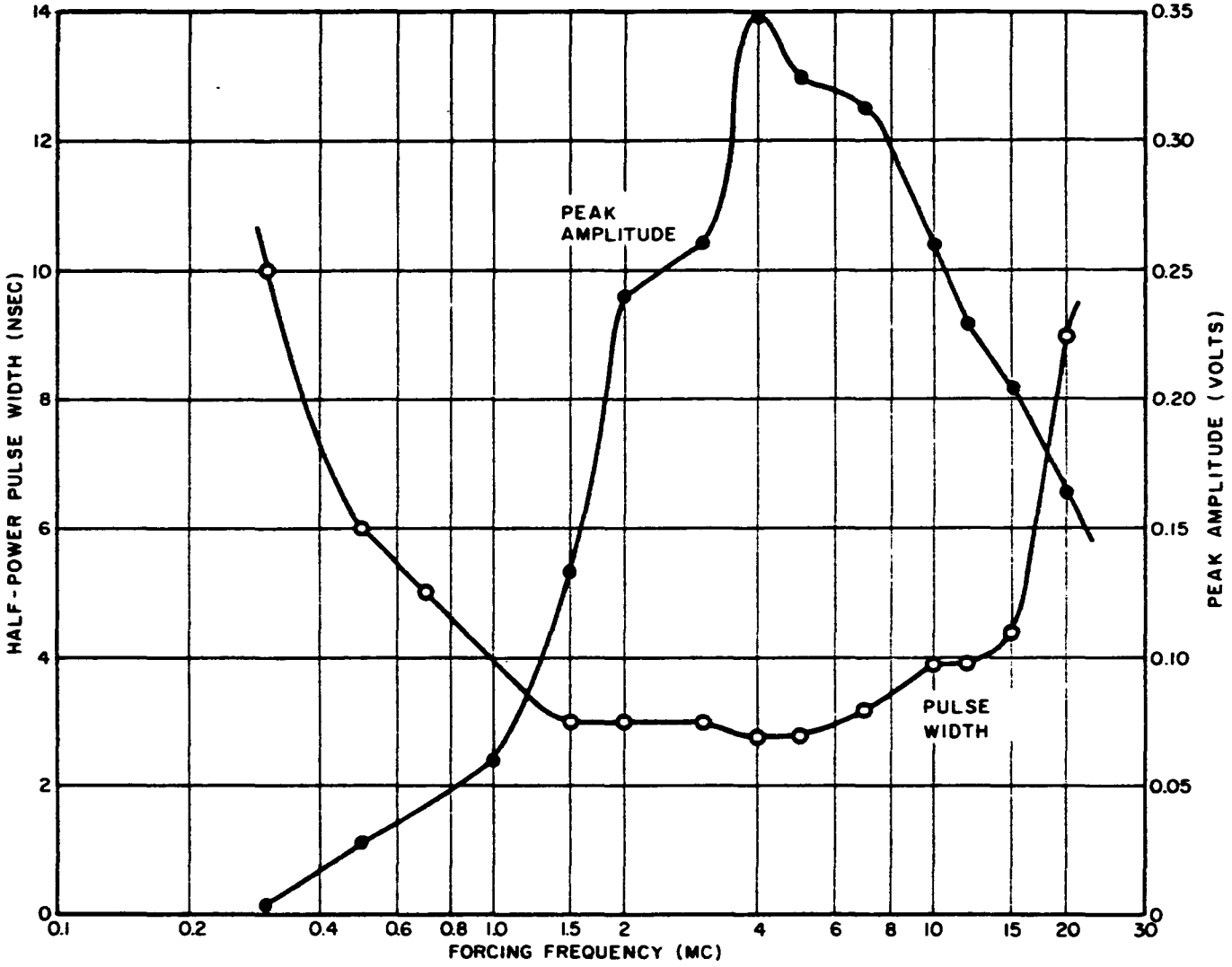

FIGURE 17. Dispersion Effects Upon Pulse Width

EDGE SHIFT AND m_e^* IN GaSb AS A FUNCTION OF FERMI LEVEL

by

H. Piller, V. A. Patton, and G. Zaeschmar

INTRODUCTION

In order to predict or interpret many of the electronic properties of semiconductors, it is necessary to have a detailed picture of the energy band structure. An important parameter in the energy band structure is the effective mass m_0^*. Faraday rotation in the free carrier region, where the rotation is proportional to the square of the wavelength, has emerged as a very useful technique for the determination of the effective mass. The Faraday effect can also give the temperature dependence of the direct optical edge shift as a function of doping level.

The Faraday effect is the rotation of the plane of polarization of a beam of linear polarized radiation in a material in the presence of a static magnetic field. In NOLC experiments it is assumed that the rotation is positive when it is clockwise for radiation propagated along the direction of the magnetic field toward the observer. In GaSb the Faraday rotation at photon energies below the absorption edge is dependent upon the free charge carriers present in all the conduction bands, but the low Fermi level precludes the use of more than two conduction bands, ([000] and <111>), in the calculation of the free carrier densities.

In gallium antimonide, the free carrier rotation[1] is the sum of the rotations resulting from the carriers in both conduction bands

$$\theta = \frac{e^3 B \ell}{\omega^2 2nc\epsilon_0} \left(\frac{n_0}{m_0^{*2}} + \frac{n_1}{m_1^{*2}} \right) \qquad (1)$$

where

B = magnetic induction

ℓ = thickness of the sample

[1] H. Piller, J. Phys. Chem. Solids, Vol. 24, p. 425 (1963).

n = refractive index

c = velocity of light

ϵ_0 = dielectric constant of vacuum

ω = angular frequency of the incident radiation

n_0 = carrier concentrations in the [000] bands

n_1 = carrier concentrations in the <111> band

The average effective mass in the <111> band, m_1^*, is much larger than the effective mass in the [000] band, m_0^*.

The average effective mass for parabolic bands with ellipsoidal energy surfaces is[2]

$$m_1^* = m_{1t}\left(\frac{3K}{K+2}\right)^{\frac{1}{2}} \tag{2}$$

where

$$K = \frac{m_{1\ell}}{m_{1t}}$$

$m_{1\ell}$ = longitudinal effective mass

m_{1t} = transverse effective mass

The ratio K can be determined by comparing an average effective mass from Faraday rotation measurements, m_1^*, with an average effective mass from reflection measurements, m_{1r}^*. The following expression is obtained for the transverse effective mass:

$$m_{1t} = m_1^{*2}\left[\frac{1}{m_{1r}^*} - \left(\frac{1}{m_{1r}^{*2}} - \frac{1}{m_1^{*2}}\right)^{\frac{1}{2}}\right] \tag{3}$$

where m_1^* is given by equation (2) and $m_{1r}^* = m_{1t}\left(\frac{3K}{1+2K}\right)$ (4)

According to the two-band model and neglecting the terms with $(\mu_1/\mu_0)^2$, the expression for the Hall coefficient is

[2] C. Kittel, Introduction to Solid State Physics, New York: John Wiley & Son, Inc. (1956); also B. Hartmann and B. Kleman, Arkiv Fysik, Band 18, No. 6 (1960).

$$R_H = \frac{1}{n_0 e}\left(1 + 2\frac{n_1}{n_0}\cdot\frac{\mu_1}{\mu_0}\right)^{-1} \tag{5}$$

For temperature-independent effective masses, the ratio of the Faraday rotations at temperatures T_a and T_b is

$$\frac{\theta_a}{\theta_b} = \frac{n_{0a} + n_{1a}\left(m_0^*/m_1^*\right)^2}{n_{0b} + n_{1b}\left(m_0^*/m_1^*\right)^2} \tag{6}$$

For a small value of $(m_0^*/m_1^*)^2$ and small carrier concentrations in the <111> band, this ratio is approximately

$$r = \frac{\theta_a}{\theta_b} = C(n_{0a}/n_{0b}) \tag{6a}$$

where C is a correction factor depending on the average mass ratio and the carrier concentrations in the two bands. The average effective mass in the <111> band is about one-third of the density-of-states mass; and the density-of-states mass was found to be $m_{d1} = 14.3\ m_{d0}$.[1] In this case, taking C = 1 introduces a negligible error in equation (6a). The error m_r in the determination of the ratio r reduces to an error m_n in the determination of the carrier concentrations n, as given by

$$\frac{m_n}{n} = \frac{m_r}{r(r-1)} \tag{7}$$

From equations (5) and (6), the carrier concentrations in the [000] band at temperature T_a is given by

$$n_{0a} = \frac{r(1/R_{Ha} - 1/R_{Hb})}{e(r-1)(1 - 2\mu_1/\mu_0)} \qquad \frac{\mu_1}{\mu_0} = 1/6 \tag{8}$$

For samples with small carrier concentrations (in GaSb, where $n = <10^{18}\text{cm}^{-3}$) this equation, together with equation (1), determines the effective mass in the [000] band.

The [000] conduction band is not parabolic. The effective mass around the [000] minimum in GaSb is given by the following approximation:[1]

$$m^* = \frac{\left(E_g^2/4 + k_F^2\gamma^2\right)^{\frac{1}{2}}}{\gamma^2} \tag{8a}$$

where

$$\gamma^2 = P^2 \frac{E_g + \frac{2}{3}\Delta}{E_g + \Delta} \tag{9}$$

and

Δ = 0.86 ev (the spin orbit splitting)

E_p = 20 ev (based on $E_p = \frac{2m}{\hbar} \cdot P^2$, where P is the momentum matrix element)

E_g = energy gap

For $k_F = 1.2 \times 10^{-2}$ atomic units ($n_0 = 3.8 \times 10^{17} cm^{-3}$)

$$m_0^* = 0.053\ m_e$$

Figure 1 shows the Faraday rotation at room temperature as a function of the wavelength squared for three samples of n-type GaSb with different carrier concentrations. The free carrier rotation in the samples with small carrier concentrations show the expected linear dependence well below the frequency corresponding to the energy gap. At the absorption edge a change in sign is observed corresponding to direct transitions. The sample with $n_e = 4.3 \times 10^{18} cm^{-3}$ has a minimum near the edge. The small shift of the edge corresponds to the filling of the conduction band.

Figure 2 shows the rotation at liquid nitrogen temperature. The free carrier rotation increased by the factor indicated for each of the samples:

$n = 1.3 \times 10^{17} cm^{-3}$ r = 2.3

$n = 5.0 \times 10^{17} cm^{-3}$ r = 2.8

$n = 4.3 \times 10^{18} cm^{-3}$ r = 1.5

By using the Hall coefficient and the refractive indices for the same temperatures and concentrations, the effective mass was determined for the samples with low carrier concentration. These samples show

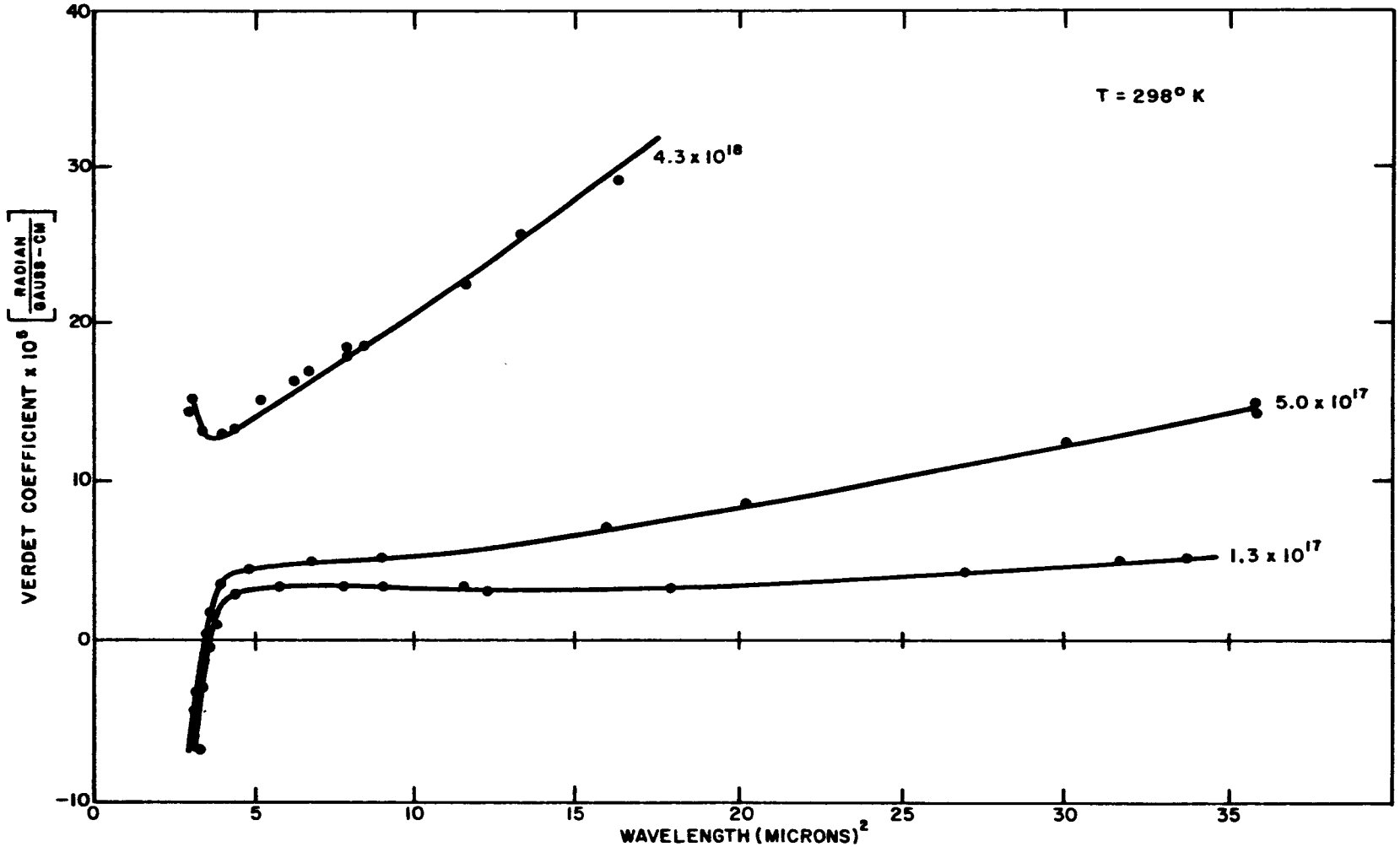

FIGURE 1. Faraday Rotation in n-Type GaSb, at Room Temperature

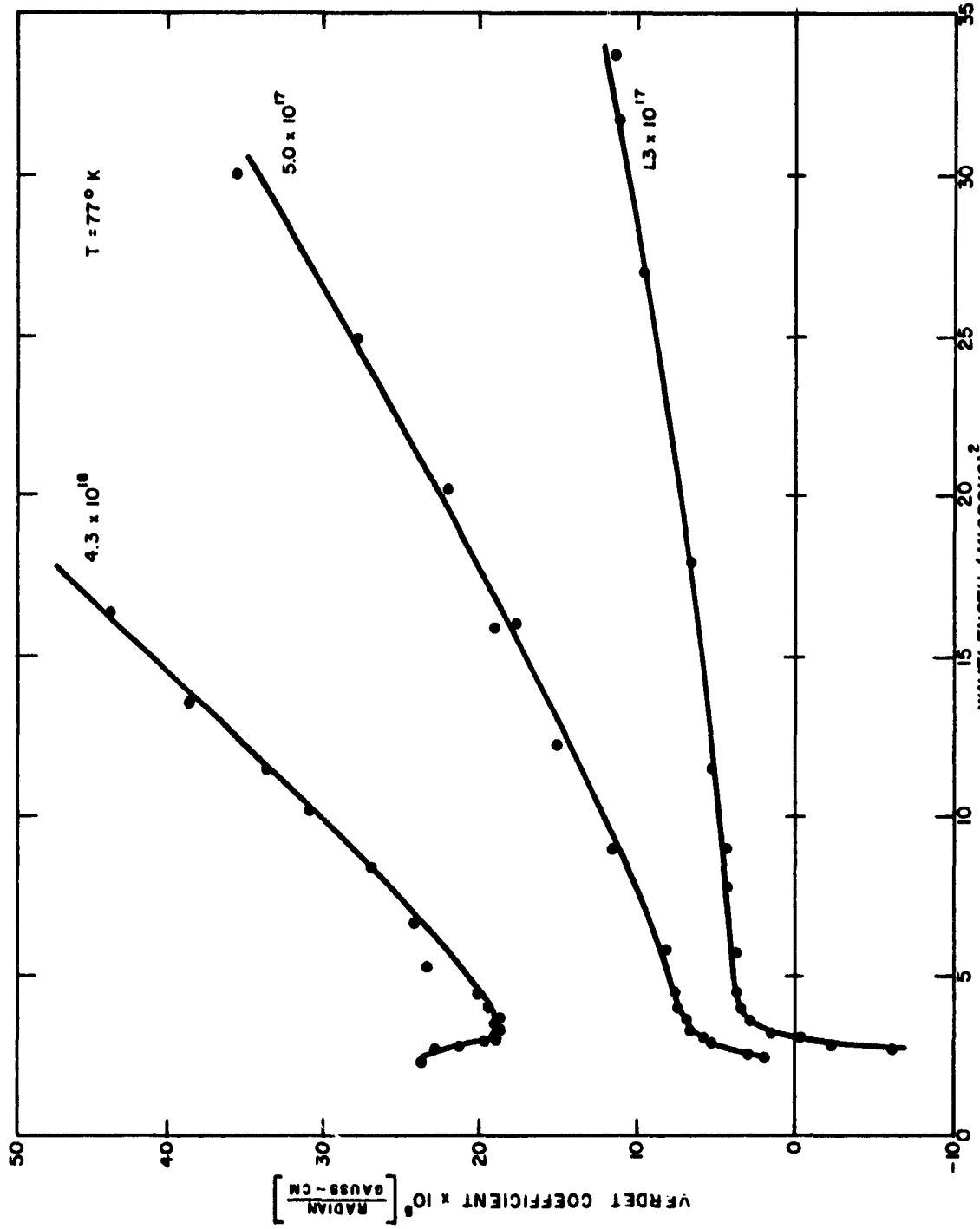

FIGURE 2. Faraday Rotation in n-Type GaSb, at Liquid Nitrogen Temperature

agreement with the calculated values obtained by use of Kane's k·p perturbation approach.[3] The effective mass $m_0^* = (0.049 \pm 0.004)\, m_e$ for a carrier concentration of $n_0 = 3.8 \times 10^{17}\ cm^{-3}$ in the [000] band. The temperature dependence of the separation between the two band minima was obtained by calculating the Fermi levels and separations, using the separation between the band minima $\Delta E_b = 80$ mev at 296°K. The separation increases at the rate of $1.1 \times 10^{-4}\ ev(°K)^{-1}$. The Hall coefficient at high magnetic fields for the sample with $n = 4.3 \times 10^{18}\ cm^{-3}$ at low temperature can be written[4]

$$R_H = \frac{1}{e(n_{0a} + n_{1a})}$$

Using the ratio $K = m_l/m_t$ for germanium and the density-of-states mass given before, one gets also approximate agreement. As mentioned previously, a combination of Faraday rotation results and reflection experiments on the same sample would allow a more precise determination.

The Burstein-Moss shift,[5,6] which is the shift of the direct optical gap, is much larger at 77°K for the different doping levels than at room temperatures. An edge shift of 90 mev for a carrier concentration of $n_{0a} = 3.8 \times 10^{17}\ cm^{-3}$ was observed at 77°K. The results indicate a temperature dependence of the direct optical gap

$$\frac{\Delta E_{opt}}{\Delta T} = \frac{\Delta E_g}{\Delta T} - 4\kappa$$

where κ is the Boltzmann constant. This temperature dependence shows agreement with Burstein's relation for the optical gap at k = 0.

CONCLUSION

The temperature dependence of the direct optical gap for different doping levels can be found from Faraday rotation measurements. To see this effect for the high concentration sample would require very thin samples. Using the two-band model applied to GaSb with the Verdet and Hall coefficients, the calculated effective mass agrees with the mass

---

[3] E. O. Kane, J. Phys. Chem. Solids, Vol. 1, p. 249 (1957).

[4] J. A. Swanson, Phys. Rev., Vol. 99, p. 1799 (1955).

[5] E. Burstein, Phys. Rev., Vol. 93, p. 632 (1954).

[6] T. S. Moss, Proc. Phys. Soc., B, Vol. 67, p. 775 (1954).

INFRARED ABSORPTION SPECTRUM OF Ce^{3+} IN LaF_3

by

R. A. Buchanan, J. Murphy, and H. H. Caspers

INTRODUCTION

The spectra being reported were taken from crystals of $LaCl_3$ and LaF_3 doped with trivalent cerium. Atomic lanthanum has the electronic structure of xenon plus $5d^1\ 6s^2$ electrons which partake in the binding with the fluoride or chloride ions; hence La^{3+} has no visible or infrared electronic absorption spectrum. Trivalent cerium, on the other hand, has one additional 4f electron which produces an absorption spectrum in the near infrared.

The $4f^1$ electronic configuration gives rise, by means of the spin-orbit interaction, to a $^2F_{7/2}$ and a $^2F_{5/2}$ level in the free ion. These levels have been determined by free ion spectroscopy[1] to be separated by 2253 cm^{-1}. The spin-orbit interaction for type 4f rare-earth ions is in general quite constant; that is, regardless of the perturbations placed on a given ion, the splitting due to the spin-orbit interaction is not strongly changed. The spectrum for Ce^{3+} in any crystal would thus be expected to appear in the vicinity of 2253 cm^{-1}, or about 4.5 microns.

A cerium ion in a crystal experiences a strong electric field from its neighbor ions. This crystalline field causes a Stark splitting of the free ion levels. The resultant number of Stark or crystalline field split levels depends upon the J value of the free ion level and the symmetry of the crystalline field. The separation of these levels is sensitive to the strength of the field and hence can vary from one crystal to another. These interactions are summarized in Figure 1. Several studies[2,3] indicate that the maximum separation in a given Stark split level is about 250 cm^{-1} or less for Pr^{3+} and Nd^{3+} in $LaCl_3$.

---

[1] R. J. Lang, Can. J. Research, Vol. 14, p. 127 (1936).

[2] E. Y. Wong and I. Richman, J. Chem. Phys., Vol. 36, p. 1889 (1962).

[3] I. Richman and E. Wong, J. Chem. Phys., Vol. 37, p. 2270 (1962).

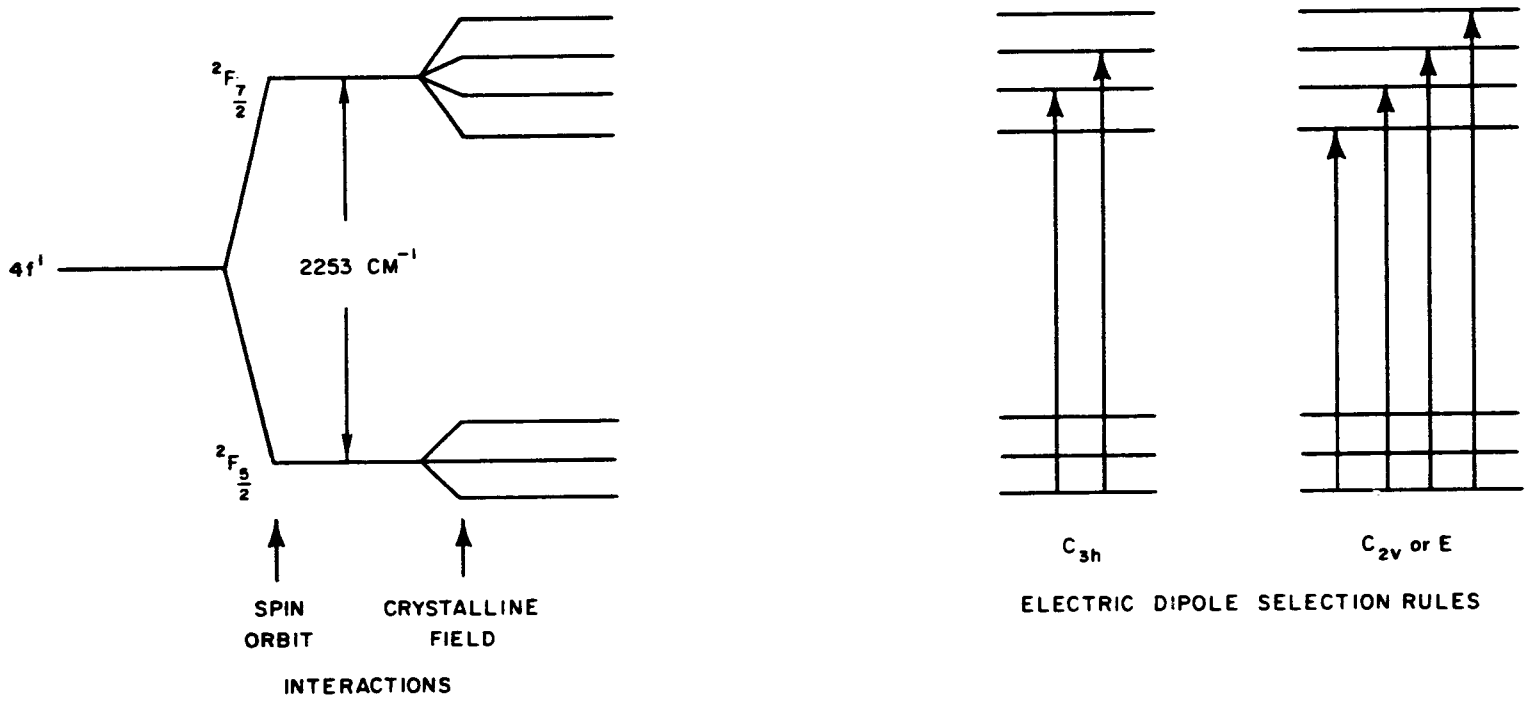

FIGURE 1. Energy Levels and Electric Dipole Selection Rules for Ce^{3+} in LaF_3

The site symmetries for La in $LaCl_3$ and LaF_3 are C_{3h} and C_{2v}, respectively. It is assumed that cerium enters these hosts by substituting for a lanthanum ion and hence should be subject to a crystalline field of the appropriate symmetry. Electron paramagnetic resonance data[4] have confirmed that the site symmetry for Ce^{3+} in $LaCl_3$ is C_{3h}. In LaF_3, electron paramagnetic resonance data[5] indicate, surprisingly, that no symmetry at all exists at the Ce^{3+} site. Furthermore, the electron paramagnetic resonance data reveal that while Gd^{3+} has the lanthanum site symmetry C_{2v}, most other rare earth ions have no symmetry when substituted into LaF_3.

The cerium site symmetry determines the selection rules governing transitions between various crystalline field split levels.[6] Two electric dipole transitions from the ground state to the upper multiplet states are allowed in Ce^{3+} in $LaCl_3$. Four such transitions can occur for Ce^{3+} in LaF_3. From these considerations alone, one would predict that the electric dipole absorption spectrum of Ce^{3+} in $LaCl_3$ and LaF_3 near absolute zero temperature should consist of 2 and 4 absorption lines, respectively. If, in addition, magnetic dipole transitions are important as well as the electric dipole transitions, then each spectrum should consist of 4 lines.

EXPERIMENTAL

Crystals of 0.1 mole-% Ce in $LaCl_3$ were prepared by Dr. Eugene Wong of the UCLA Physics Department. A sample of 1 mole-% Ce in LaF_3 was purchased from Crystal Technology, Inc. Each crystal was approximately 4 mm thick. Spectra were taken on a Cary Model 14b spectrophotometer, which maintained a resolving power of 2000 to 2500 in the 3- to 5-micron region. Samples were cooled by conduction through a copper sample-holder in contact with liquid helium, to a temperature near 4.2°K. The spectra thus obtained are presented in Figure 2.

DISCUSSION OF SPECTRA

The spectra of Ce^{3+} in LaF_3 and $LaCl_3$ exhibit many similarities. The very weak lines at low cm^{-1} become more intense at liquid nitrogen

[4] C. A. Hutchison, Jr. and E. Wong, J. Chem. Phys., Vol. 29, p. 754 (1958).

[5] J. M. Baker and R. S. Rubins, Proc. Phys. Soc., Vol. 78, p. 1353 (1961).

[6] J. Murphy, H. H. Caspers, and R. A. Buchanan, NAVWEPS Report 7237, Quarterly Report: Foundational Research Projects, July-September 1962, p. 111 (1962).

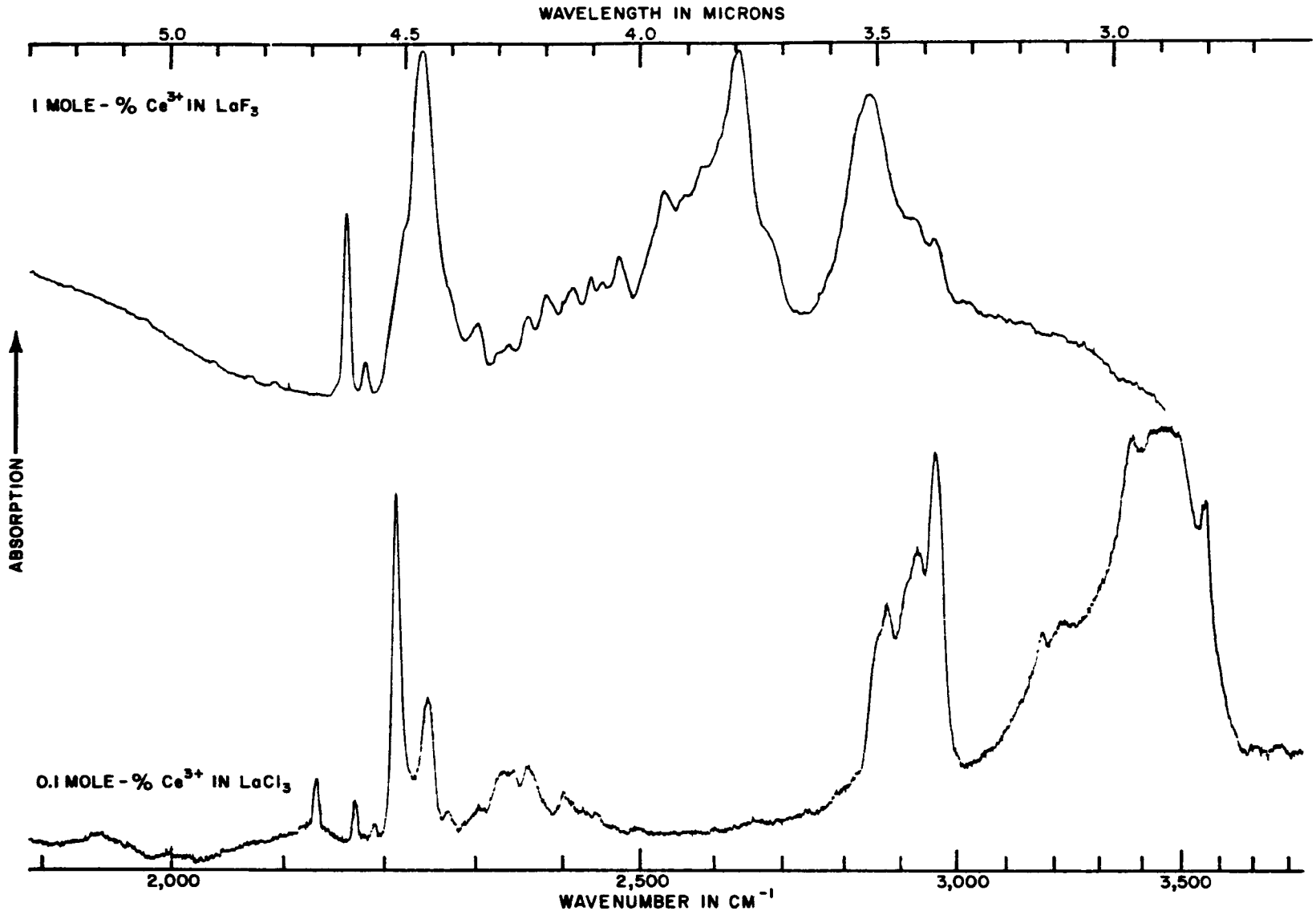

FIGURE 2. Absorption Spectra of Crystals of Ce^{3+} in $LaCl_3$ and LaF_3, Near 4.2°K

temperature and therefore must be associated with transitions which originate on excited energy levels. Intense and sharp lines are observed between 2100 and 2200 cm^{-1}. Two intense and broad lines containing complex structures are observed between 2500 and 3500 cm^{-1}. In between the sharp line region and the broad line region lies a region that contains many weak broad lines. Clearly, there are too many lines to be accounted for by pure electronic transitions. The sharp lines between 2100 and 2200 cm^{-1} are most likely pure electronic transitions. The weak broad lines in the central region are vibronic lines, i.e., lattice vibration frequencies coupled to the electronic lines which are sharp between 2100 and 2200 cm^{-1}. These vibronic lines will be discussed shortly.

The intense broad lines in the 2500 to 3500 cm^{-1} region are more difficult to understand. If these are indeed electronic transitions, they may be broadened and intensified by mixing with lattice vibration frequencies coupled to the lower electronic levels. Such effects have been noted previously.[7] The over-all multiplet splitting is about 700 cm^{-1} in LaF_3 and about 1200 cm^{-1} in $LaCl_3$—much larger than the 250 cm^{-1} observed for Pr^{3+} and Nd^{3+} in $LaCl_3$. A crystalline field splitting of 1000 cm^{-1} has been reported[8] for Ce^{3+} and Yb^{3+} in CaF_2. Although the exact assignments of the absorption peaks of Ce^{3+} in $LaCl_3$ and LaF_3 are not known at this time, it appears probable that the crystalline field splitting of the Ce^{3+} multiplet levels is anomalously large.

Polarization spectra have been taken of these crystals. Some polarization is noted in the sharp lines of Ce^{3+} in $LaCl_3$, but no polarization of any line could be found for Ce^{3+} in LaF_3. These results agree with the Ce^{3+} site symmetries C_{3h} and C_{2v} in $LaCl_3$ and LaF_3, respectively.

It was mentioned previously that the weak broad lines between about 2200 and 2500 cm^{-1} were due to interactions of lattice frequencies with the electronic transitions. The vibronic lines in $LaCl_3$ have been covered adequately elsewhere.[9] The following statements will be limited to the Ce^{3+} in LaF_3 spectrum. Table 1 contains a list of the lattice frequencies that have been observed experimentally in LaF_3. Three possible electronic transitions have been chosen at 2160, 2180, and 2235 cm^{-1}. Each of the lattice frequencies has been added to the electronic

---

[7] G. H. Dieke, "Spectroscopic Observations on Maser Materials" in Advances in Quantum Electronics, ed. by J. R. Singer, New York: Columbia University Press, 1961.

[8] Z. J. Kiss, Phys. Rev., Vol. 127, p. 718 (1962).

[9] R. A. Buchanan, J. Murphy, and H. H. Caspers, NAVWEPS Report 8141, Quarterly Report: Foundational Research Projects, October-December 1962, pp. 73-101 (1963).

transition and compared with the observed spectrum. Good agreement between the calculated and observed vibronic lines is noted.

TABLE 1. Vibronic Lines for Ce^{3+} in LaF_3

Lattice Vibrations (cm^{-1})	Electronic Transitions (cm^{-1})					
	2160		2180		2235	
	Calc.	Obs.	Calc.	Obs.	Calc.	Obs.
176 IR	2336	2335	2356	2357	2411	2412
210 IR	2370	--	2390	2390	2445	2447
277 IR	2437	2434	2457	2459	2512	2515
293 Raman	2453	2447	2473	2469	2528	2528
358 IR	2518	2515	2538	2535	2593	--
368 Raman	2528	2528	2548	--	2603	2604

CONCLUSIONS

1. More lines are observed in the Ce^{3+} spectrum than can be accounted for by pure electronic transitions alone.

2. The evidence seems to indicate a larger crystalline field splitting in Ce^{3+} than in other trivalent rare earths (4f type), with the possible exception of Yb.

3. The higher polarization studies confirm the absence of symmetry higher than C_{2v} at the Ce^{3+} site in LaF_3.

4. Lattice vibrations couple to electronic transitions to produce many vibronic lines.

NAVWEPS Report 8150 - WepTasks R360 FR-104/211-1/R011-01-001 and RMGA-41-031/211-1/F009-07-002

INITIAL DISTRIBUTION

	Copies
Chief, Bureau of Naval Weapons Navy Department Washington 25, D. C.	
Attn: Code R-3	1
R-5	1
R-12	1
RM	1
RMMO	1
RMWC	1
RRMA-3	1
RRRE	1
DLI-31	4
Director National Security Agency Fort George G. Meade, Md.	
Attn: REMP-2	1
Chief, Bureau of Ships Navy Department Washington 25, D. C.	
Attn: Code 681A	1
687C1	1
694E, D. Wilson	1
452F	1
Chief of Naval Research Navy Department Washington 25, D. C.	
Attn: Code 407	1
420	1
Commanding Officer Office of Naval Research Pasadena Branch 1030 East Green Street Pasadena 1, Calif.	1
Officer in Charge Naval Civil Engineering Laboratory Port Hueneme, Calif.	
Attn: Technical Library	1
Director Naval Research Laboratory Washington 25, D. C.	
Attn: Richard Wallis	1
Commander Naval Weapons Laboratory Dahlgren, Va.	1
Officer in Charge Naval Weapons Services Office U. S. Naval Station (Washington Navy Yard Annex) Washington 25, D. C.	
Attn: Code 120	2
Commander Naval Ordnance Laboratory White Oak Silver Spring 19, Md.	
Attn: E. H. Jackson, LX Division	1
Dr. F. Stern, Solid State Division	1
Dr. E. P. Trounson, Physics Research Department	1
Commander Naval Ordnance Test Station China Lake, Calif.	
Attn: Technical Library	1
B. O. Seraphin, Code 5019	1

	Copies
Commanding Officer Naval Ordnance Test Station Pasadena Annex 3202 E. Foothill Blvd. Pasadena 8, Calif. Attn: Library	1
Director Navy Electronics Laboratory San Diego, Calif. Attn: H. E. Lee Technical Library	1 1
Superintendent Naval Postgraduate School Monterey, Calif. Attn: Library E. C. Crittenden, Jr.	1 1
Commanding Officer and Director Naval Radiological Defense Laboratory San Francisco 24, Calif. Attn: L. D. Miller, Code 944A	1
Commander Pacific Missile Range Naval Missile Center Point Mugu, Calif. Attn: Technical Library	1
NOLC Washington Office Naval Ordnance Laboratory White Oak Silver Spring 19, Md. Attn: W. F. Stuart	1
Commanding Officer Office of Ordnance Research 55 South Grand Avenue Pasadena, Calif. Attn: Dr. W. N. Arnquist	1
Commander U. S. Army Material Command Harry Diamond Laboratories Washington 25, D. C. Attn: Dr. W. K. Saunders	1
Commanding General Army Electronics Proving Ground Fort Huachuca, Ariz. Attn: SIGPG-DCGES-2	1
Commander Cambridge Research Center L. G. Hanscom Field Bedford, Mass. Attn: CROTLA	1
Armed Services Technical Information Agency Arlington Hall Station Arlington 12, Va.	10
Director National Bureau of Standards Washington 25, D. C. Attn: Dr. H. P. R. Frederikse, Code 4.04 Dr. R. D. Huntoon, Code 30	1 1
Aerojet-General Corporation Advanced Research Division Azusa, Calif. Attn: R. C. Carlston, Bldg. 415	1
Armour Research Foundation Illinois Institute of Technology Technology Center 10 West 35th Street Chicago 18, Ill. Attn: J. W. Buttrey	1
Avco Corporation Research and Development Division Physics Department - T430 Wilmington, Mass. Attn: Dr. T. Wentink, Jr.	1
Barnes Engineering Company Stamford, Conn. Attn: R. DeWaard	1
Bell and Howell Research Center 360 Sierra Madre Villa Pasadena, Calif. Attn: R. K. Willardson, Solid State	1

	Copies
Bulova Research and Development Laboratories 6210 Woodside Avenue Woodside 77, Long Island, N. Y. Attn: Dr. T. K. Steele	1
California Institute of Technology 1201 East California Street Pasadena 4, Calif. Attn: I. E. Newland, Reports Group, JPL	1
Eastman Kodak Company Naval Ordnance Division 50 West Main Street Rochester 14, N. Y. Attn: W. McKusick	1
Ford Motor Company Aeronutronics Division Research Operations Newport Beach, Calif. Attn: L. M. Lambert	1
General Electric Company One River Road Schenectady 5, N. Y. Attn: G. C. Dodson	1
General Telephone and Electronics Laboratory 1015 Corporation Way Palo Alto, Calif. Attn: K. A. Wickersheim	1
Hughes Research Laboratory Hughes Aircraft Company Malibu, Calif. Attn: C. Asawa	1
Johns Hopkins University Applied Physics Laboratory Silver Spring, Md. Attn: Dr. A. I. Mahan A. Nagy	1 1
Lockheed Aircraft Corporation Plant B-1 Burbank, Calif. Attn: Dr. L. G. Mundie, Dept. 7210, Bldg. 167A	1
Lockheed Aircraft Corporation Missile Systems Division Sunnyvale, Calif. Attn: M. Eisenberg Dr. C. Kooi	1 1
Massachusetts Institute of Technology Lincoln Laboratory Lexington 73, Mass. Attn: J. H. Chisholm	1
Motorola, Inc. 8201 East McDowell Road Phoenix, Ariz. Attn: J. C. Cacheris	1
Pennsylvania State College State College, Pa. Attn: Director, Ordnance Research Laboratory	1
Servo Corporation of America 111 New South Road Hicksville, Long Island, N. Y. Attn: I. Melman	1
Syracuse University Syracuse 10, N. Y. Attn: Dr. N. Ginsburg, Physics Department H. Levenstein, Solid State Laboratory	1 1
University of Arizona Lunar and Planetary Laboratory Tucson, Ariz. Attn: R. B. Goranson	1
University of California Riverside, Calif. Attn: A. Lawson	1

	Copies
University of Michigan Willow Run Laboratories P. O. Box 618 Ann Arbor, Mich. Attn: W. Wolfe	1
Washington University St. Louis, Mo. Attn: Dr. E. U. Condon	1
Royal Radar Establishment Ministry of Aviation St. Andrews Road Malvern Worchestershire, England Attn: E. H. Putley Via: BuWeps, Code DSC-3	1
Signals Research and Development Establishment Ministry of Aviation Christchurch Hampshire, England Attn: Dr. M. R. Brown (ZSP/5/08) Via: BuWeps, Code DSC-3	1
Royal Aircraft Establishment Radio Department Farnsborough, Hants, England Attn: T. S. Moss Via: BuWeps, Code DSC-3	1

NOLC:	Copies
J. A. Hart, Code 04	1
C. J. Humphreys, Code 40	2
E. Paul, Jr., Code 40	1
R. L. Conger, Code 42	1
R. W. Sharp, Code 422	1
J. H. Johnson, Code 422	1
R. L. King, Code 422	1
L. T. Long, Code 422	1
J. A. Parks, Code 422	1
R. F. Potter, Code 43	1
J. Bernstein, Code 432	1
V. A. Patton, Code 432	1
G. Zaeschmar, Code 432	1
R. A. Buchanan, Code 433	1
H. H. Caspers, Code 433	1
J. Murphy, Code 433	1
H. Piller, Code 433	1
C. P. Haber, Code 44	1
W. C. Spindler, Code 441	1
W. S. Harris, Code 441	1
R. E. Panzer, Code 441	1
C. M. Douglas, Code 442	1
D. L. Herring, Code 442	1
K. L. Paciorek, Code 442	1
P. J. Slota, Jr., Code 443	1
R. H. Kratzer, Code 443	1
F. C. Essig, Code 45	1
E. W. Seeley, Code 452	1
J. R. Alday, Code 452	1
B. F. Husten, Code 50	1
L. L. Parker, Code 50	1
H. A. Bulgerin, Code 51	1
R. L. Bauer, Code 53	1
J. J. Nastronero, Code 54	1
R. J. Hardy, Code 57	1
F. C. Alpers, Code 71	1
W. F. Meggers, Jr., Code 72	1
T. B. Jackson, Code 73	1
A. C. Sevy, Code 75	1
Technical Library, Code 234	2

Naval Ordnance Laboratory Corona. (NAVWEPS Report 8150)
QUARTERLY REPORT: FOUNDATIONAL RESEARCH PROJECTS, JANUARY-MARCH 1963. 1 June 1963. 96 pp. UNCLASSIFIED

During the third quarter of fiscal year 1963, Foundational Research projects were conducted in the following general areas: Coder Components; High Temperature Polymers; Infrared Atomic Spectra; Lasers; Nonaqueous Electrochemistry; Nonlinear Transmission Lines; Semiconductor Physics; and Solid State Spectroscopy.

1. Naval research
2. Polymerization—Theory
3. Infrared spectrum—Analysis
4. Lasers
5. Electrochemistry—Applications
6. Transmission lines—Electromagnetic effects
7. Semiconductor physics
8. Spectroscopy
I. Foundational Research Projects

WepTasks:
R360 FR-104/211-1/R011-01-001
RMGA-41-031/211-1/F009-07-002

This card is UNCLASSIFIED

Naval Ordnance Laboratory Corona. (NAVWEPS Report 8150)
QUARTERLY REPORT: FOUNDATIONAL RESEARCH PROJECTS, JANUARY-MARCH 1963. 1 June 1963. 96 pp. UNCLASSIFIED

During the third quarter of fiscal year 1963, Foundational Research projects were conducted in the following general areas: Coder Components; High Temperature Polymers; Infrared Atomic Spectra; Lasers; Nonaqueous Electrochemistry; Nonlinear Transmission Lines; Semiconductor Physics; and Solid State Spectroscopy.

1. Naval research
2. Polymerization—Theory
3. Infrared spectrum—Analysis
4. Lasers
5. Electrochemistry—Applications
6. Transmission lines—Electromagnetic effects
7. Semiconductor physics
8. Spectroscopy
I. Foundational Research Projects

WepTasks:
R360 FR-104/211-1/R011-01-001
RMGA-41-031/211-1/F009-07-002

This card is UNCLASSIFIED

Naval Ordnance Laboratory Corona. (NAVWEPS Report 8150)
QUARTERLY REPORT: FOUNDATIONAL RESEARCH PROJECTS, JANUARY-MARCH 1963. 1 June 1963. 96 pp. UNCLASSIFIED

During the third quarter of fiscal year 1963, Foundational Research projects were conducted in the following general areas: Coder Components; High Temperature Polymers; Infrared Atomic Spectra; Lasers; Nonaqueous Electrochemistry; Nonlinear Transmission Lines; Semiconductor Physics; and Solid State Spectroscopy.

1. Naval research
2. Polymerization—Theory
3. Infrared spectrum—Analysis
4. Lasers
5. Electrochemistry—Applications
6. Transmission lines—Electromagnetic effects
7. Semiconductor physics
8. Spectroscopy
I. Foundational Research Projects

Weptasks:
R360 FR-104/211-1/R011-01-001
RMGA-41-031/211-1/F009-07-002

This card is UNCLASSIFIED

Naval Ordnance Laboratory Corona. (NAVWEPS Report 8150)
QUARTERLY REPORT: FOUNDATIONAL RESEARCH PROJECTS, JANUARY-MARCH 1963. 1 June 1963. 96 pp. UNCLASSIFIED

During the third quarter of fiscal year 1963, Foundational Research projects were conducted in the following general areas: Coder Components; High Temperature Polymers; Infrared Atomic Spectra; Lasers; Nonaqueous Electrochemistry; Nonlinear Transmission Lines; Semiconductor Physics; and Solid State Spectroscopy.

1. Naval research
2. Polymerization—Theory
3. Infrared spectrum—Analysis
4. Lasers
5. Electrochemistry—Applications
6. Transmission lines—Electromagnetic effects
7. Semiconductor physics
8. Spectroscopy
I. Foundational Research Projects

WepTasks:
R360 FR-104/211-1/R011-01-001
RMGA-41-031/211-1/F009-07-002

This card is UNCLASSIFIED